AD-A041 257 AIRESEARCH MFG CO OF CALIFORNIA TORRANCE F/G 10/2
SUBSYSTEM DESIGN ANALYSIS LIGHTWEIGHT ALTERNATOR (MODEL TEST PR--ETC(U)
MAR 77 C H LEE, D BERKER, G TATRO, P WALIA F29601-74-C-0055
UNCLASSIFIED AFWL-TR-75-66-ADD-2 NL

1 OF 2
AD A041257

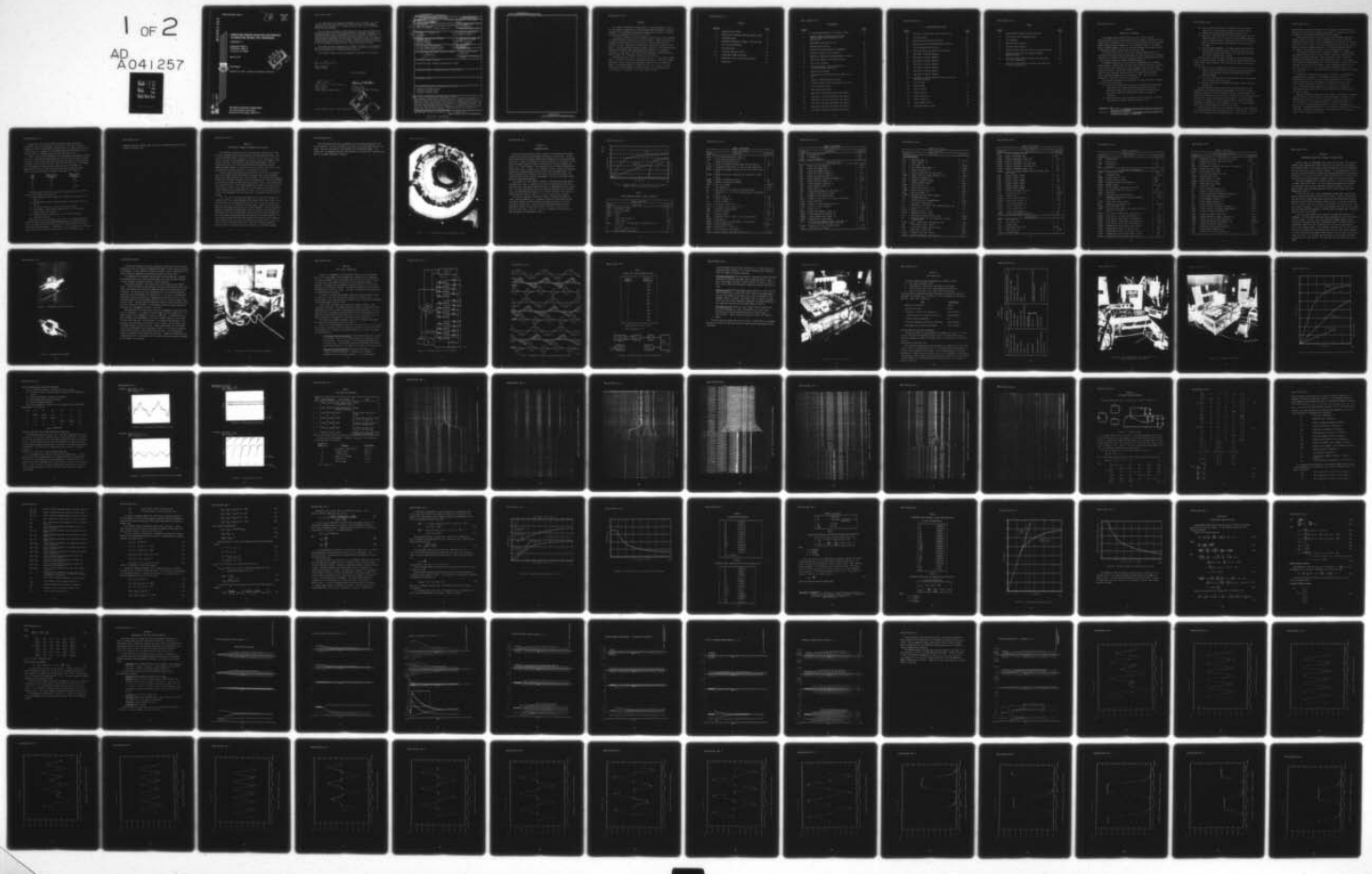

AFWL-TR-75-66, Add. 2

AFWL-TR-
75-66
Add. 2

SUBSYSTEM DESIGN ANALYSIS LIGHTWEIGHT ALTERNATOR (MODEL TEST PROGRAM)

Addendum 2

AiResearch Mfg Co.
2525 West 190th St.
Torrance, CA 90509

March 1977

Final Report

Approved for public release; distribution unlimited.

AIR FORCE WEAPONS LABORATORY
Air Force Systems Command
Kirtland Air Force Base, NM 87117

AFWL-TR-75-66, Adden. 2

This final report was prepared by AiResearch Mfg Co, Torrance, CA, under Contract F29601-74-C-0055, Job Order 317J1217, with the Air Force Weapons Laboratory, Kirtland AFB, NM. Mr. James O'Loughlin (ALE) was the Laboratory Project Officer-in-Charge.

When US Government drawings, specifications, or other data are used for any purpose other than a definitely related Government procurement operation, the Government thereby incurs no responsiblility nor any obligation whatsoever, and the fact that the Government may have formulated, furnished, or in any way supplied the said drawings, specifications, or other data is not to be regarded by implication or otherwise as in any manner licensing the holder or any other person or corporation or conveying any rights or permission to manufacture, use, or sell any patented invention that may in any way be related thereto.

This report has been reviewed by the Information Office and is releasable to the National Technical Information Service (NTIS). At NTIS, it will be available to the general pbulic, including foreign nations.

This technical report has been reviewed and is approved for publication.

James O'Loughlin

JAMES O'LOUGHLIN
Project Officer

FOR THE COMMANDER

Peter D. Tannen

PETER D. TANNEN
Lt Col, USAF
Chief, Electrical Laser Branch

Armand D. Maio

ARMAND D. MAIO
Lt Colonel, USAF
Chief, Advanced Laser Technology Division

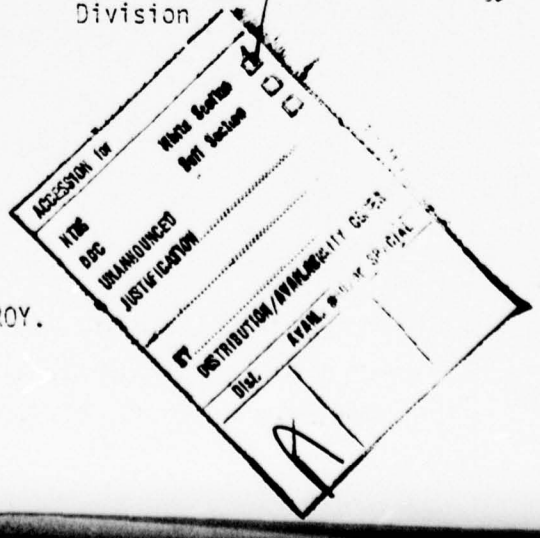

DO NOT RETURN THIS COPY. RETAIN OR DESTROY.

UNCLASSIFIED

SECURITY CLASSIFICATION OF THIS PAGE (When Date Entered)

REPORT DOCUMENTATION PAGE

READ INSTRUCTIONS BEFORE COMPLETING FORM

1. REPORT NUMBER: AFWL-TR-75-66, Addendum-2
2. GOVT ACCESSION NO.:
3. RECIPIENT'S CATALOG NUMBER:
4. TITLE (and Subtitle): SUBSYSTEM DESIGN ANALYSIS LIGHTWEIGHT ALTERNATOR (MODEL TEST PROGRAM) • Addendum 2.
5. TYPE OF REPORT & PERIOD COVERED: Final Report.
6. PERFORMING ORG. REPORT NUMBER:
7. AUTHOR(s): C. H./Lee, P./Walia, D./Berker, G./Tatro
8. CONTRACT OR GRANT NUMBER(s): F29601-74-C-0055
9. PERFORMING ORGANIZATION NAME AND ADDRESS: AiResearch Mfg Co, 2525 West 190th St, Torrance, CA 90509
10. PROGRAM ELEMENT, PROJECT, TASK AREA & WORK UNIT NUMBERS: 317J1217
11. CONTROLLING OFFICE NAME AND ADDRESS: Air Force Weapons Laboratory (ALE), Kirtland Air Force Base, NM 87117
12. REPORT DATE: March 1977
13. NUMBER OF PAGES: 102
14. MONITORING AGENCY NAME & ADDRESS (if different from Controlling Office): 104p.
15. SECURITY CLASS. (of this report): Unclassified
15a. DECLASSIFICATION/ DOWNGRADING SCHEDULE:
16. DISTRIBUTION STATEMENT (of this Report): Approved for public release; distribution unlimited.
17. DISTRIBUTION STATEMENT (of the abstract entered in Block 20, if different from Report):
18. SUPPLEMENTARY NOTES:
19. KEY WORDS (Continue on reverse side if necessary and identify by block number):
Alternator Transient Analysis
Alternator Computer Analysis
Alternator Transient Model
20. ABSTRACT (Continue on reverse side if necessary and identify by block number):
This report discusses the test and computer simulation activities conducted on a modified-design, small-rating aircraft alternator. These activities were intended to provide additional verifications of the alternator analytical approach utilized in designing two specialized large-rating lightweight alternators. The latter designs have been previously detailed in Air Force technical reports AFWL-TR-75-66, "Subsystem Design Analysis Report for Lightweight Alternator (AC Load Case)," and AFWL-TR-75-66, Addendum 1, "Subsystem Design Analysis Report for Lightweight Alternator (DC Load Case)".

DD FORM 1 JAN 73 1473 EDITION OF 1 NOV 65 IS OBSOLETE

UNCLASSIFIED

SECURITY CLASSIFICATION OF THIS PAGE (When Date Entered)

387 343

PREFACE

This report is submitted in compliance with the requirements of the U.S. Air Force Special Weapons Center Contract Number F29601-74-C-0055 "Lightweight Alternator" by the AiResearch Manufacturing Company of California, a division of The Garrett Corporation, Torrance, California.

The report discusses the test and computer simulation activities conducted on a modified-design, small-rating aircraft alternator. These activities were intended to provide additional verifications of the alternator analytical approach utilized in designing two specialized large-rating lightweight alternators. The latter designs have been previously detailed in Air Force technical reports AFWL-TR-75-66, "Subsystem Design Analysis Report for Lightweight Alternator (AC Load Case)," and AFWL-TR-75-66, Addendum 1, "Subsystem Design Analysis Report for Lightweight Alternator (DC Load Case)".

Detailed technical direction was provided by the Air Force Special Weapons Center, Kirtland Air Force Base, Albuquerque, New Mexico. Major Frank Zimmermann and Mr. James O'Loughlin provided continuing direction, guidance, and support. The program manager at AiResearch was Mr. T.E. Brown. Principal investigators and contributors on technical activities at AiResearch were: Dr. C.H. Lee, Mr. D. Berker, Mr. G. Tatro, and Mr. P. Walia.

CONTENTS

ILLUSTRATIONS

ILLUSTRATIONS (Continued)

TABLES

SECTION 1

OBJECTIVES AND APPROACH

This addendum report documents the final activities on Contract F29601-74-C-0055 consisting of alternator test and computer modeling activities accomplished in accordance with: (1) the Air Force Statement of Work (Purchase Request FY3592-75-10147, Amendment No. 2 to Statement of Work for Purchase Request FY3592-74-10084), and (2) the technical approach and program specified in AiResearch proposal 75-11176, dated January 28, 1975.

The primary objective of this work was to demonstrate and verify the alternator analytical methods and techniques utilized to attain the full-scale, large-rating, lightweight alternator designs previously conducted and described in the preceding reports on Contract F29601-74-C-0055.[1,2]

A secondary objective of this work was to demonstrate the ac resonant loading concept. Meeting these two objectives involved correlation of results from an experimental (test) activity and a companion computer modeling and analytical activity. Achieving thorough quantitative definition of the alternator that was tested and modeled, and realizing complete and accurate dynamic modeling methods that simulated actual tests, were of paramount importance in meeting the primary work objective.

The technical approach used to accomplish the above objectives consisted of the following major tasks:

(a) Analyze an existing small rating test alternator; determine needed modifications to simulate the previously designed full-scale alternator hardware configuration and operating characteristics, and, as the final step, quantitatively define the modified alternator.

(b) Modify the small rating alternator per the final step in (a) above and construct a special loading and control circuit.

Reference 1: AFWL-TR-75-66, Subsystem Design Analysis Report for Lightweight Alternator (ac Load Case)

Reference 2: AFWL-TR-75-66, Addendum 1, Subsystem Design Analysis Report for Lightweight Alternator (dc Load Case)

(c) Test the modified alternator in combination with the special loading circuit under specified transient load conditions to experimentally determine the alternator characteristics.

(d) Construct a simulation model of the modified alternator and the specialized load circuit using the Air Force SCEPTRE transient analysis computer program. Quantitative basis for the alternator model was the design description obtained as the final step in (a) above.

(e) Using the model developed in (d) above, analytically determine the alternator performance under the specified transient load conditions and compare these results with the actual alternator test results obtained from (c) above.

The small-scale alternator used was an existing and available 6-kva, 400-Hz, 12,000-rpm (4-pole), 120/208-v, self-excited laminated salient pole rotor aircraft type of machine. Basic modifications made to the machine consisted of:

(a) Constructing a replacement solid nonsalient pole rotor for the machine, closely simulating the rotor configuration selected for the full-scale machinery previously designed under Contract F29601-74-C-0055.

(b) Providing direct excitation of the machine by removing and replacing its self-excitation provisions.

(c) Adding to the machine instrumentation needed to monitor key test information.

The modified machine design description was established using the AiResearch digital computer design program ROUND, which also was used to develop the previous full-scale alternator designs. The replacement rotor designed and constructed was a solid-core, nonsalient pole, distributed-winding configuration without rotor amortisseur provisions (i.e., the same basic configuration selected for the full-scale designs). The design constants developed using ROUND were, as noted above, utilized in the later computer modeling and transient behavior simulation activities.

The modified alternator first was separately tested for basic characteristics and performance using procedures similar to those defined in the IEEE No. 115 Test Procedures for Synchronous Machines. This testing included

determination of saturation characteristics, design point verification, and definition of key machine reactances and constants for comparison with those developed for the design by the ROUND analytical program.

A specialized loading circuit and controls were designed, constructed, checkout tested, and then utilized in combination tests with the modified alternator to obtain actual transient performance of the machine. An original objective for this loading circuit was to demonstrate the ac resonant loading concept at precise resonance conditions. This specific objective was not met; however, the machine was tested at two off-resonance conditions.

Two different transient analysis computer programs (i.e., SCEPTRE and an AiResearch program) were utilized to perform transient simulations of the alternator and specialized load. These two programs differ in solution methods but both handle the same basic mathematical model. In this model, the alternator is represented by a six-circuit equivalent, consisting of three armature, one field, one direct damper, and one quadrature damper circuit. The latter two circuits in this case represent the damping action of the solid rotor core (i.e., no discrete amortisseur or damper windings are included in this rotor).

Treatment of the SCR switching network is different in the SCEPTRE and AiResearch analysis programs. In the SCEPTRE program, the SCR's are approximated by resistors in series with the load capacitor. The resistor value is appropriately varied between two set extremes so that it has a value near zero ohms when the capacitor is charging, and a high value (e.g., 10,000 ohms) when the capacitor is maintaining or discharging. In the AiResearch program the SCR is directly treated as a switch that may be set open or closed.

Modeling treatment of the effect of the magnetic saturation on the model's inductive values is also different in these two programs. Inherently, the SCEPTRE program requires that the inductance matrix be symmetrical. This is not a prerequisite in the AiResearch program. The numerical method of solution used in the AiResearch program is a modified or improved Euler's technique. The SCEPTRE program can utilize any one of three explicit integrating techniques: Runga-Kutta, trapezoidal, or XPO technique. The latter has been utilized in conducting this work.

Comparison of results using these two programs shows no essential differences, that is, both programs yield identical solutions. The Euler technique utilized in the AiResearch program results in a negligible sacrifice in precision (i.e., compared with the SCEPTRE program XPO technique), which is more than offset by reduced computational and compilation time.

Overall, results of the alternator tests and computer simulations correlate very well. Load cases were established for both the test and simulation tasks, involving initiation from steady-state operating conditions on the alternator and loading circuit of various field, load, and fault conditions. For example, partial comparison of percent deviation of analytical with respect to experimental results for stabilized alternator phase voltage and current quantities after application of transient load cases is as follows:

Load Case	Phase Voltage, percent	Phase Current, percent
(a)	-2.8	-3.5
(b)	-12	-1.25
(c)	-7.2	1
(d)	7	-12.5
(e)	0	4

The above comparison data are taken from Figures 29, 30, 31, 32, and 34 herein and load cases referred to are:

(a) Step increase of field voltage from 30 percent to rated with full load on.

(b) Step decrease of field voltage from rated to 30 percent with full load on.

(c) Initiate no load to full load at rated field voltage.

(d) Single-phase, line-to-neutral sudden short circuit from rated load at rated field voltage.

(e) 3-phase to ground, sudden short circuit from rated load at rated field voltage.

Based upon the results obtained in this work, it is concluded that the AiResearch alternator design program ROUND does develop machine saturation data, resistances, and constants that may be utilized confidently to predict alternator transient behavior. Furthermore, it is concluded that the alternator dynamic modeling and simulation mode, using either the SCEPTRE or the

AiResearch computer programs, does give valid and resonably accurate results compared with actual test.

SECTION II

DESCRIPTION OF REQUIRED ALTERNATOR MODIFICATIONS

The alternator selected for use in this work was a 6-kVA aircraft type, originally manufactured by Leland Corporation and designated AGH 329-3. This unit was selected primarily because of its small kVA rating (which minimized overall size and rating requirements for the test circuit) and because it was readily available. Modifications to the machine were needed to make its configuration similar to the full-scale machine designed under Contract F29601-75-C-0055; however, a condition for using the machine was that it would be restored to original condition at the conclusion of the work.

The basic machine modification was the use of a solid rotor of nonsalient pole (distributed winding) configuration to replace the original laminated salient pole (nondistributed coil) rotor structure. The shaft bearing journals of the rotor were made wide enough to allow interference fit rings to be pressed on the bearing journals to permit loading the bearing races. The original rotor had a center bore with a drive shaft extending the length of the rotor shaft so that the thrust bearing inner races could be preloaded by torque applied to a bolt located at the threaded end of the shaft, but with the inclusion of slip rings on the replacement nonsalient pole rotor, a center-bore design could not be used.

Slip rings and a brush setup were added to allow the field voltage and current to be directly monitored under the transient conditions of test. Since the alternator is a brushless design that has a built-in exciter machine, no space was available to incorporate the brush-holder assembly inside the stator housing without major modification to the stator assembly. The slip ring/brush assembly was therefore located opposite the driving end of the alternator and was sized so that the ring would pass through the inner race of the bearings. The ring assembly extended externally past the end of the stator housing. The brush-holder assembly was bolted onto the end of the existing stator housing. Leads connecting the slip ring to the field circuit passed along a slot cut in the shaft under the bearing inner race. These modifications allowed the existing stator to be used without major structural or electrical changes.

The final modification was the addition of an air-gap voltage search coil to the armature. The coil was wound in the first slot of the phase belt for one phase. Two coils were wound in this manner for two different phases. The second coil was redundant and was to be used only if the first coil malfunctioned. The coil is shown installed in Figure 1.

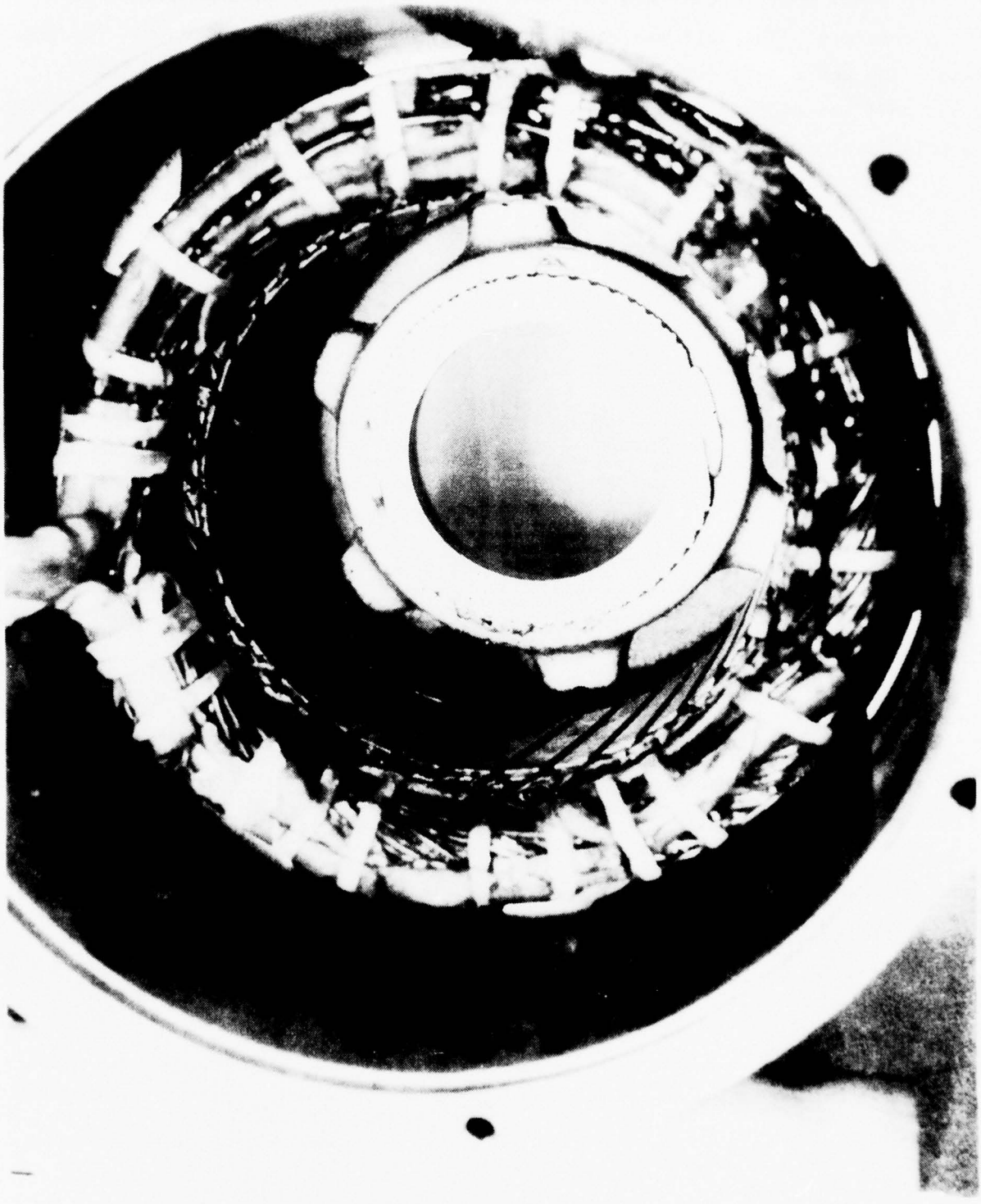

Figure 1. Air Gap Voltage Search Coil Installed in Stator

SECTION III

ALTERNATOR DESIGN

Use of an existing stator without winding or other modifications placed inherent restrictions on the attainable reactances of the machine. (The only modification made in the stator element was the addition of an air-gap voltage search coil.) Machine reactances are used to determine the inductances for the analytical model and many of these are functions of the stator geometry and design (e.g., tooth thickness, slot dimensions, end turn length and extensions, winding turns, etc.); however, basic changes do result in machine subtransient and transient reactance quantities due to the rotor replacement made. With careful consideration in design of the field circuit and slot winding, the solid-core rotor without squirrel cage damper in the rotor slots does to some degree increase these reactances.

The selection of rotor material required a steel possessing good magnetic characteristics, that is, capable of 70 to 90 kilolines average rotor tooth flux densities without severe saturation and with reasonable structural properties. The steel selected was 4130, which exhibits good saturation characteristics with good mechanical capability, is readily available, and requires no special material handling, tools or fixtures, or special heat treatment.

The original machine was examined in detail to determine dimensions, stator winding parameters, etc. AiResearch computer program ROUND was then utilized to develop the machine design including optimization of the new solid-rotor configuration. Basic alternator performance data also were predicted by ROUND, including the no-load, full-load, and short-circuit saturation data shown in Figure 2. The major parameters for the resulting modified design are summarized in Table 1.

AGE 2604

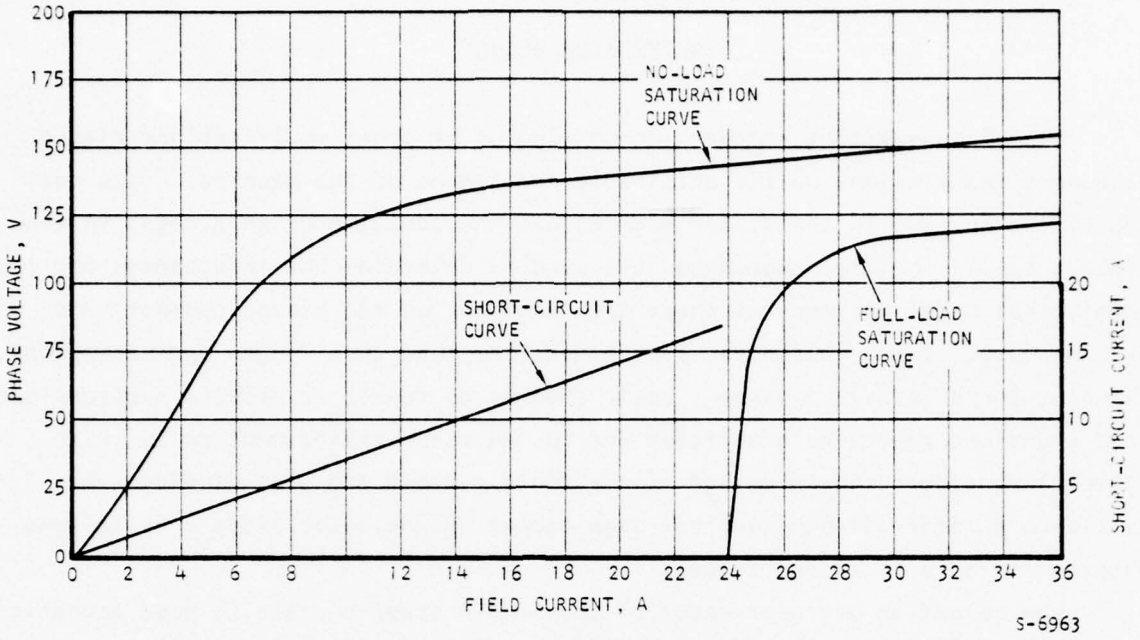

Figure 2. Computer Result for No-Load and Full-Load (Constant Rated Current) Saturation and Short-Circuit

TABLE 1

MAJOR PARAMETER SUMMARY OF MODEL ALTERNATOR

Stator Input Data		
Symbol	Definition	Quantity
VBASE	Base phase voltage	115.0
ABASE	Base phase amperes	17.4
PHASE	Phases	3.0
POLES	Poles	4.0
AI	Stator stack length, in.	1.625
D	Stator bore, in.	3.63
DSTAK	Stator OD, in. (either BETAC or DSTAK must be 0.0)	5.66
G	Air gap, in.	0.015
Y	Coil span, teeth or per unit	8.0
Q	Total number stator slots	36

TABLE I (Continued)

Stator Input Data		
Symbol	Definition	Quantity
TOLH	Slot stacking tolerance, height, in.	0
TOLW	Slot stacking tolerance, width, in.	0
C	Number of parallel circuits	1.0
CTHK	Round or rectangular strand height over insulation, in.	0.04
CWIDT	Rectangular strand width, in. (set 0.0 for round wire)	0
CHORI	Number of horizontal strands per slot (set 0.0 for round wire)	0
CVERT	Number of vertical strands per slot (set 0.0 for round wire)	0
CONDS	Number of conductors per slot	12.0
STRDS	Number of strands per conductor	2.0
ASTR	Net sq in./strand	0.00102
BO	Slot opening, in.	0.08
BT	Tooth width (BT = 0 except for straight tooth)	0.12
BI	Slot width, in. (BI = 0 for straight tooth or rectangular wire)	0
HO	Height of BO, in.	0.02
HT	Height of taper, in.	0.02
HW	Height of wedge, in.	0.03
TLINR	Thickness of slot liner, in.	0.015
TMID	Thickness of slot middle stick, in.	0.015
RNUM	Quotient of Q/poles/phase	3.0
SCU	Slot fill factor	0.24
SFE	Stacking factor	0.94
EMU	Current distortion factor (=1.0 for sine current)	1.0
TSKEW	Slot skew, in.	0.317
BETAC	Desired stator core flux density, kilolines/sq in.	0
TEMPS	Stator temperature, ^{o}F	350.00
CMODE	Alternator (0.), Motor (1.)	0
VENT	Total length of stack vents, in.	0
DENIR	Density, stator and rotor iron, lb/cu in.	0.276

TABLE 1 (Continued)

Stator Input Data		
Symbol	Definition	Quantity
BIRON	Flux density, kl/in^2	77.0
FIRON	Frequency, Hz	400.0
PIRON	Iron Loss, Watts/lb	10.0
	Rotor Input Data	
RS1	Rotor slot grip height, in.	0.06
RS2	Rotor slot wedge height, in.	0.02
RS3	Rotor slot damper height, in.	0.
RS4	Rotor slot liner thickness, in.	0.02
RS5	Rotor slot cushion height, in.	0.
RS6	Rotor conductor insulation thickness, in.	0.001
RS7	Rotor conductor height, in.	0.05
RS8	Rotor bottom stick height, in.	0
RS9	Rotor conductor width, in.	0.1
RSW	Rotor width, in.	0.14
SFCU	Slope and tolerance for slot height, in.	0.
QW	Number of wound slots per pole	6.
QV	Number of vent slots per pole	0.
QTAUP	Number of rotor slots if all slots were punched	8.
SFPOL	Rotor LAM factor	1.
CONDF	Number of field conductors per slot	12.00
CONCU	Net sq in./field conductor	0.004
DRI	Rotor ID, in.	0.0001
ROTRL	Rotor axial magnetic length, in.	1.85
EXTRV	Field extension for venting, in.	0.0
BENDR	Field conductor bend radius, in.	0.25
TEMPF	Temperature of field copper	350.00
PFWI	Friction and windage at FIRON. watts (set = -1. to calculate power loss due to friction)	-1.00
FSTRA	Percent stray loss at ABASE, percent	1.00
PPOLI	Pole head loss at FIRON	21.00

TABLE 1 (Continued)

Rotor Input Data		
Symbol	Definition	Quantity
Derived Constants		
GE	Equivalent gap, in.	0.0177
DR	Rotor diameter, in.	3.6
BI	Slot width, in.	0.2036
HI	Slot height above wedge, in.	0.3776
HS	Total slot height, in.	0.4474
KR	Carter's coefficient for rotor slots	1.34
ACOND	Copper area for a stator conductor, sq in.	0.0020
EXT	Stator coil extension, in.	1.64
ELE	Length of conductor length	4.67
ELC	Stator conductor length	6.296
TAUP	Pole pitch at D, in.	2.85
TAUS	Stator slot pitch at D, in.	0.317
TAURO	Rotor slot pitch at DR, in.	0.353
RSD	Rotor slot depth, in.	0.751
AVCON	Average length of a field conductor	3.64
CM	Demagnetizing factor	1.00
CP	Field form ratio, average/maximum	0.528
CF	Field self-linkage factor	0.435
CI	Fundamental flux factor, peak fundamental/peak total	0.866
SCU	Stator slot fill factor	0.24
TALPF	Temperature factor, field	1.61
TALPS	Temperature factor, stator	1.61
RA	Resistance per phase at TEMPS, ohms	0.4883
RF	Field resistance, all coils and poles in series at TEMPF, ohms	0.2881
TPDO	L_F/R_F = open circuit time constant, sec	0.0687
WKP	Pitch factor, stator winding	0.985
WKD	Distribution factor, stator winding	0.959
WKS	Skew factor, stator slot	0.995
WKPDS	Product of WKP, WKD, and WKS	0.9404
YLAME	Specific permeance, stator end coils	10.24

TABLE 1 (Continued)

Rotor Input Data		
Symbol	Definition	Quantity
ELF	Field inductance, henries	0.0198
YLAMA	Specific permeance, gap	327.
YLAMI	Specific permeance, stator slot	3.34
SLAMR	Specific permeance, rotor slot	4.2
ELAMR	Specific permeance, rotor end faces	1.1
RLAFE	Specific permeance, field end coils	5.9
DLAMD	Specific permeance, damper slot	3.8
RLAME	Specific permeance, damper end coils (double layer, full cage)	5.9
FBS	Barne's factor, stator	2.4
FBF	Barne's factor, field	1.9
FBD	Barne's factor, damper	1.54
FKS	Barne's factor, stator	1.0
FKF	Barne's factor, field	0.7
FKD	Barne's factor, damper	0.89
ABI	Stator core area, net sq in.	0.55
HC	Stator core, height, in.	0.5674
DSTAK	Stack, OD, in.	5.66
DENEM	WTOT x 0.785 x $DSTAK^2$ x AI	0.3
WCORE	Stator core, weight, lb	3.83
WFLD	Field copper weight, lb	1.4
WROIR	Rotor iron weight, lb	4.00
WSCU	Stator copper weight, lb	2.44
WTETH	Stator teeth weight, lb	0.9
WTOT	Total electromagnetic weight, lb	12.
Load Condition		
VPU	AC volts, PU	1.
APU	AC current, PU	1.
PF	Power factor	-1.
RPM	Revolutions per minute	12000.
EFF	Efficiency, PU	0.803
Volts	Phase voltage	115.

TABLE 1 (Continued)

Load Condition		
Symbol	Definition	Quantity
AMPS	Phase current	17.4
KVA	KVA rating	6.
FREQ	Frequency, Hz	400.
KW	Load, kW	6.
	Variable Derived Parameters	
AMPSF	Field current, A dc	29.2
CHI	Reactance factor	0.0137
DENFD	Current density, field	7301.
DENST	Current density, stator	8529.
ELOAD	Electrical loading, A-conductor/in.	619.
HEATF	ELOAD x DENST	5.3×10^{6}
PHILK	Field leakage flux per pole, kilolines	8.7
PHIPL	Air gap flux per pole, kilolines	100.
QUALF	kVA/lb/rpm	4.5×10^{-5}
RAPU	RA/Z base, per unit ohms (hot)	0.074
TA	Armature time constant for the dc component, $X_2/2$ FRAPU, sec	0.0012
THETA	Power factor angle, radian	0.
TPO	Transient time constant, sec	0.0055
ZBASE	Base resistance, ohms	6.6
BROOT	Flux density at root of rotor tooth next to pole center, kilolines/sq in.	127.
BETAC	Flux density, stator core, kilolines/sq in.	43.
BETAG	Flux density, air gap, kilolines/sq in.	40.7
BPCNT	Flux density, pole center, kilolines sq in.	46.7
BETAT	Flux density, stator teeth, kilolines/sq in.	114.00
BETCO	Flux density, rotor core, kilolines/sq in.	28.
FCORE	Magnetomotive force, stator core, A-turns	3.4
FGAP	Magnetomotive force, air gap, A-turns	225.
FPCNT	Magnetomotive force, pole center, A-turns	29.
FTETH	Magnetomotive force, stator teeth, A-turns	142.
FROCO	Magnetomotive force, rotor core, A-turns	14.

TABLE 1 (Continued)

Variable Derived Parameters		
Symbol	Definition	Quantity
FIELD	Magnetomotive force, field per pole, A-turns	1051.
FFL	Magnetomotive force, behind XP, A-turns	862.
HRC	Height, rotor core, in.	1.04
BRC	Flux density, maximum in rotor core, kilolines $in.^2$	31.
PCORE	Stator core loss, watts	31.
PFLDT	Field copper loss, watts	245.
PFW	Friction and windage loss, watts	39.
PPOLH	Pole head loss, watts	665.
PSCU	Stator copper loss, watts	443.
PSTRA	Stray load loss, watts	3.5
PTETH	Stator teeth loss, watts	47.
PTOT	Total loss, watts	1476.
XAD	Direct armature reaction, PU	3.84
X2	Negative sequence reactance, PU	0.219
XD	Direct unsaturated synchronous reactance, PU	4.028
XDDL	Direct damper leakage reactance, PU	0.0266
XO	Zero sequence reactance, PU	0.085
XF	Field leakage reactance, PU	0.195
XL	Stator leakage reactance, PU	0.184
XPD	Direct transient reactance, saturated, PU	0.323
XPDU	Direct transient reactance, unsaturated, PU	0.367
XPPD	Direct subtransient reactance, PU	0.210
XDQ	Quadrature damper reactance, PU	3.35
XDQL	Damper quadrature leakage, reactance, PU	0.0449
XPPQ	Quadrature subtransient reactance, PU	0.228
TPPD	Direct subtransient time constant, sec	0.00525
XAQ	Quadrature armature reaction, PU	3.31
XQ	Quadrature synchronous reactance, PU	3.49
XDD	Direct damper reactance, PU	3.87
XPQ	Quadrature transient reactance, PU	0.2286

SECTION IV

ALTERNATOR FABRICATION, ASSEMBLY, AND TEST SETUP

Figure 3 shows the replacement rotor after milling slots. The smallest diameter shaft extention was later knurled to retain the slip ring assembly. The slotted diameter is the bearing journal through which the lead connecting the slip rings to the field circuit is passed. On the opposite end of the core the long shaft extension carries the drive end bearing and drive coupling provisions. This area of the shaft in the original brushless (salient pole) rotor held the rotating rectifier assembly armature for the main exciter.

The final assembled rotor is shown in Figure 4. The slip ring assembly is shown fitted to the rotor. The slip rings were separated and insulated from the rotor shaft by Astrel 360 (polyarylsulfone) plastic, which is a good dielectric that provides mechanical stability and strength and high-temperature capability.

A 0.010-in.-thick slot liner of Nomex-Kapton-Nomex (NKN) insulator was used to insulate the pole turns from the rotor core. Each turn consisted of two parallel No. 16 AWG round magnet wires having polyamide-imide insulation meeting Class 220 (220°C continuous) thermal rating. To achieve the maximum slot fill factor, the turns of two No. 16 wires were laid side by side in the slot without crossovers. As each coil was completed the slot liner was folded over the turns and 310 nonmagnetic stainless steel top wedges were inserted to retain the coils in the slot.

After all poles had been wound, the coils on each pole were series-connected. All pole groups were then series-connected and solder-terminated to the field leads. The end turns on each pole were banded together using a prestressed fiberglass tape, and a prestressed band of fiberglass tape was then wound around the OD of all pole end turns to restrain them against centrifugal loading forces. The fiberglass tape was cured for 4 hr at 325°F. The slip ring assembly was then pressed onto the rotor shaft and the adapter for the drive coupling was copper flash-coated and press-fitted into the drive end of the rotor. All surfaces were then masked, and the rotor was vacuum impregnated in silicon varnish. The cure cycle for the varnish was 5 hr at 325°F.

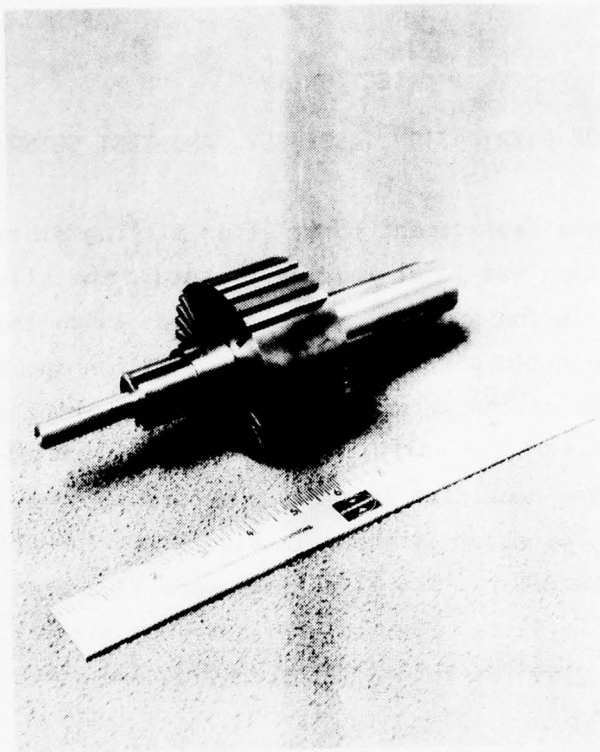

Figure 3. Replacement Rotor After Milling

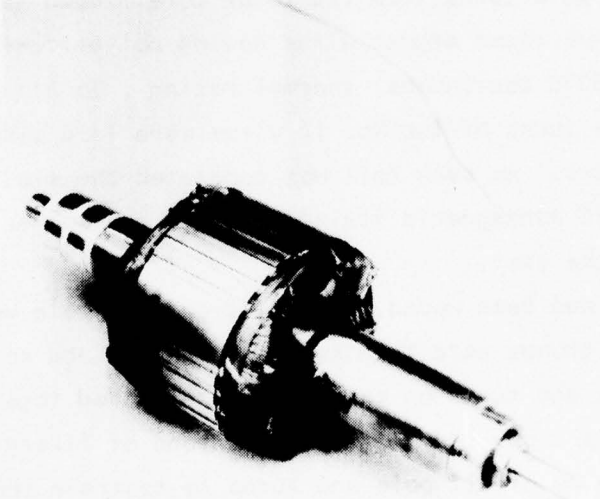

Figure 4. Completed Rotor Assembly

Insulation resistance tests were conducted at 500 vdc during the winding procedure as each coil group was completed and again at end of each cure cycle. No breakdown in rotor conductor insulators occurred. The dc resistance of the rotor winding was measured at completion and was 0.195 ohm at 70°F.

The completed rotor assembly was balanced including bearings. Balance was accomplished by drilling and grinding away rotor core and shaft material. A final unbalance tolerance of 0.003 in.-oz was achieved.

The rotor was placed in the stator after installing the stator search coils. The two end bearing race loading rings were interference-fitted on the shaft, and bearing inner races were loaded by pressing from both ends of the alternator. The machine was then reassembled and the brush-holder assembly containing four electrographitic brushes of 0.5 in. by 0.25 in. surface area was bolted to the stator housing. Brushes were contoured to the slip ring surface by means of fine sand paper placed on the slip ring while slowly rotating the shaft. Care was taken to remove any remaining abrasive material from the slip ring and brush holder. The assembled structure was then coupled to the electrical dynamometer as shown in Figure 5.

The alternator was driven by the electrical dynamometer, which was structurally connected to it by means of the alternator end bell flange bolts. The power output of the dynamometer is 9 hp at 12,000 rpm. The alternator shaft was connected to the dynamometer drive shaft through a specially constructed flexible shaft coupling. The alternator is a forced-air-cooled design, and cooling air was provided by a test facility air system. The cooling air was introduced through the existing ducts. Stator output power and field leads (from the brush assembly) were connected to Jones strip connectors located on a metal plate bolted to the alternator mounting base. This allowed easy removal and change of test leads during the test. Temperature sensors and the voltage search coils incorporated into the stator housing also were terminated on the Jones strip connector.

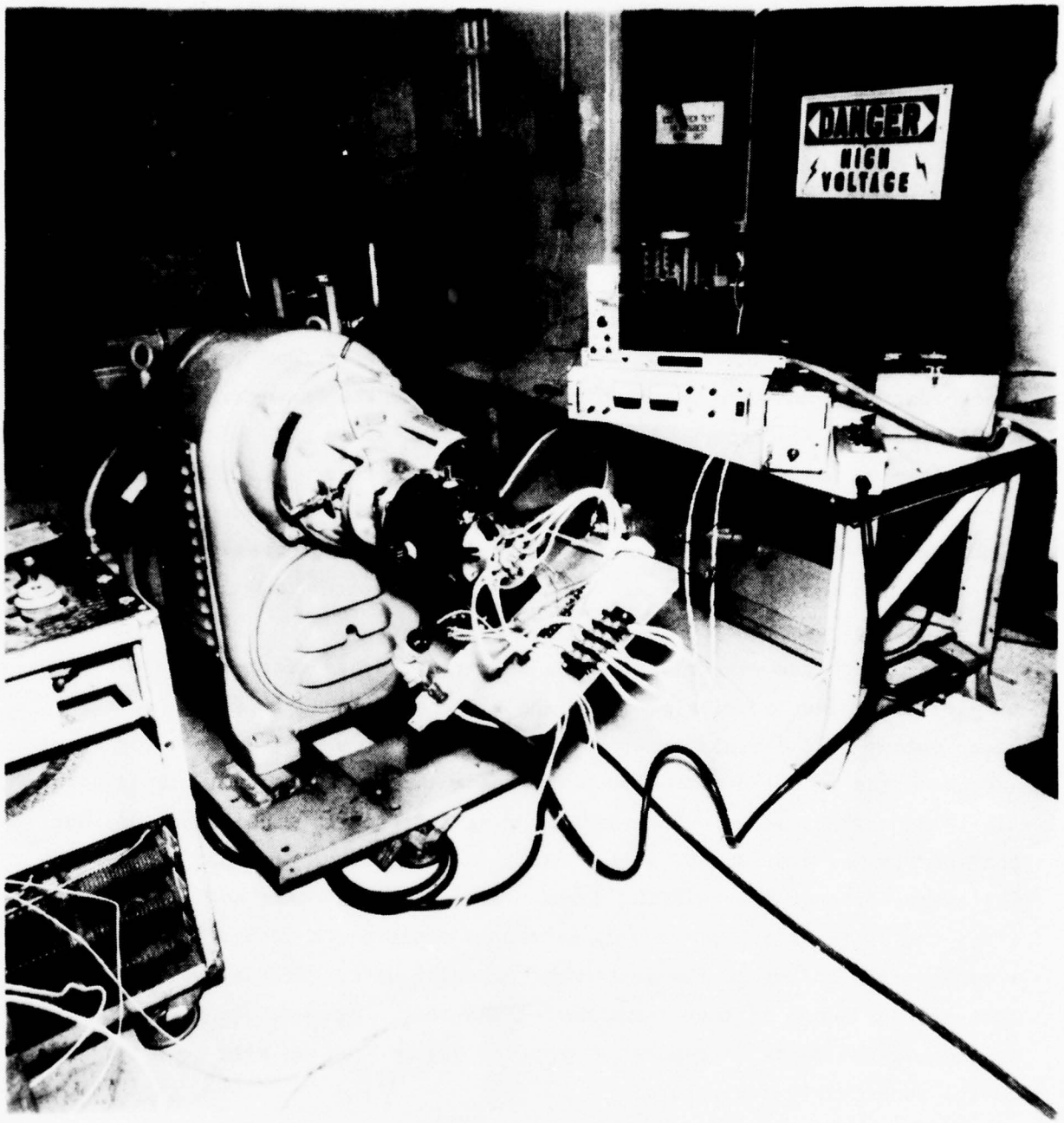

Figure 5. Assembled Alternator Coupled to Dynamometer

SECTION V

TEST CIRCUIT DESCRIPTION

Figure 6 is a schematic of the alternator loading circuit constructed. Each of the three phases of the alternator was connected to four capacitors (12 total) arranged so that the two capacitors on the positive half cycle and two capacitors on the negative half-cycle of each phase were charged. The charging of the capacitors was sequential and was controlled by turning the SCR's on or off at proper intervals. The gate firing logic circuit for each SCR determined its on or off state. There were 12 charge SCR's (Q1C-Q12C) and 12 discharge SCR's (Q1D-Q12D).

The gate firing logic was designed so that each charging SCR was turned on once in two full cycles, and the SCR stayed on for one-half cycle. In a similar manner, each discharge SCR was turned on once in two cycles, and stayed on for approximately one-third cycle.

Figure 7 shows the capacitor charge and discharge currents at ideal (resonance) conditions. The resonant charging frequency is determined by the capacitance and effective phase inductance value of the alternator. The discharge period of the capacitor was determined by the RC time constant of the capacitor and load resistor adjusted to allow five RC time constants for the total discharge of the capacitor in the one-third cycle time period.

The actual test parameter component values for the resonant load capacitors and the load resistors are listed in Table 2.

Figure 8 is a block diagram for the load firing control circuit of Figure 6. The following functional description explains the control from the input of the air gap search coil voltage to the outputted sequential firing of the charge and discharge SCR's.

The Frequency Reference Generator--The alternator search coil provides a sync signal, that is, the air gap voltage to the frequency reference generator. The sync signal is then phase-displaced 180 deg to eliminate noise. The phase-displaced signal generates a square wave signal whose frequency is the same as the frequency of the search coil.

Phase Lock and Clock Generator--The square wave output of the frequency reference generator is compared with a frequency feedback signal from the phase generator. This provides phase

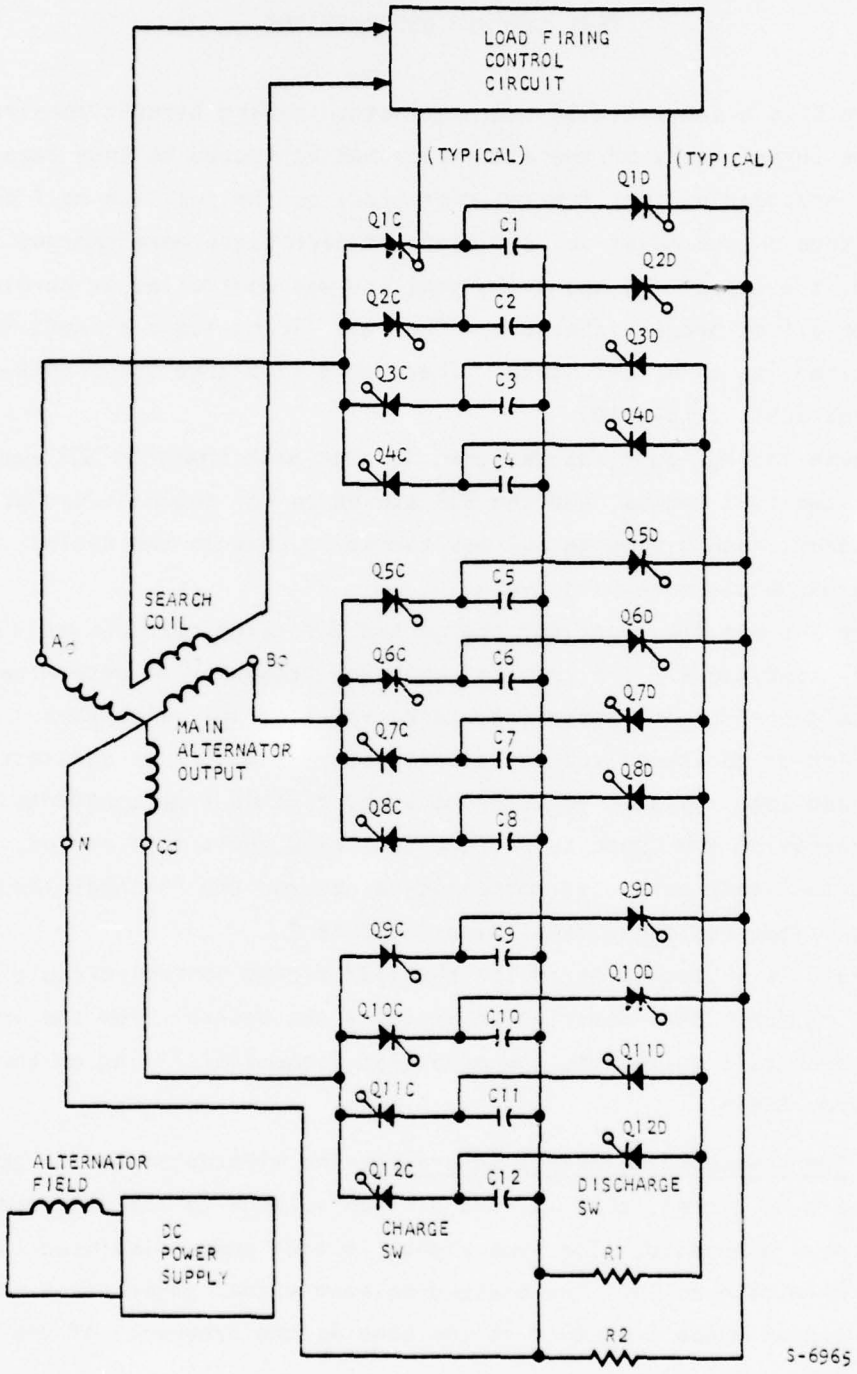

Figure 6. Alternator Loading Circuit Schematic

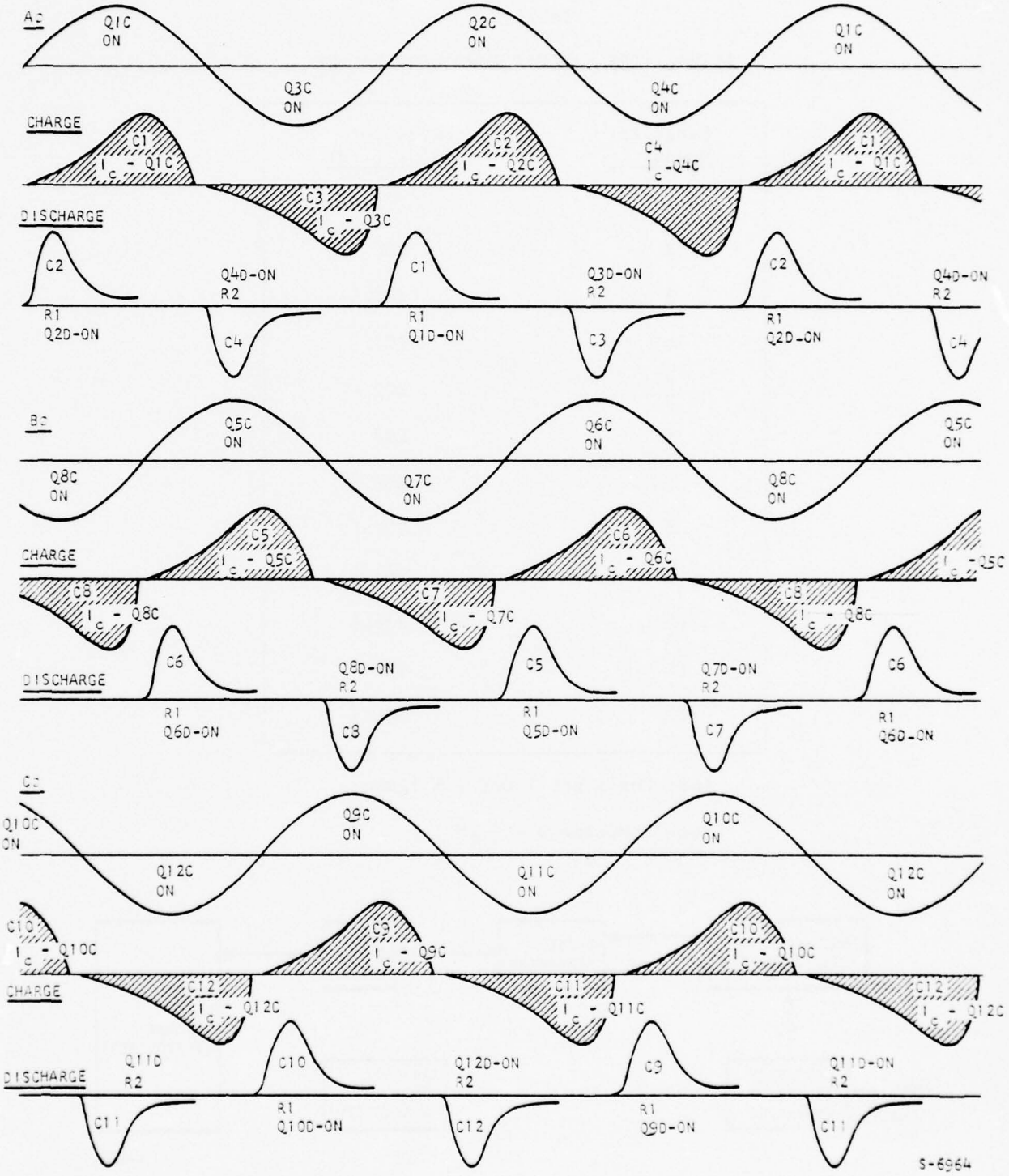

Figure 7. Sequence of Charge and Discharge Capacitor Current

TABLE 2

ACTUAL TEST CIRCUIT COMPONENT VALUES

Capacitor Number	Capacitor Value (μfd)
1	207.5
2	208
3	208.5
4	207.5
5	207
6	208
7	206.5
8	207
9	206.5
10	206.5
11	206
12	206.5

Load resistors 1 and 2 = 1 ohm

Load inductance - 8 μH

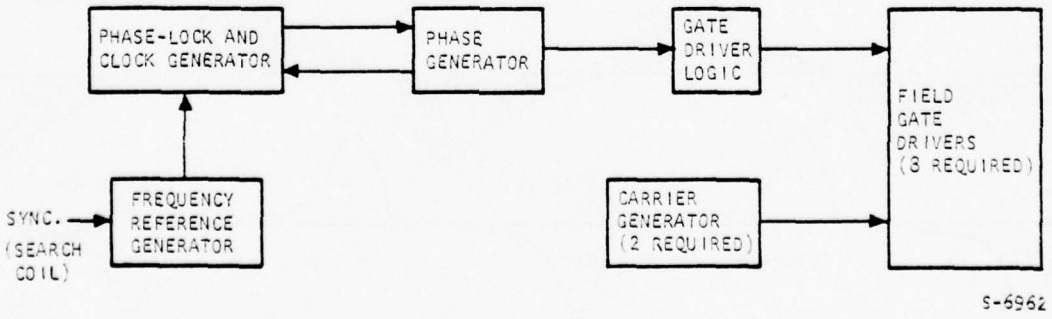

Figure 8. Load Firing Control Circuit Block Diagram

locking between the two signals and results in a clock pulse to be generated whose frequency is six times the square wave's frequency from the frequency reference generator.

The Phase Generators--The clock pulse is inputted to three flip-flops connected to provide three phase logic signals called A, B, and C, each 120 deg apart and their inverses called $\overline{A}$, $\overline{B}$, and $\overline{C}$. The A, B, and C logic signals are fed back to complete the phase lock control loop.

Gate Driver Logic--The three phase logic signals A, B, and C and the three inverted logic signals $\overline{A}$, $\overline{B}$ and $\overline{C}$ from the two phase generators are terminated into the gate driver logic to generate firing command signals to the SCR. Each phase, that is A and $\overline{A}$, provides the driver logic signal command to charge and discharge sequentially four capacitors according to the order shown in Figure 7.

Field Gate Drivers--The driver logic signals from the gate driver logic are terminated by eight field gate driver circuit cards. The drivers provide the necessary gate driver power signal to fire the SCR's. Each circuit card contains drivers for three SCR gates.

Figure 9 shows the actual test circuit layout. The SCR heat sink assembly and the logic card rack rest upon the top of the table and the capacitor bank underneath.

Figure 9. Test Circuit Assembly

SECTION VI

TEST DESCRIPTION

The test alternator program encompassed four successive tasks:

- Basic machine magnetic tests
- Determination of alternator resistances and reactances
- Tests with the load circuit under steady-state conditions
- Tests with the load circuit under transient conditions

Tests conducted to determine alternator reactances and saturation data were performed in accordance with the IEEE No. 115 Test Procedures for Synchronous Machines. Specifically these were:

Test	Test Section
Open-circuit saturation	3.05.35
Short-circuit curve	3.05.50
Direct-axis transient and subtransient	7.25.15 Method 1
Reactance test from sudden short-circuit	7.30.10 Method 1
Direct synchronous reactance	7.15
Direct and quadrature subtransient reactance	7.30.25 Method 3
Zero-sequence resistance and reactance	7.45.10 Method 1

TEST EQUIPMENT AND MONITORED PARAMETERS

The test equipment and test parameters are summarized in Table 3. Figures 10 and 11 show the test equipment physical layout including power supplies, transient recorder, and metering equipment used in the testing with the loading circuit.

BASIC MAGNETIC CHARACTERISTICS

Basic machine characteristics were obtained at (1) open-circuit, (2) short-circuit, and (3) full-load conditions. The full-load tests were performed using a constant value 3-phase resistive load. The full-load saturation curve was determined in a manner similar to that for the circuit saturation by terminating the alternator with a 3-phase resistive load, which at rated full line to neutral voltage, develops full-load phase current and power output. Test results are shown in Figure 12.

TABLE 3

TEST EQUIPMENT

Description	Manufacturer	Parameter Controlled or Monitored
Laboratory power supply	Sorenson DCR 20-1000A	Field voltage power supply
Laboratory power supply	Sorenson QR36-4A	Logic power supply
Oscilloscope	TEKTRONIX 502	Steady-state voltage and currents
Digital converter	Systron-Donner 7014	Speed
g-meter	Unholtz-Dickie Mod 8 PMCV	Vibration
Oscillograph	Consolidated Electrodynamics	Transient-state recorder of ac and dc voltages and currents
Galvonometer	Type 169	
Isolation amplifier	Neff Amplifier	
Current monitor transformer	Pearson 2025	ac current pickup
Current shunt		dc field current pickup

Figure 10. Transient Recorder, Isolation Amplifiers, and dc Power Supply Test Layout

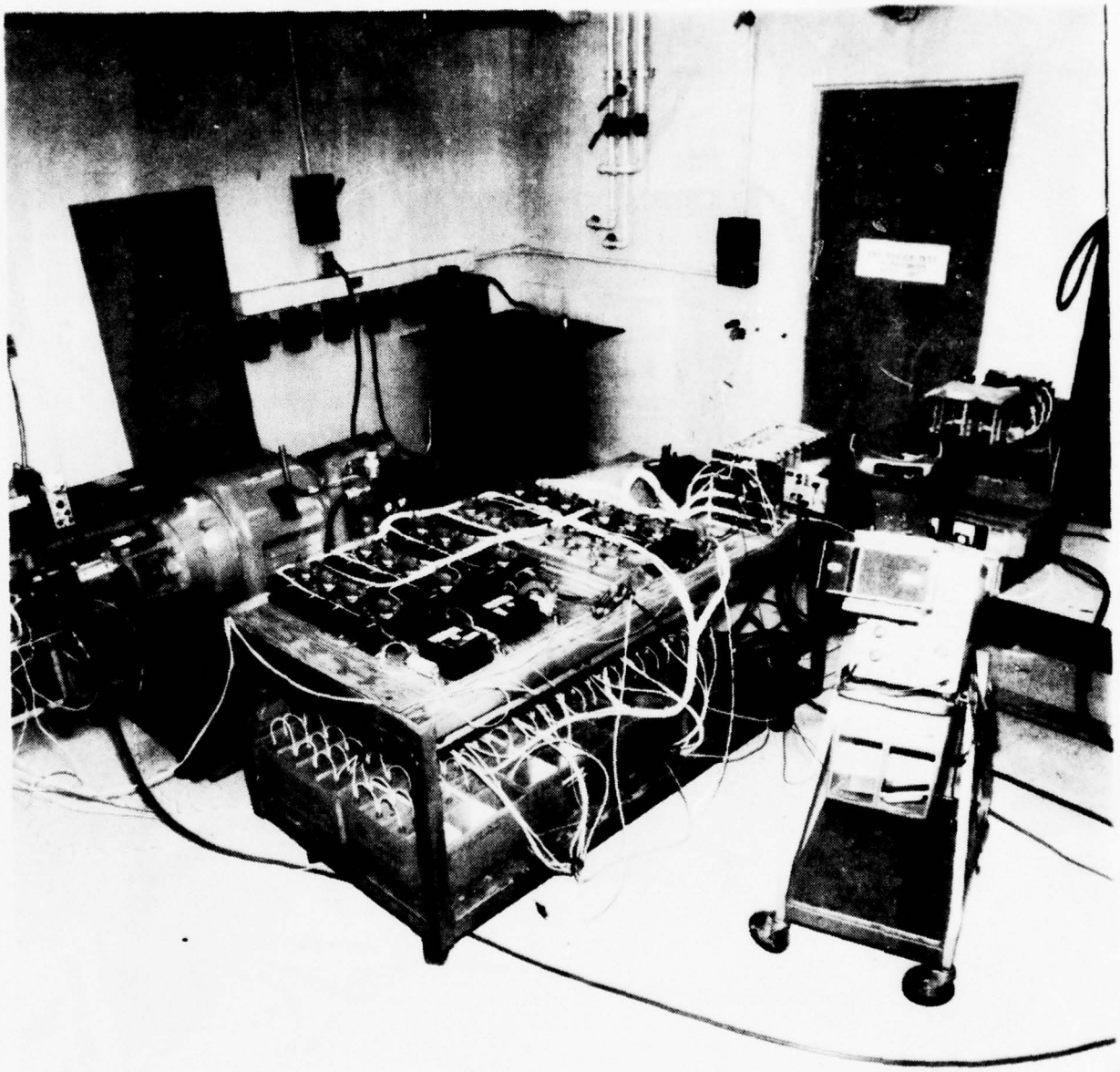

Figure 11. Completed Test Assembly

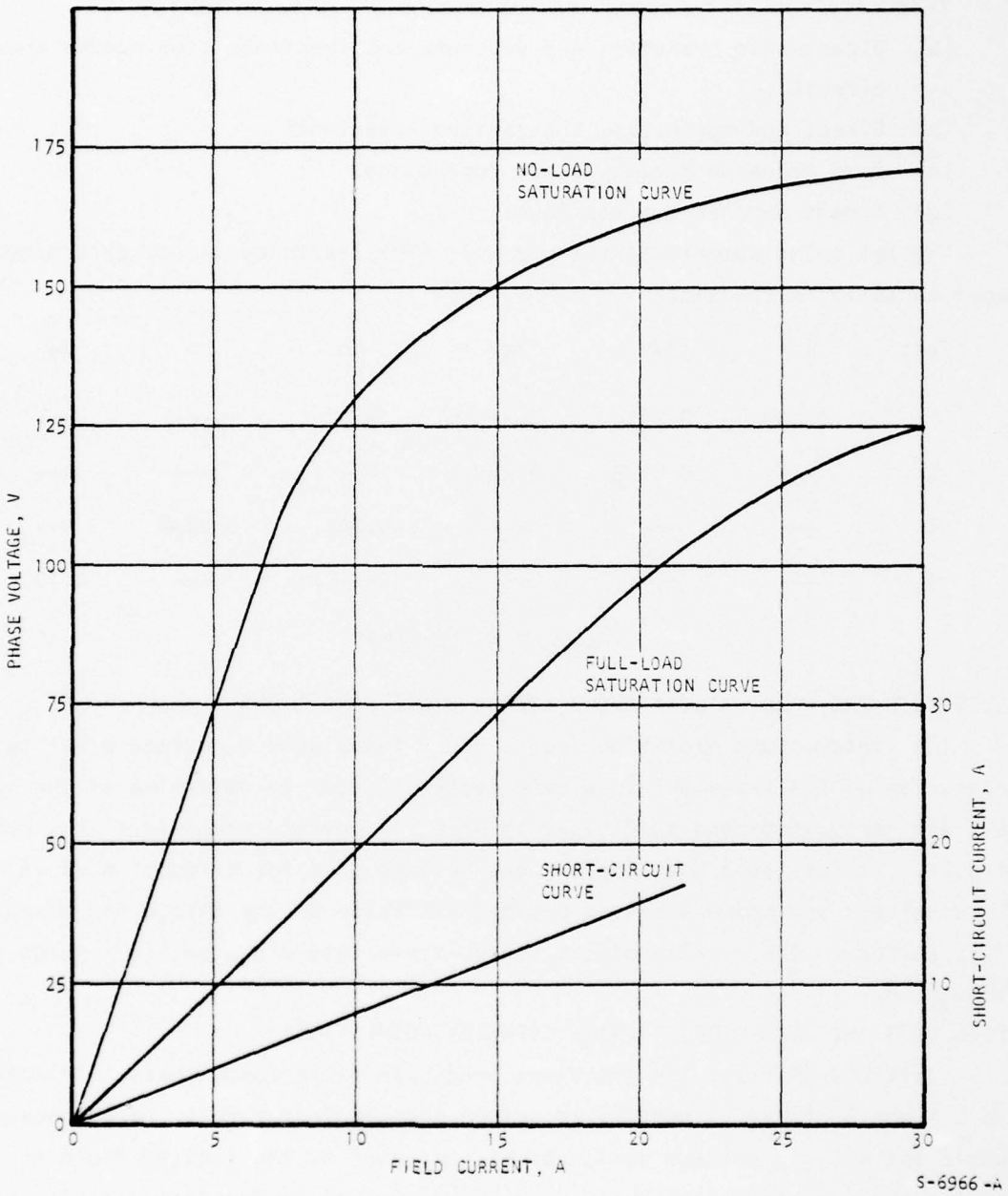

Figure 12. No-Load and Full-Load Saturation and Short-Circuit Test

TEST OF ALTERNATOR RESISTANCES AND REACTANCES

Test of alternator parameters included the following tests:

(a) Direct-axis transient and subtransient reactance from sudden short-circuit.

(b) Direct and quadrature subtransient reactance

(c) Zero sequence reactance and resistance

(d) Direct synchronous reactance

The following summarizes the per unit (PU) reactance values determined experimentally in the test:

Test	Xd'	Xd''	Xq''	Ro	Xo	Xd
1	0.449	0.201	---	---	---	---
2	---	0.2175	0.2451	---	---	---
3	---	---	---	0.0451	0.0958	---
4	---	---	---	---	---	2.72

Z_{base} = 6.609 ohms

TESTS WITH THE LOAD CIRCUIT UNDER STEADY-STATE CONDITIONS

The steady-state operation load circuit tests were conducted prior to the initiation of the transient load case tests in order to determine if the search coil air gap voltage was sufficient to properly operate the load firing control circuit. It was found that the air gap voltage used for triggering at rated field voltage and speed achieved proper initiation of the charge and discharge of capacitors. The results of the steady-state test are shown in Figures 13 through 16.

TESTS WITH THE LOAD CIRCUIT UNDER TRANSIENT-CONDITIONS

Table 4 summarizes the transient load case performance tests. In load cases 1 and 2, field voltage could not be stepped from zero to rated because sufficient air gap voltage could not be generated by the excited field to develop the sync lock feedback previously described in the test circuit descriptions. It was found that a minimum of approximately 30 percent of full rated field voltage was necessary to maintain the sync lock under a step change in field voltage.

CALIBRATION: PHASE CURRENT: 20 A/CM
PHASE VOLTAGE: 50 V/CM
TIME: 0 5 MS/CM

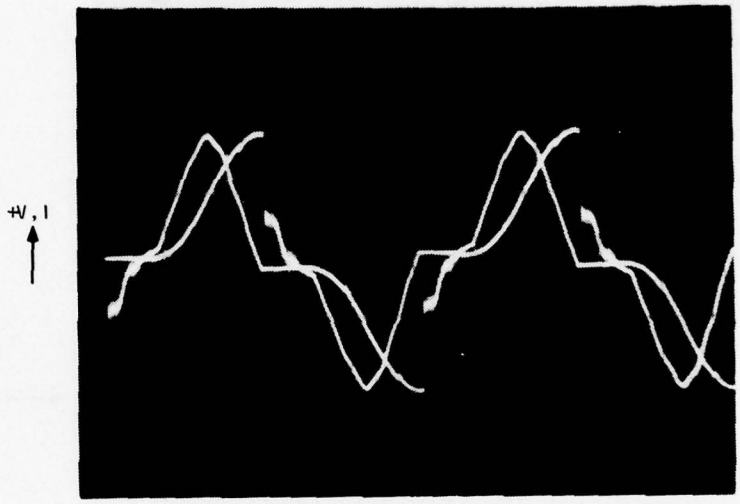

Figure 13. Alternator Phase-Voltage and Current

CALIBRATION: PHASE CURRENT: 20 A/CM
SEARCH COIL VOLTAGE: 5 V/CM
TIME: 1.0 MS/CM

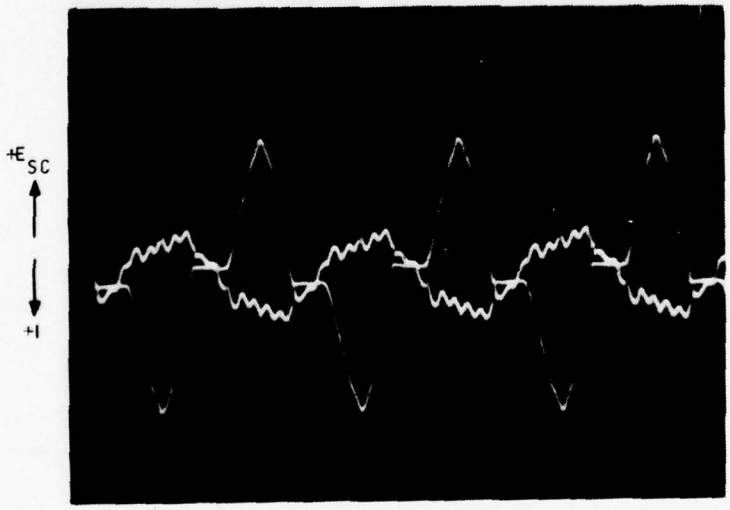

F-23736

Figure 14. Alternator Phase Current and Search Coil Voltage

CALIBRATION: FIELD CURRENT: 6 A/CM
FIELD VOLTAGE: 2 V/CM
TIME: 1.0 MS/CM

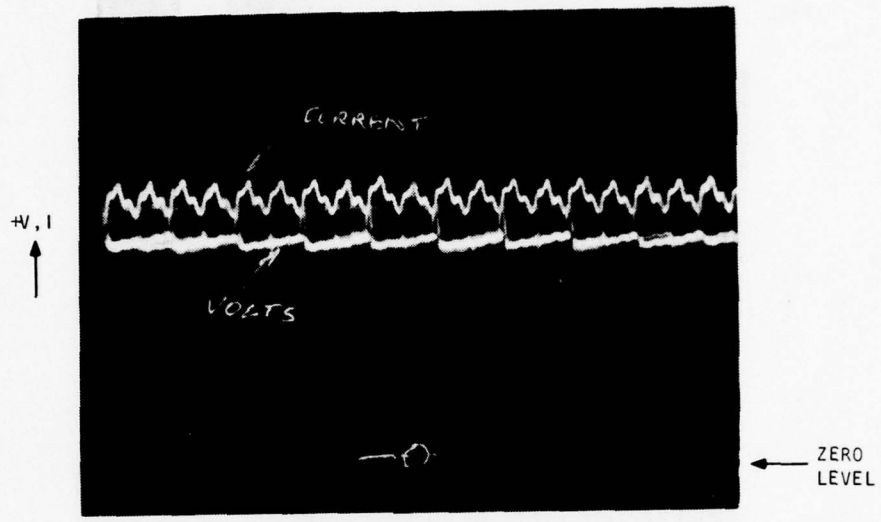

Figure 15. Field Voltage and Current

CALIBRATION: LOAD CURRENT: 20 A/CM
LOAD VOLTAGE: 20 V/CM
TIME: 0.5 MS/CM

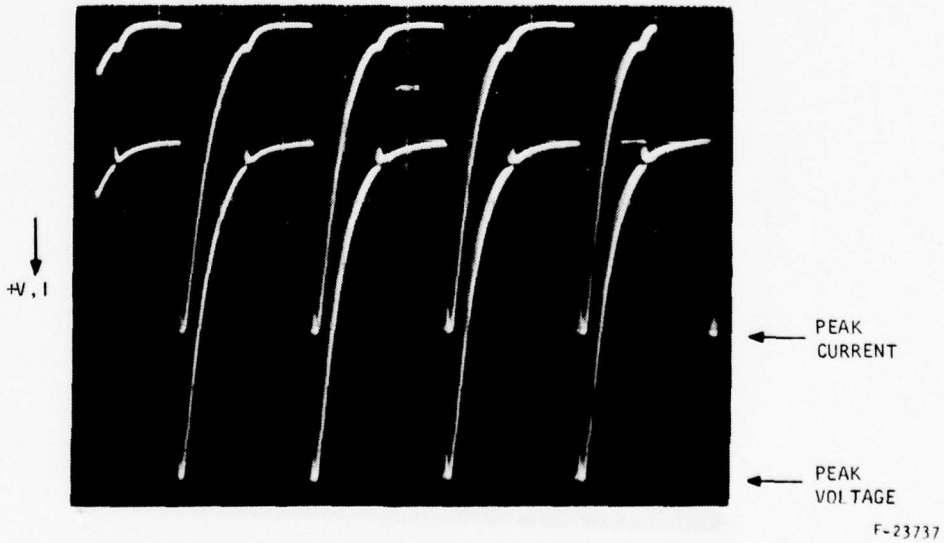

Figure 16. Load Voltage and Current

TABLE 4

LOAD CASES FOR ALTERNATOR

Case No.	Torque	Speed	Field Voltage	Load
1	Rated	Rated	Step increase from 30 percent to rated	Rated
2	Rated	Rated	Step decrease from rated to 30 percent	Rated
3	Rated	Rated	Rated	Step increase from zero to rated
4	Rated	Rated	Rated	1-phase, line-to-neutral short circuit from rated load
5	Rated	Rated	Rated	1-phase, line-to-line, short circuit from rated load
6	Rated	Rated	Rated	3-phase to ground, short circuit from rated load
7	Rated	Rated	Rated	Open-circuit from rated load, 1-phase line-to-neutral

The test results are presented in Figures 17 through 23. The calibration of the recordings is as follows:

Galvanometer Number	Parameter	Calibration
1	A voltage, line-to-neutral	260 V/in.
4	A phase current	80 A/in.
11	B phase current	80 A/in.
14	Search coil voltage	7 V/in.
15	Field current	10 A/in.
18	Field voltage	5 V/in.

Time: 0.0156 s/in.

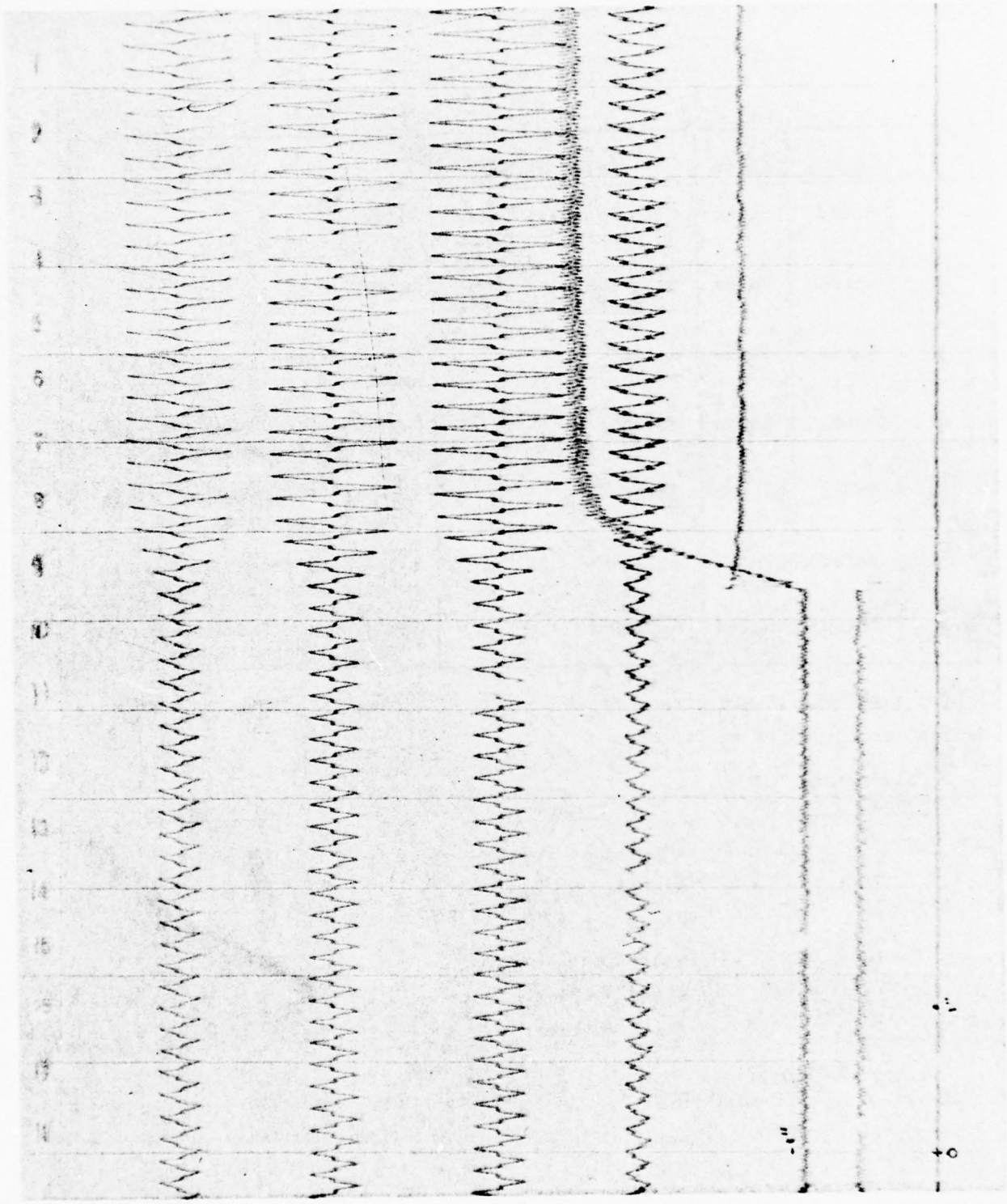

F-23749

Figure 17. Load Case 1 Transient Performance Test Results

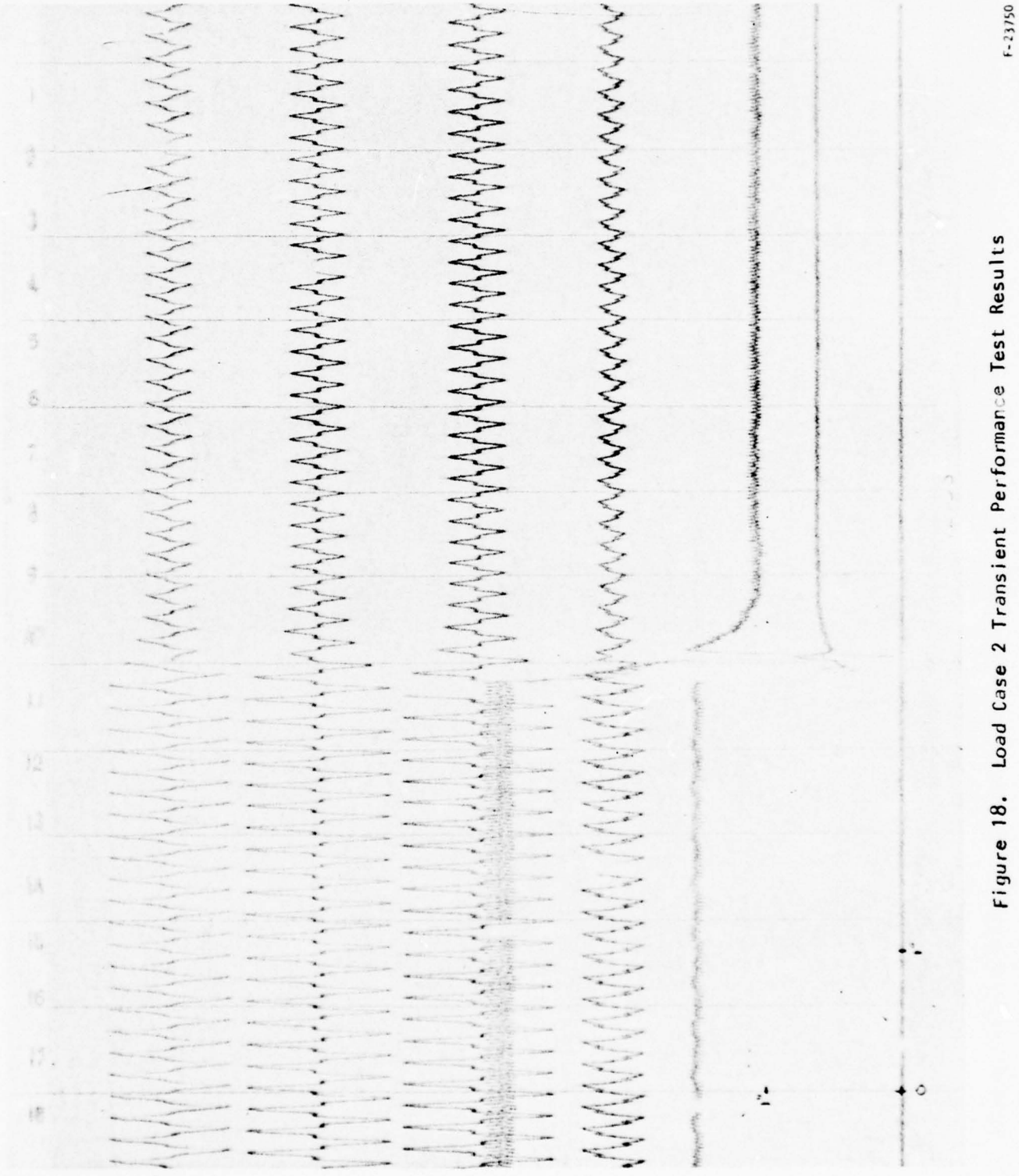

F-23750

Figure 18. Load Case 2 Transient Performance Test Results

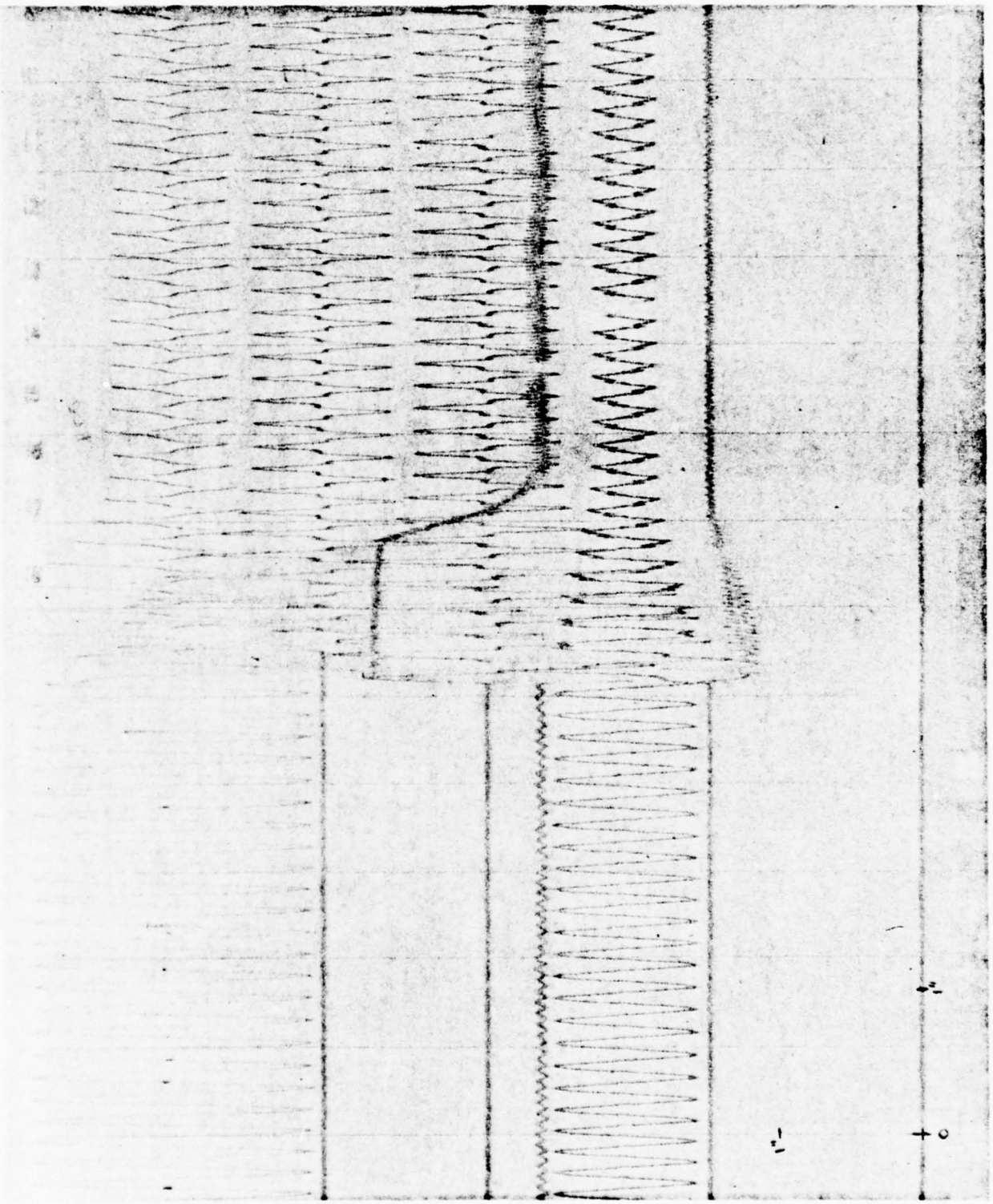

Figure 19. Load Case 3 Transient Performance Test Results

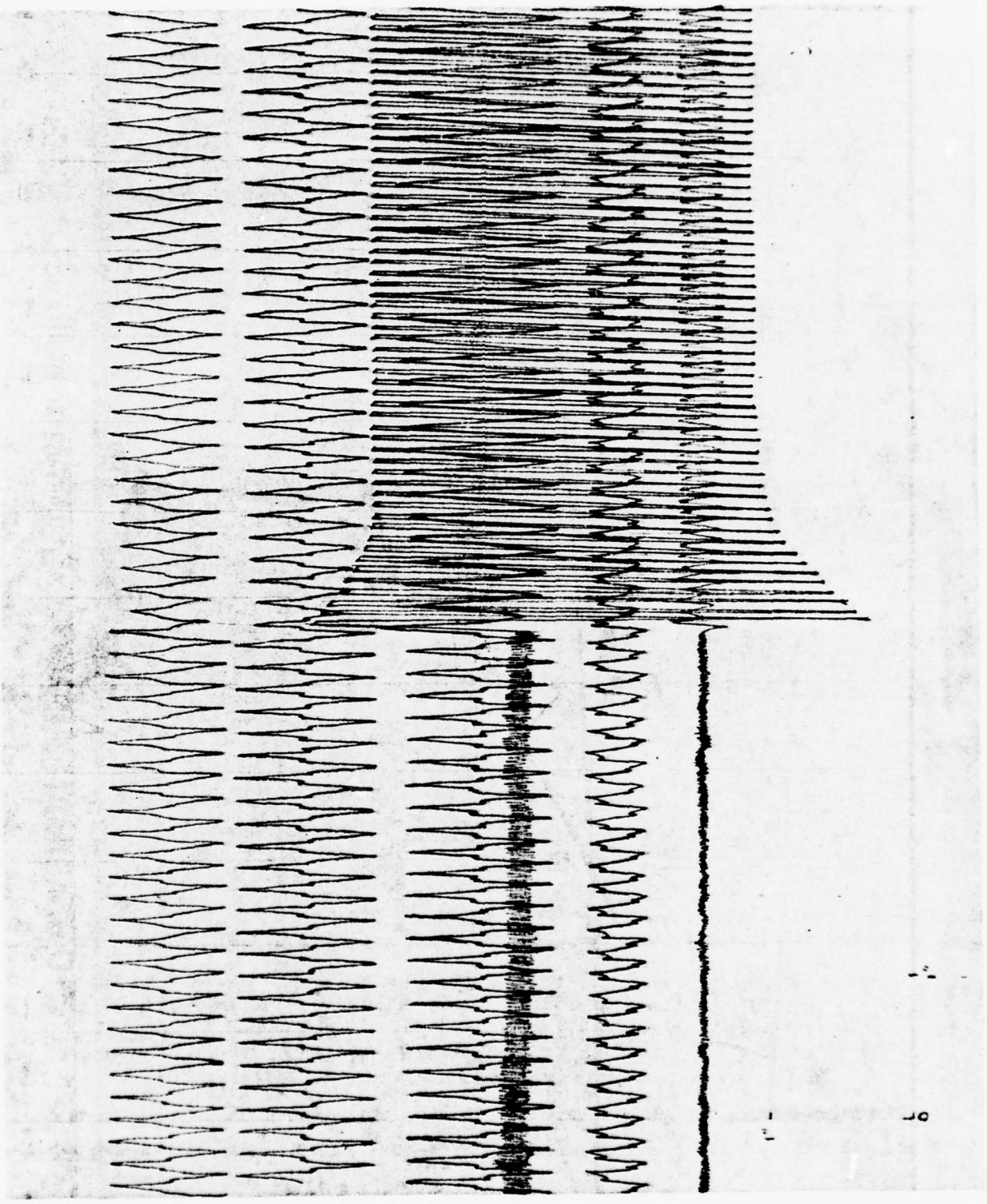

F-23751

Figure 20. Load Case 4 Transient Performance Test Results

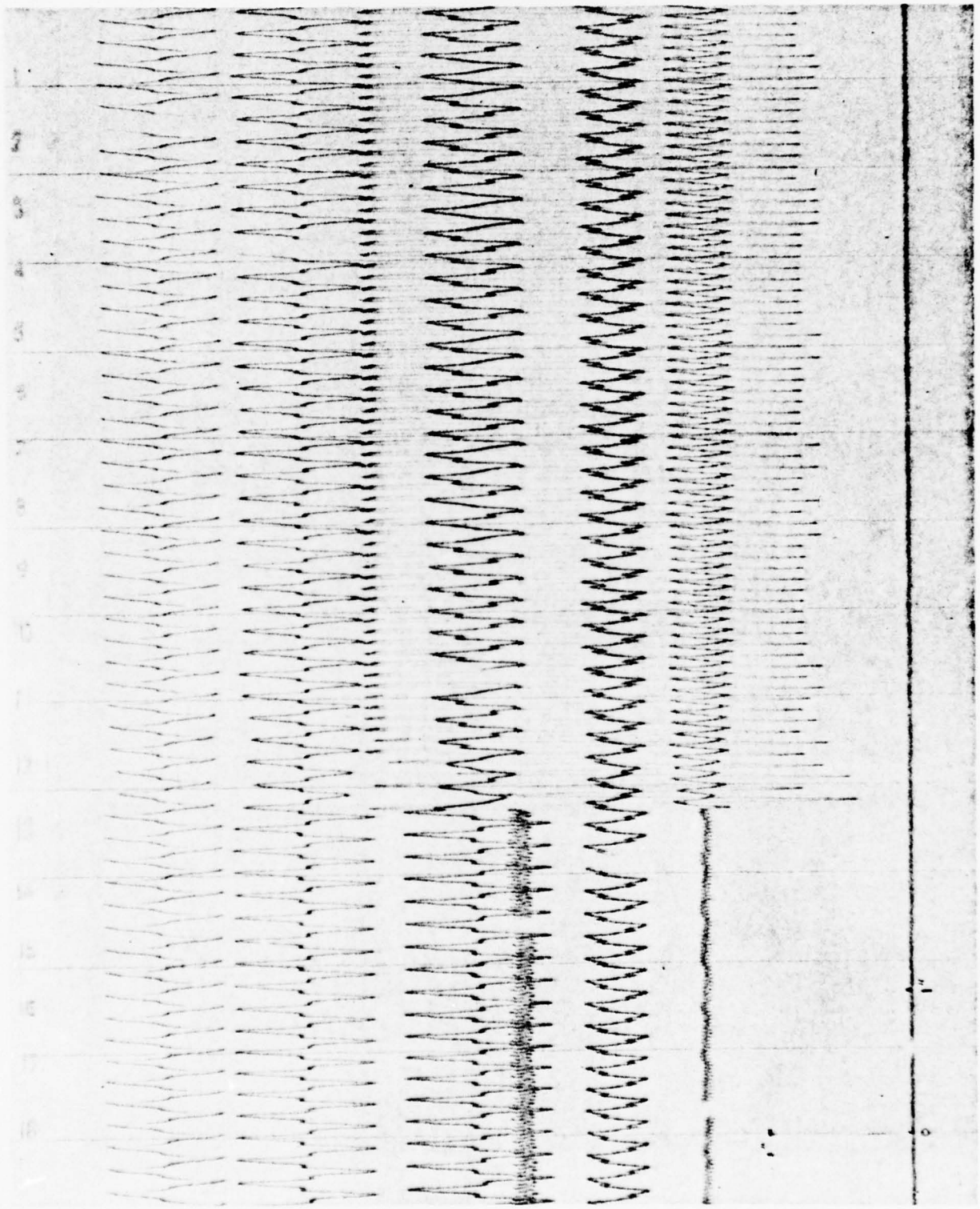

F-23753

Figure 21. Load Case 5 Transient Performance Test Results

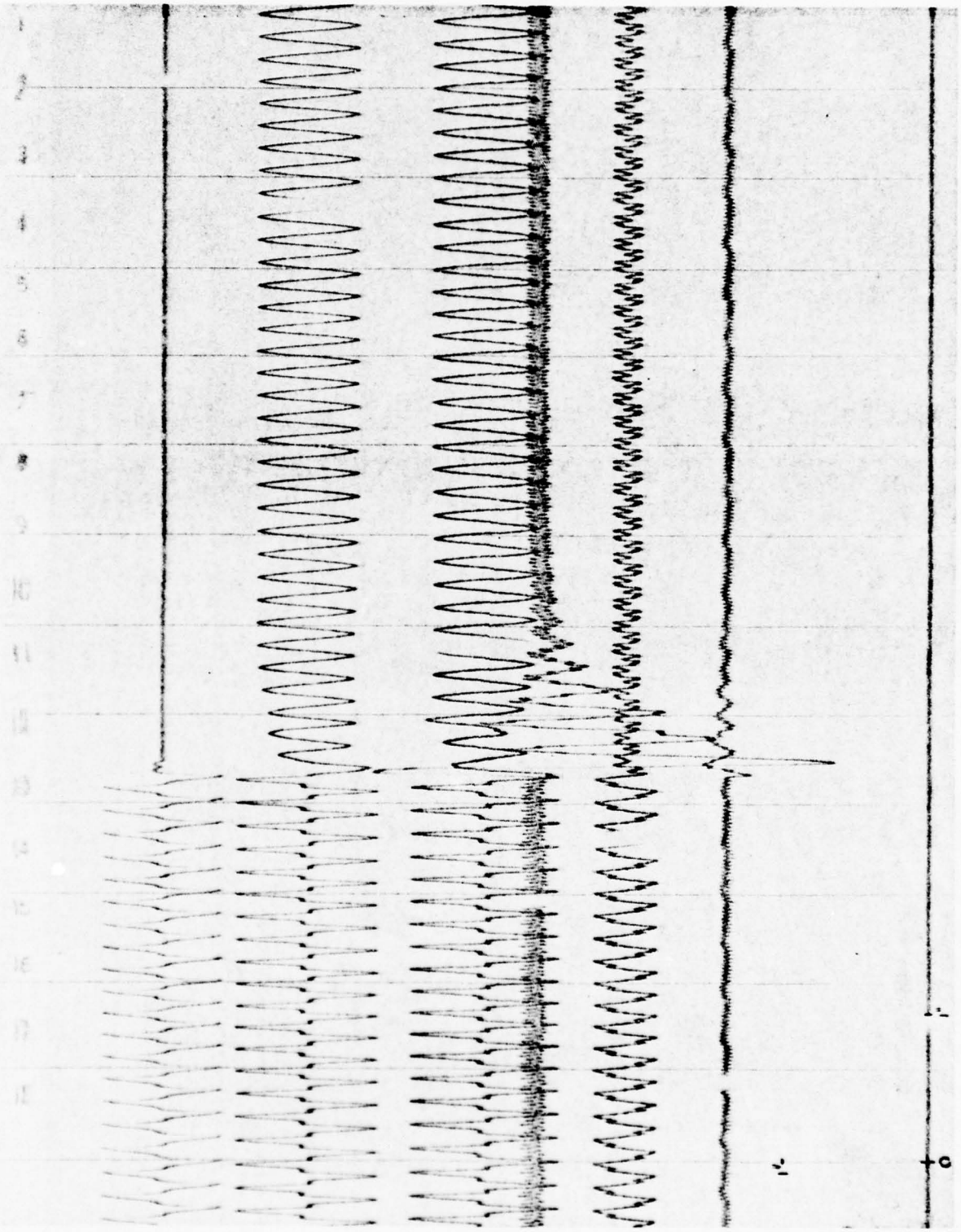

Figure 22. Load Case 6 Transient Performance Test Results

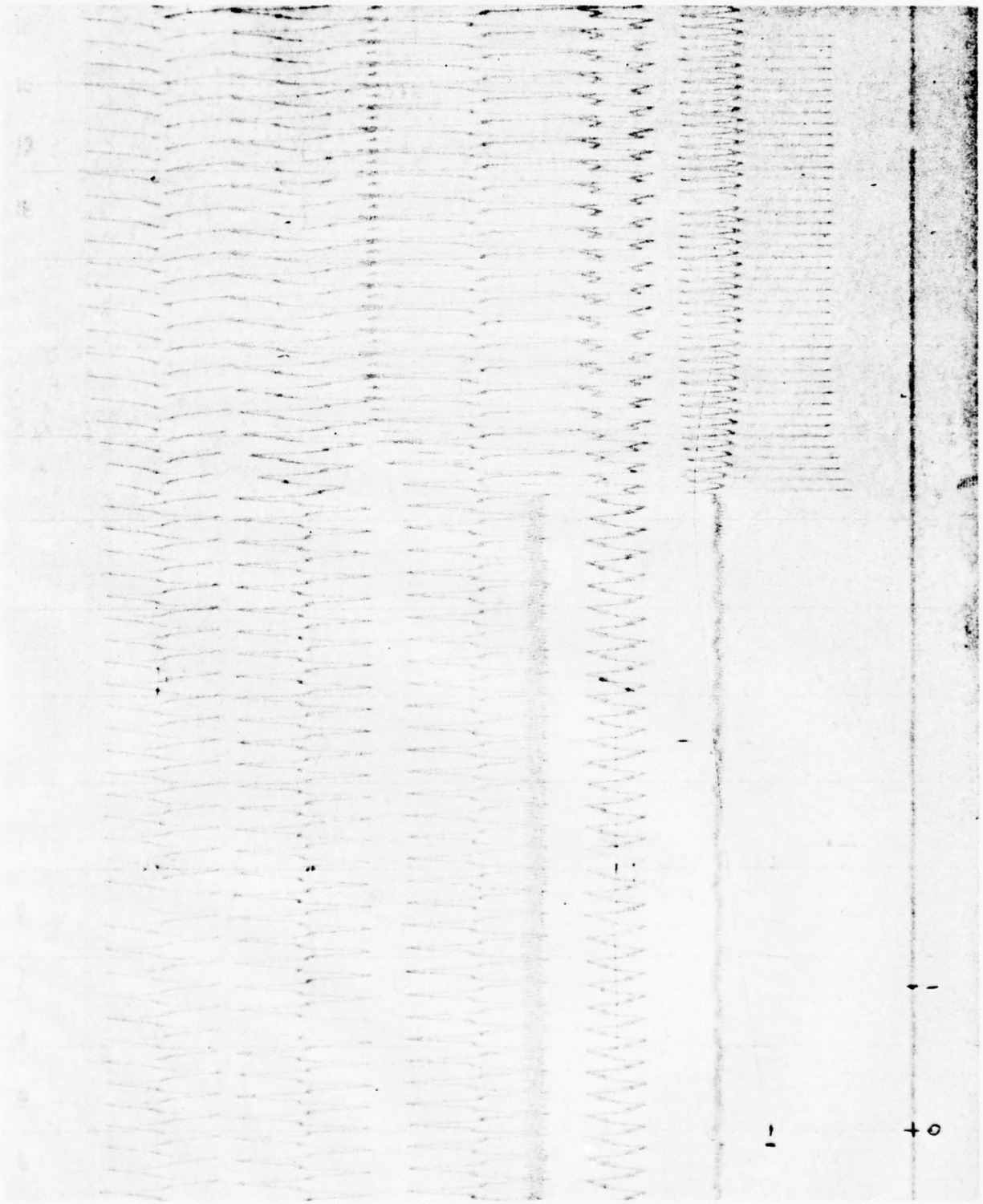

F-23754

Figure 23. Load Case 7 Transient Performance Test Results

SECTION VII
ALTERNATOR MODELING APPROACH

The alternator model used in this analysis is shown in Figure 24.

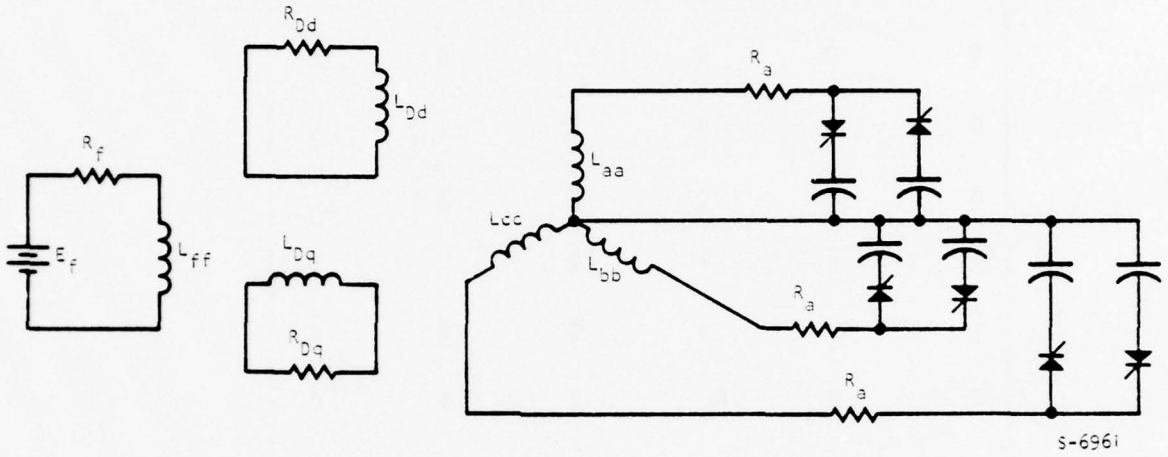

Figure 24. Alternator Model

This model consists of six circuits: three armature phase windings; one field winding; one direct axis damper winding; and one quadrature axis damper winding. The equivalent damper windings usually have the same number of turns as the armature windings. The field winding, on the other hand, usually retains its own number of turns. There will be mutual inductances between these windings. The speed of the machine is assumed constant.

The matrix equation for the six-circuit model is given by:

$$\frac{d}{dt}\left(\tilde{M}I\right) + \tilde{R}I + V = E \tag{1}$$

Since inductances are affected by saturation, Equation (1) can be written as

$$\frac{d}{dt}\left[\left(\tilde{L}_1 + f\,\tilde{M}_s\right)I\right] + \tilde{R}I + V = E \tag{2}$$

where

$$\tilde{M}_s \equiv \begin{bmatrix} L_{aa} - L_{al} & M_{ab} & M_{ac} & M_{af} & M_{aDd} & M_{aDq} \\ M_{ab} & L_{bb} - L_{al} & M_{bc} & M_{bf} & M_{bDd} & M_{bDq} \\ M_{ac} & M_{bc} & L_{cc} - L_{al} & M_{cf} & M_{cDd} & M_{cDq} \\ M_{af} & M_{bf} & M_{cf} & L_{ff} - L_{fl} & M_{fDd} & 0 \\ M_{aDd} & M_{bDd} & M_{cDd} & M_{fDd} & L_{Dd} - L_{Ddi} & 0 \\ M_{aDq} & M_{bDq} & M_{cDq} & 0 & 0 & L_{Dq} - L_{Dql} \end{bmatrix} \tag{3}$$

$$\tilde{L}_1 \equiv \begin{bmatrix} L_{al} & 0 & 0 & 0 & 0 & 0 \\ 0 & L_{al} & 0 & 0 & 0 & 0 \\ 0 & 0 & L_{al} & 0 & 0 & 0 \\ 0 & 0 & 0 & L_{fl} & 0 & 0 \\ 0 & 0 & 0 & 0 & L_{Ddl} & 0 \\ 0 & 0 & 0 & 0 & 0 & L_{Dql} \end{bmatrix} \tag{4}$$

$$\tilde{R} \equiv \begin{bmatrix} R_a & 0 & 0 & 0 & 0 & 0 \\ 0 & R_a & 0 & 0 & 0 & 0 \\ 0 & 0 & R_a & 0 & 0 & 0 \\ 0 & 0 & 0 & R_f & 0 & 0 \\ 0 & 0 & 0 & 0 & R_{Dd} & 0 \\ 0 & 0 & 0 & 0 & 0 & R_{Dq} \end{bmatrix} \tag{5}$$

$$I \equiv \begin{bmatrix} i_a \\ i_b \\ i_c \\ i_f \\ i_{Dd} \\ i_{Dq} \end{bmatrix} \tag{6} \qquad V \equiv \begin{bmatrix} V_a \\ V_b \\ V_c \\ 0 \\ 0 \\ 0 \end{bmatrix} \tag{7} \qquad E \equiv \begin{bmatrix} 0 \\ 0 \\ 0 \\ E_f \\ 0 \\ 0 \end{bmatrix} \tag{8}$$

also $$\frac{dV_a}{dt} = \frac{i_a}{C} \tag{9}$$

$$\frac{dV_b}{dt} = \frac{i_b}{C} \tag{10}$$

$$\frac{dV_c}{dt} = \frac{i_c}{C} \tag{11}$$

Before discussing the solution of this set of differential equations, it is necessary to discuss the alternator constants. The AiResearch alternator design computer program ROUND calculates the unsaturated parameters (based on an air gap line) X_d, X_q, X_{al}, X'_d, X_d'', X_q'', X_{Dd}, X_{Dq}, X_{Ddl}, X_{Dql}, X_2, X_o, X_{fl} and L_{ff}, as well as a predicted no-load saturation curve. From these values, together with rated frequency and the machine base impedance, the following unsaturated machine inductances can be obtained:

L_d	Direct axis inductance, H
L_q	Quadrature axis inductance, H
L_{al}	Armature leakage inductance per phase, H
L'_d	Direct axis transient inductance, H
L''_d	Direct axis subtransient inductance, H
L''_q	Quadrature axis subtransient inductance, H
L_{Dd}	Direct axis damper winding inductance, H
L_{Dq}	Quadrature axis damper winding inductance, H
L_{Ddl}	Direct axis damper winding leakage inductance, H
L_{Dql}	Quadrature axis damper winding leakage inductance, H
L_2	Negative sequence inductance, H
L_o	Zero sequence inductance, H
L'_{fl}	Field winding leakage inductance, in terms of armature, H
L_{ff}	Field winding self-inductance (in its own term), H

The inductances and resistance of the alternator model are as follows. (These inductances can be derived from the direct and quadrature axes inductances listed above).

L_{aa}	Self inductance of armature winding phase A, H
L_{bb}	Self inductance of armature winding phase B, H
L_{cc}	Self inductance of armature winding phase C, H

M_{ab}, M_{ba}	Mutual inductance between armature windings A and B, H
M_{bc}, M_{cb}	Mutual inductance between armature windings B and C, H
M_{ca}, M_{ac}	Mutual inductance between armature windings C and A, H
L_{ff}	Self inductance of field winding, in its own term, H
L_{Dd}	Self inductance of direct damper winding, in armature terms, H
L_{Dq}	Self inductance of quadrature damper winding, in armature terms, H
M_{af}, M_{fa}	Mutual inductance between field and armature winding Phase A, H
M_{bf}, M_{fb}	Mutual inductance between field and armature winding Phase B, H
M_{cf}, M_{fc}	Mutual inductance between field and armature winding Phase C, H
M_{aDd}, M_{Dda}	Mutual inductance between direct damper and armature winding Phase A, H
M_{bDd}, M_{Ddb}	Mutual inductance between direct damper and armature winding Phase B, H
M_{cDd}, M_{Ddc}	Mutual inductance between direct damper and armature winding Phase C, H
M_{aDq}, M_{Dqa}	Mutual inductance between quadrature damper and armature winding Phase A, H
M_{bDq}, M_{Dqb}	Mutual inductance between quadrature damper and armature winding Phase B, H
M_{cDq}, M_{Dqc}	Mutual inductance between quadrature damper and armature winding Phase C, H
M_{fDd}, M_{Ddf}	Mutual inductance between field and direct damper windings, H
L_{a1}	Armature winding leakage inductance, same for all three phases, H (portion of the armature inductance not subject to saturation)
L_{f1}	Field winding leakage inductance (in its own term), H
L_{Dd1}	Direct damper winding leakage inductance, H
L_{Dq1}	Quadrature damper winding leakage inductance, H
R_a	Armature winding resistance per phase, ohms
R_f	Field winding resistance, ohms

R_{Dd} Direct damper winding resistance, ohms

R_{Dq} Quadrature damper winding resistance, ohms

The mutual inductances between the field and the quadrature damper as well as between the direct and the quadrature damper windings are assumed to be zero even though the saturation effect would cause some slight coupling between them.

The alternator under consideration has a round, solid rotor. Uneven slotting gives a slight saliency to the machine. Damping effect comes from eddy currents induced in the solid rotor structure.

The self and mutual inductances of the armature windings can be approximated by the following expressions (the saliency is approximated by a double-frequency sinusoidal term.)

$$L_{aa} = L_s + L_m \cos 2\omega t \tag{12}$$

$$L_{bb} = L_s + L_m \cos (2\omega t + 120) \tag{13}$$

$$L_{cc} = L_s + L_m \cos (2\omega t - 120) \tag{14}$$

$$M_{ab} = M_{ba} = -M_s - L_m \cos (2\omega t + 60) \tag{15}$$

$$M_{bc} = M_{cb} = -M_s + L_m \cos 2\omega t \tag{16}$$

$$M_{ca} = M_{ac} = -M_s - L_m \cos (2\omega t - 60) \tag{17}$$

where ωt is expressed in electrical degrees.

The mutual inductances between field or damper windings with armature windings vary with relative winding positions. This variation is approximated by a sinusoidal function. The positive direction of the quadrature axis is taken as 90^o ahead of that of the direct axis.

$$M_{af} = M_{fa} = M_{AF} \cos \omega t \tag{18}$$

$$M_{bf} = M_{fb} = M_{AF} \cos (\omega t - 120) \tag{19}$$

$$M_{cf} = M_{fc} = M_{AF} \cos (\omega t + 120) \tag{20}$$

$$M_{aDd} = M_{Dda} = M_{ADD} \cos \omega t \tag{21}$$

$$M_{bDd} = M_{Ddb} = M_{ADD} \cos (\omega t - 120) \tag{22}$$

$$M_{cDd} = M_{Ddc} = M_{ADD} \cos (\omega t + 120) \tag{23}$$

$$M_{aDq} = M_{Dqa} = M_{ADQ} \cos (\omega t + 90) \tag{24}$$

$$M_{bDq} = M_{Dqb} + M_{ADQ} \cos (\omega t - 30) \tag{25}$$

$$M_{cDq} = M_{Dqc} = M_{ADQ} \cos (\omega t + 210) \tag{26}$$

Other mutual inductances are

$$M_{fDd} = M_{Ddf} = \text{a constant } M_{FDD} \tag{27}$$

$$M_{fDq} = M_{Dqf} = 0 \tag{28}$$

$$M_{DdDq} = M_{DqDd} = 0 \tag{29}$$

Those constants not listed in the computer output are calculated as follows:

$$L_s = 1/3 \ (L_d + L_q + L_o) \tag{30}$$

$$M_s = 1/2 \ (L_s - L_o) \tag{31}$$

$$L_m = 2/3 \ (L_d - L_s - M_s) \tag{32}$$

$$M_{AF} = \sqrt{\frac{2}{3} L_{ff} \ (L_d - L'_d)} \tag{33}$$

(L_{ff} is in field terms, not in terms of the armature)

Let k_{af} = effective turns ratio, armature (one phase only, not three-phase equivalent) to field.

$$M_{ADD} = k_{af} M_{AF} \tag{34}$$

$$M_{ADQ} = \sqrt{\frac{2}{3} L_{Dq} (L_q - L''_q)} \tag{35}$$

The value of M_{FDD} can be obtained by solving the following quadratic equation.

$$M_{FDD}^2 - \frac{3 M_{ADD} M_{AF}}{Ld - Ld''} M_{FDD} + \left[\frac{3}{2} \frac{L_{Dd} M_{AF}^2 + L_{ff} M_{ADD}^2}{Ld - Ld''} - L_{Dd} L_{ff} \right] = 0 \tag{36}$$

The smaller root is used, which is the physical solution. This quadratic equation comes from the relation:

$$L_d - L_d'' = \frac{3}{2} \frac{L_{Dd}M_{AF}^2 - 2M_{FDD}M_{ADD}M_{AF} + L_{ff}M_{ADD}^2}{L_{Dd}L_{ff} - M_{FDD}^2} \tag{37}$$

In a solid rotor alternator without pole face type damper winding, the subtransient component decays very rapidly. Using one damping winding on each direct and quadrature axis, a good compromised open-circuit subtransient time constant is 1/3 cycle. In a 400-Hz machine,

$$T_{do}'' = T_{qo}'' \cong 0.00083 \text{ sec}$$

and

$$R_{Dd} = \frac{L_{Dd}}{T_{do}''} \tag{38}$$

$$R_{Dq} = \frac{L_{Dq}}{T_{qo}''} \tag{39}$$

In this experimental alternator with round rotor construction it is considered reasonable to use one saturation factor for all inductances. The saturation factor is determined by the resultant MMF (field ampere-turns plus the armature reaction).

The resultant MMF can be resolved into two components, MMF_d along the direct axis and MMF_q along the quadrature axis. Armature, field, and direct damper currents contribute to MMF_d. Armature and quadrature damper currents contribute to MMF_q. The MMF producedby any armature phase current is pulsating in magnitude and stationary in space. This MMF can be resolved into two opposite-revolving MMF's, each with one half the magnitude of the pulsating MMF. The forward revolving component, which is stationary with respect to the rotating field, is the armature reaction component. The three backward revolving components of the three phases will cancel each other in the case of a balanced load. In case of unbalanced load, the resultant MMF will revolve with double speed relative to the field structure. The contribution of this double-speed MMF to saturation of inductances is ignored in the analysis.

If the MMF's are expressed in terms of equivalent field amperes, and at time zero, the field axis coincides with the axis of armature winding phase A, the instantaneous values of MMF_d and MMF_q can be expressed in terms of the instantaneous currents as follows:

$$MMF_d = i_f + k_{af} i_{Dq} + \frac{1}{2} K_{af} \left[i_a \cos \omega t + i_b \cos (\omega t - 120^\circ) + i_c \cos (\omega t + 120^\circ) \right] \quad (40)$$

$$MMF_q = k_{af} i_{Dq} - \frac{1}{2} k_{af} \left[i_a \sin \omega t + i_b \sin (\omega t - 120^\circ) + i_c \sin (\omega t + 120^\circ) \right] \quad (41)$$

As mentioned previously, the positive direction of this quadrature axis is assumed to be 90 deg ahead of that of the direct axis. The resultant MMF can then be obtained:

$$MMF = \sqrt{MMF_d^2 + MMF_q^2} \quad (42)$$

With unbalanced load and during transient, these MMF's vary with time. From the no-load saturation curve and the air gap line, a saturation factor can be defined from Figure 25 such that at a certain resultant MMF of I_{f1},

$$F_{sat} = \frac{AB}{AC}$$

Figure 26 shows the result of this calculation.

Since in general, MMF is a function of time, the saturation factor is also a function of time.

The saturated inductances are obtained by multiplying the unsaturated inductance by the saturation factor. For instance, the saturated self-inductance of armature winding phase A is:

$$L_{aa,sat} = L_{al} + F_{sat} (L_{aa} - L_{al}) \quad (44)$$

where L_{al} is leakage inductance and is for practical purposes not subject to saturation.

For the experimental alternator, the constants from the AiResearch computer design program ROUND are tabulated in Tables 5 through 7.

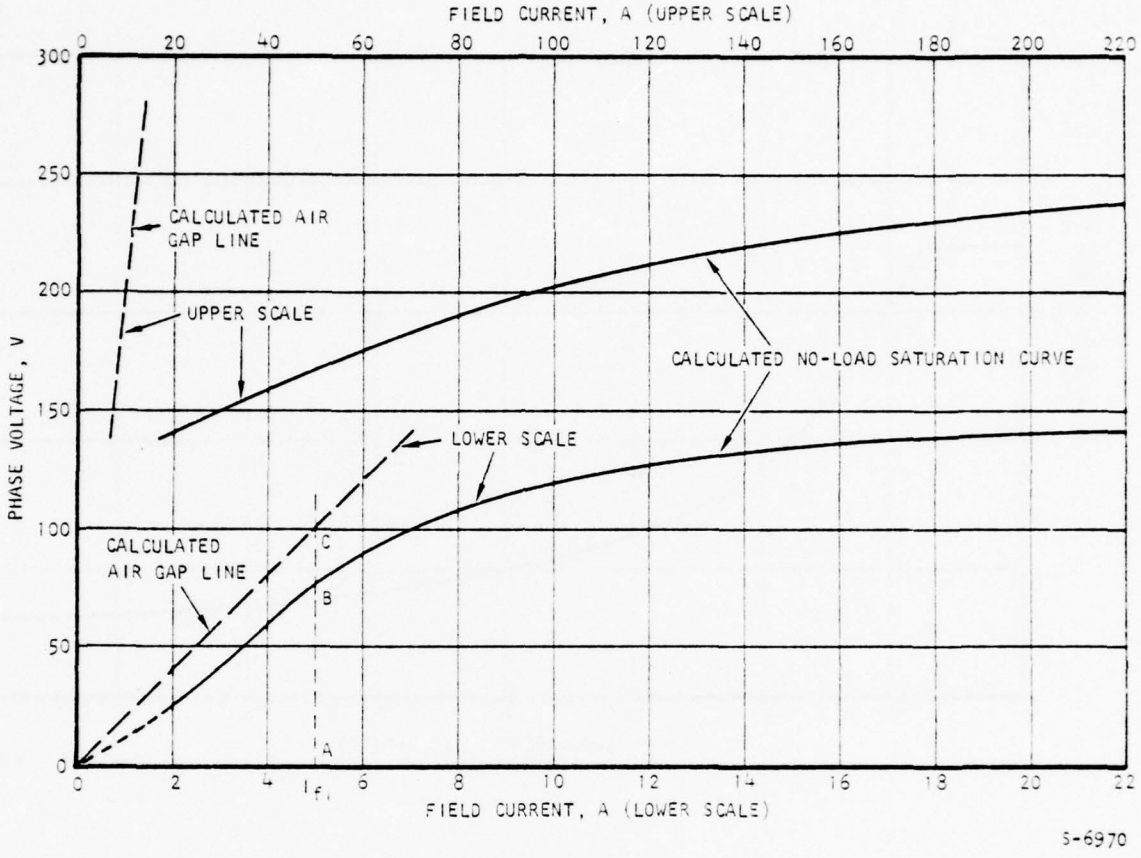

Figure 25. Computer-Calculated Saturation Curve

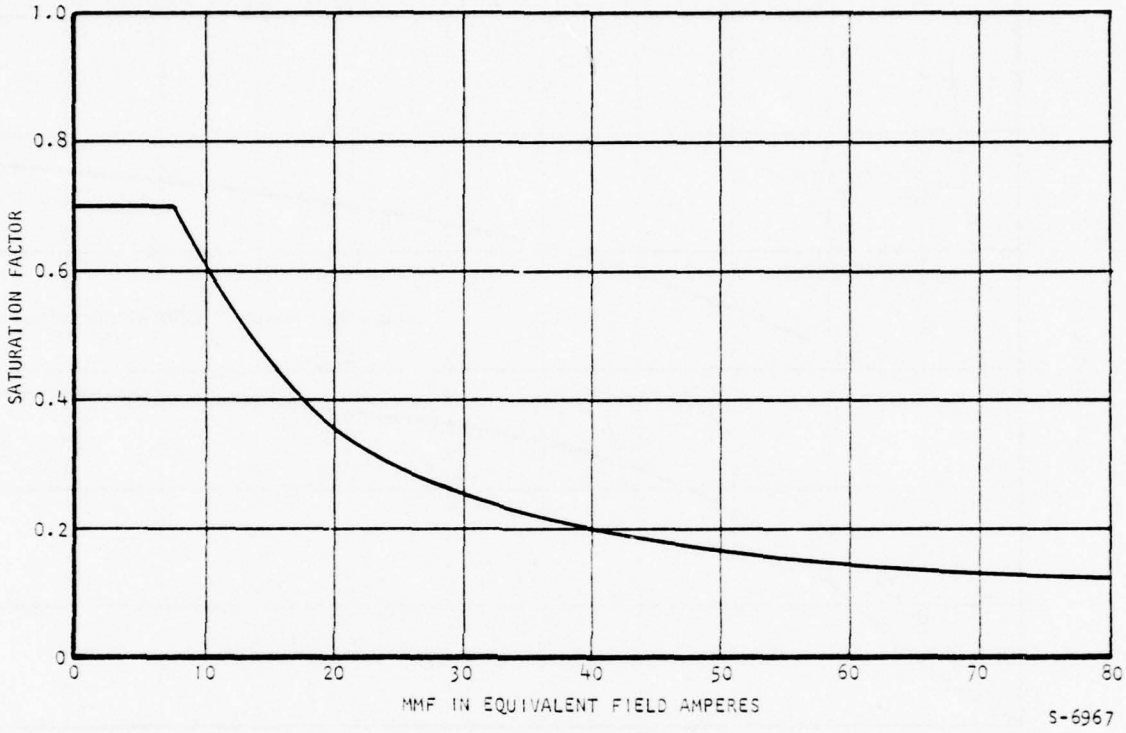

Figure 26. Saturation Factor for Computer Output Constants

TABLE 5

COMPUTER OUTPUT CONSTANT

X_d	4.028 PU
X_q	3.498 PU
X_{al}	0.1837 PU
X'_d	0.3676 PU
X''_d	0.2103 PU
X''_q	0.2286 PU
X_{Dd}	3.871 PU
X_{Dq}	3.359 PU
X_{Dd1}	0.0266 PU
X_{Dq1}	0.0449 PU
X_2	0.2195 PU
X_0	0.08535 PU
X_{f1}	0.1931 PU
L_{ff} = 0.01981 H	

TABLE 6

ALTERNATOR MODEL CONSTANTS DERIVED FROM COMPUTER OUTPUT

L_s	0.00667 H
M_s	0.00322 H
L_m	0.000467 H
L_{ff}	0.01981 H
L_{Dd}	0.01018 H
L_{Dq}	0.00883 H
M_{AF}	0.01128 H
M_{ADD}	0.00825 H
M_{ADQ}	0.00712 H
M_{FDD}	0.0142 H
L_{al}	0.000483 H
L_{f1}	0.000948 H
L_{Dd1}	0.000070 H
L_{Dq1}	0.000118 H

TABLE 6 (Continued)

R_a	0.300 ohm
R_f	0.2665 ohm (including slip ring brush drop)
R_{Dd}	12.0 ohm
R_{Dq}	10.0 ohm

TABLE 7

SATURATION FACTOR DATA (FOR COMPUTER PROGRAM ROUND CONSTANTS)

$F_{sat} = 0.700$ if resultant MMF ≤ 7.531

$F_{sat} = A + \frac{B}{MMF} + \frac{C}{MMF^2}$ if MMF > 7.531

where

$A = 0.02473334$

$B = 7.578884$

$C = -18.77908$

Using test results on the experimental alternator combined with manually calculated constants using Kilgore's design formulas (Reference 3), the circuit constants for the model are those in Table 8 and 9. These constants are used together with a different set of saturation curves, from actual test. As shown in Figure 27, a fictious air gap line is drawn tangential to the lower part of the tested no-load saturation curve. The saturation factor at a MMF of I_{f1} is again given by

$$F_{sat} = \frac{AB}{AC} \tag{45}$$

Figure 28 shows the result of Equation (45).

Reference 3: KILGORE, L. A., Calculation of Synchronous Machine Constants--Reactances and Time Constants Affecting Transient Characteristics, pp 1201-1214, AIEE Transactions, December 1931

TABLE 8

ALTERNATOR MODEL CONSTANTS DERIVED FROM COMBINATION OF TEST AND COMPUTATION

L_s	0.004650 H
M_s	0.002199 H
L_m	0.000310 H
L_{ff}	0.01553 H
L_{Dd}	0.007152 H
L_{Dq}	0.006293 H
M_{AF}	0.008334 H
M_{ADD}	0.004716 H
M_{ADQ}	0.002678 H
M_{FDD}	0.008327 H
L_{al}	0.000367 H
L_{fl}	0.000774 H
L_{Ddl}	0.000205 H
L_{Dql}	0.000278 H
R_a	0.300 ohm
R_f	0.2665 ohm
R_{Dd}	12 ohms
R_{Dq}	10 ohms

TABLE 9

SATURATION FACTOR DATA FOR CONSTANTS FROM COMBINATION OF TEST AND COMPUTATION

$F_{sat} = 1.00$ if MMF ≤ 7.0211

$F_{sat} = A + \frac{B}{MMF} + \frac{C}{MMF^2}$ if MMT > 7.0211

where

A = 0.012443137

B = 12.430776

C = -38.595227

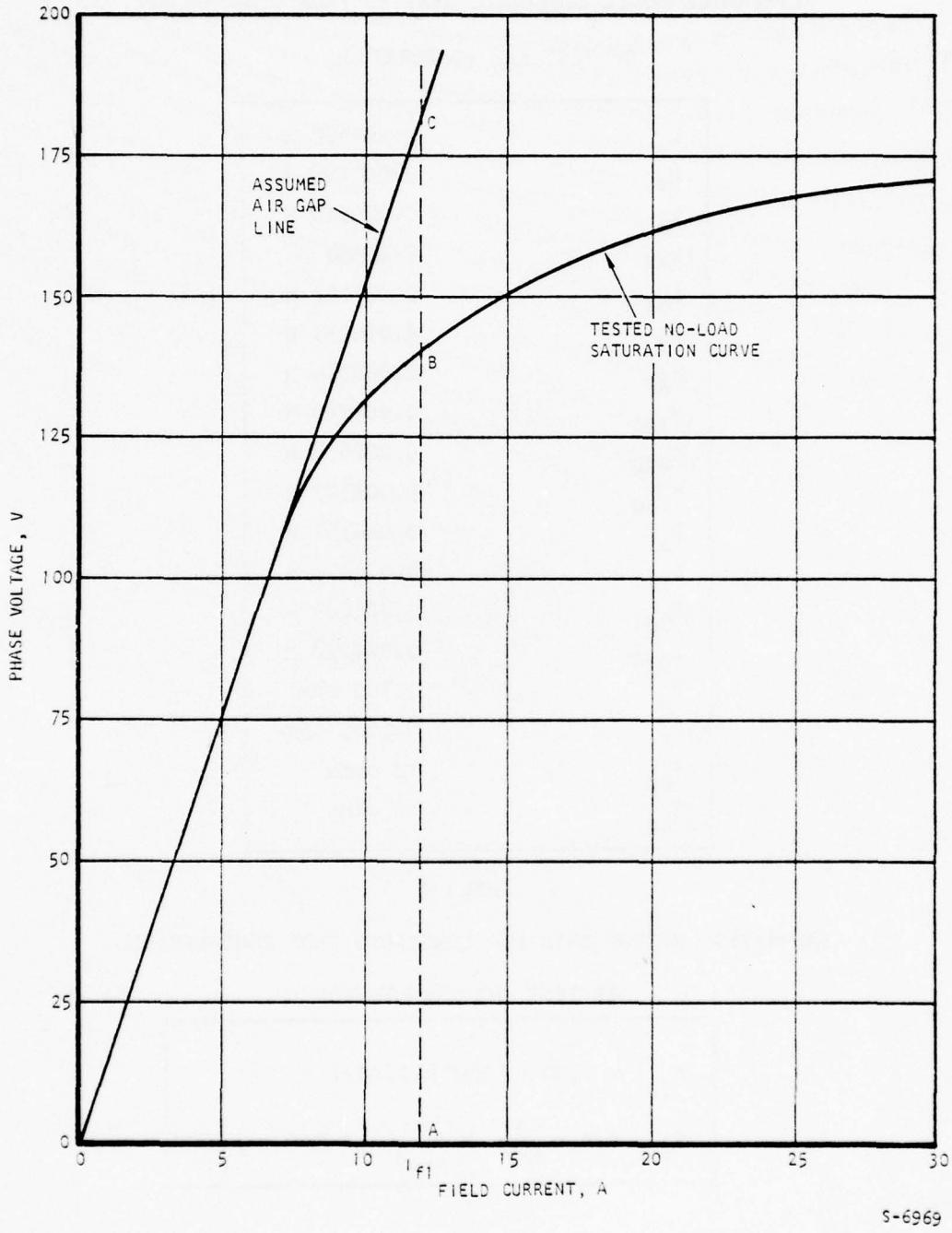

Figure 27. Actual No-Load Saturation Curve

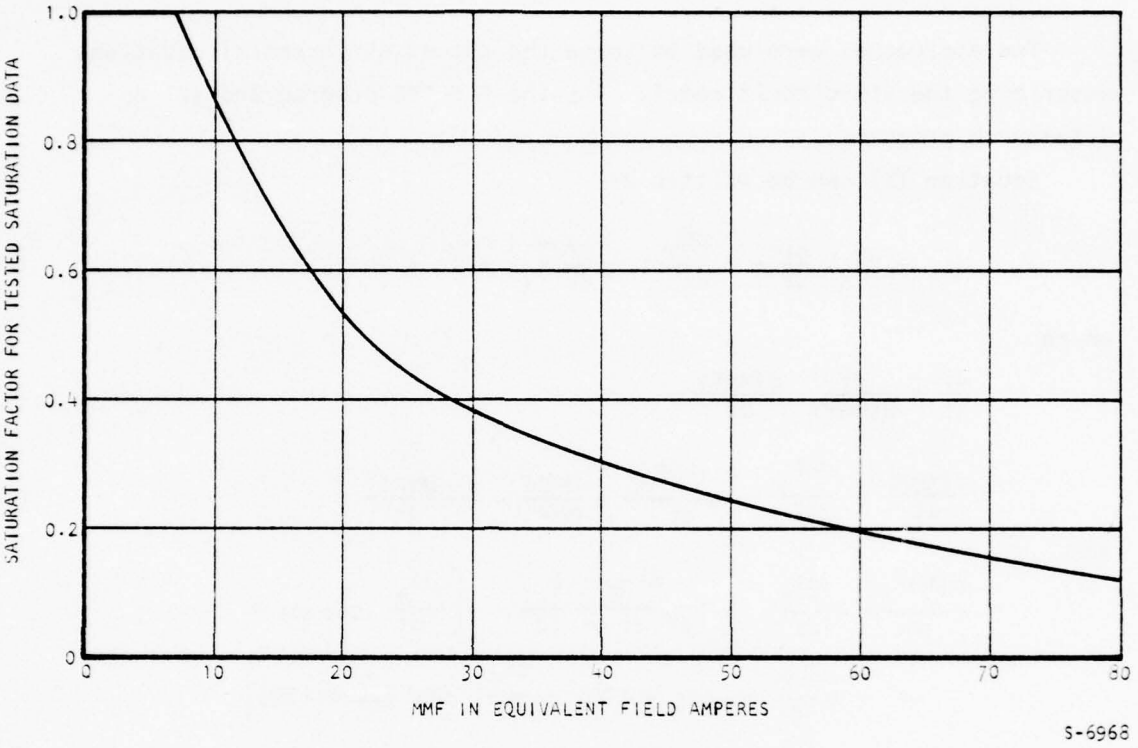

Figure 28. Saturation Factor for Tested Saturation Data

The products of machine constants and the saturation factors for test constants and for the AiResearch computer program ROUND constants do not greatly differ. The transient performance derived from the model is nearly the same whether the test constants or the AiResearch design program ROUND constants are used.

SECTION VIII

DISCUSSION OF MODEL SIMULATION

Two approaches were used to solve the set of differential equations describing the six-circuit model: (1) the SCEPTRE program and (2) an AiResearch program.

Equation (2) can be written as:

$$(\tilde{L}_1 + f\tilde{M}_s)\frac{dI}{dt} + f\frac{d\tilde{M}_s}{dt}I + \frac{df}{dt}\tilde{M}_s I + \tilde{R}I + V = E \tag{46}$$

where

$$\frac{df}{dt} = \frac{df}{d(MMF)} \cdot \frac{d(MMF)}{dt} \tag{47}$$

$$\frac{d(MMF)}{dt} = \frac{MMF_d}{MMF} \cdot \frac{d\ (MMF_d)}{dt} + \frac{MMFq}{MMF} \cdot \frac{d\ (MMFq)}{dt} \tag{48}$$

and

$$\begin{aligned}\frac{d(MMF_d)}{dt} = {} & \frac{di_f}{dt} + k_{af}\frac{di_{Dd}}{dt} + \frac{k_{af}}{2}\left[\frac{di_a}{dt}\cos\omega t + \right. \\ & \left. + \frac{di_b}{dt}\cos(\omega t - 120) + \frac{di_c}{dt}\cos(\omega t + 120)\right] \\ & - \omega\frac{k_{af}}{2}\left[i_a \sin\omega t + i_b \sin(\omega t - 120)\right. \\ & \left. + i_c \sin(\omega t + 120)\right]\end{aligned} \tag{49}$$

$$\begin{aligned}\frac{d(MMFq)}{dt} = {} & k_{af}\frac{di_{Dq}}{dt} - \frac{k_{af}}{2}\left[\frac{di_a}{dt}\sin\omega t + \frac{di_b}{dt}\sin(\omega t - 120)\right. \\ & \left. + \frac{di_c}{dt}\sin(\omega t + 120)\right] - \omega\frac{k_{af}}{2}\left[i_a\cos\omega t + i_b\cos(\omega t - 120)\right. \\ & \left. + i_c\cos(\omega t + 120)\right]\end{aligned} \tag{50}$$

Substituting equations (48) through (50) into equation (47)

$$\frac{df}{dt} = C_a\frac{di_a}{dt} + C_b\frac{di_b}{dt} + C_c\frac{di_c}{dt} + C_f\frac{di_f}{dt} - C_{Dd}\frac{di_{Dd}}{dt} + C_{Dq}\frac{di_{Dq}}{dt} - C_x \tag{51}$$

Let $$\frac{df}{d(MMF)} = f' \tag{52}$$

$$\frac{MMF_d}{MMF} = P_d \qquad \frac{MMF_q}{MMF} = P_q \tag{53}$$

then

$$C_a = f' \frac{k_{af}}{2} (P_d \cos \omega t - P_q \sin \omega t) \tag{54}$$

$$C_b = f' \frac{k_{af}}{2} \left[P_d \cos (\omega t - 120) - P_q \sin (\omega t - 120)\right] \tag{55}$$

$$C_c = f' \frac{k_{af}}{2} \left[P_d \cos (\omega t + 120) - P_q \sin (\omega t + 120)\right] \tag{56}$$

$$C_f = f' P_d \tag{57}$$

$$C_{Dd} = f' P_d k_{af} \tag{58}$$

$$C_{Dq} = f' P_q k_{af} \tag{59}$$

$$C_x = -f' \omega \frac{k_{af}}{2} \Big\{ P_d \Big[i_a \sin \omega t + i_b \sin (\omega t - 120) + i_c \sin (\omega t + 120) \Big] + P_q \Big[i_a \cos \omega t + i_b \cos (\omega t - 120) + i_c \cos (\omega t + 120) \Big] \tag{60}$$

SCEPTRE PROGRAM APPROACH

Since $\frac{df}{dt}$ contains derivatives of state variables (i.e., $\frac{di_a}{dt}$, etc.) the term $\frac{df}{dt} \tilde{M}_s I$ must be included in SCEPTRE as a fictitious voltage:

$$(\tilde{L}_1 + f\tilde{M}_s) \frac{dI}{dt} + \tilde{R} I = (E - f \frac{d\tilde{M}_s}{dt} I - \tilde{M}_s \frac{df}{dt} I - V) \tag{61}$$

Iteration and numerical integration can then be carried out like an ordinary SCEPTRE problem.

AIRESEARCH PROGRAM APPROACH

Let

$$\tilde{M}_s I = \begin{bmatrix} Y_1 \\ Y_2 \\ Y_3 \\ Y_4 \\ Y_5 \\ Y_6 \end{bmatrix} \tag{62}$$

then

$$\frac{df}{dt}\tilde{M}_s I = \tilde{C}\frac{dI}{dt} + C_X\tilde{M}_s I \tag{63}$$

where

$$\tilde{C} = \begin{bmatrix} C_aY_1 & C_bY_1 & C_cY_1 & C_fY_1 & C_{Dd}Y_1 & C_{Dq}Y_1 \\ C_aY_2 & C_bY_2 & C_cY_2 & C_fY_2 & C_{Dd}Y_2 & C_{Dq}Y_2 \\ C_aY_3 & C_bY_3 & C_cY_3 & C_fY_3 & C_{Dd}Y_3 & C_{Dq}Y_3 \\ C_aY_4 & C_bY_4 & C_cY_4 & C_fY_4 & C_{Dd}Y_4 & C_{Dq}Y_4 \\ C_aY_5 & C_bY_5 & C_cY_5 & C_fY_5 & C_{Dd}Y_5 & C_{Dq}Y_5 \\ C_aY_6 & C_bY_6 & C_cY_6 & C_fY_6 & C_{Dd}Y_6 & C_{Dq}Y_6 \end{bmatrix} \tag{64}$$

and C_x is given in Equation (60)

Equation (46) then becomes

$$(\tilde{L}_1 + f\tilde{M}_s + \tilde{C})\frac{dI}{dt} = E - V - (\tilde{R} + f\frac{d\tilde{M}_s}{dt} + C_x\tilde{M}_s)I \tag{65}$$

A modified Euler technique can now be used to integrate and solve this set of differential equations. The matrix $\tilde{C}$ is in general nonsymmetrical, and is added to the symmetrical inductance matrix $(\tilde{L}_1 + f\tilde{M}_s)$. The resultant matrix is therefore also nonsymmetrical. This is the basic reason the SCEPTRE program cannot solve Equation (65).

Since no circuit change is allowed in SCEPTRE, the thyristor switches are simulated by resistors that change in value depending on the direction of current flow. This requires extra computer time to iterate into current values. It also results in leakage currents through resistors that do not actually exist. This current leakage decreases the accuracy of the solution.

The AiResearch program needs no iteration. It actually simulates the switching phenomena and also uses much less computer time than the SCEPTRE program.

SECTION IX

COMPARISON OF TEST AND SIMULATION RESULTS

The present computer program would need considerable modification in order to simulate the line-to-line and three-line faults. Therefore, for load cases 5 and 6, double-line-to-ground fault and three-line-to-ground fault cases were simulated. The tests had been completed on the experimental alternator before this limitation in modeling had been evaluated; therefore, a direct test comparison for the model results was made in load case 5.

Figures 29 through 35 are computer plots of transient responses for various load cases using the AiResearch mode solution program and the ROUND computer-program-calculated generator constants. The figures are discussed below.

Figure 29--Step increase of applied field voltage. The corresponding test result is shown in Figure 17. The envelopes of the transient excursions in Figure 17 are shown dashed in Figure 29.

In the following figures, dash lines show the envelopes of the test transients as above.

Figure 30--Step decrease of applied field voltage.

Figure 31--Normal field excitation, suddenly applied load. The corresponding test result is shown in Figure 19. In the test, due to misfiring of the switch, phase C load did not connect until two cycles after the Phase A load is applied. For this reason the test and computer results do not exactly match during a brief transient period.

Figure 32--Single-line-to-ground fault.

Figure 33--Double-line-to-ground fault. Test results are not shown for comparison in this case, as noted above.

Figure 34--Three-line-to-ground fault.

Figure 35--One line open.

As can be seen from the figures, the transient performance predicted by the model is in good agreement with the test results.

Figure 29. Load Case 1 Transient Response

EXPERIMENTAL GENERATOR (COMPUTER CONSTANTS) --- LC 1

(DASHED LINES DENOTE TEST DATA ENVELOPE)

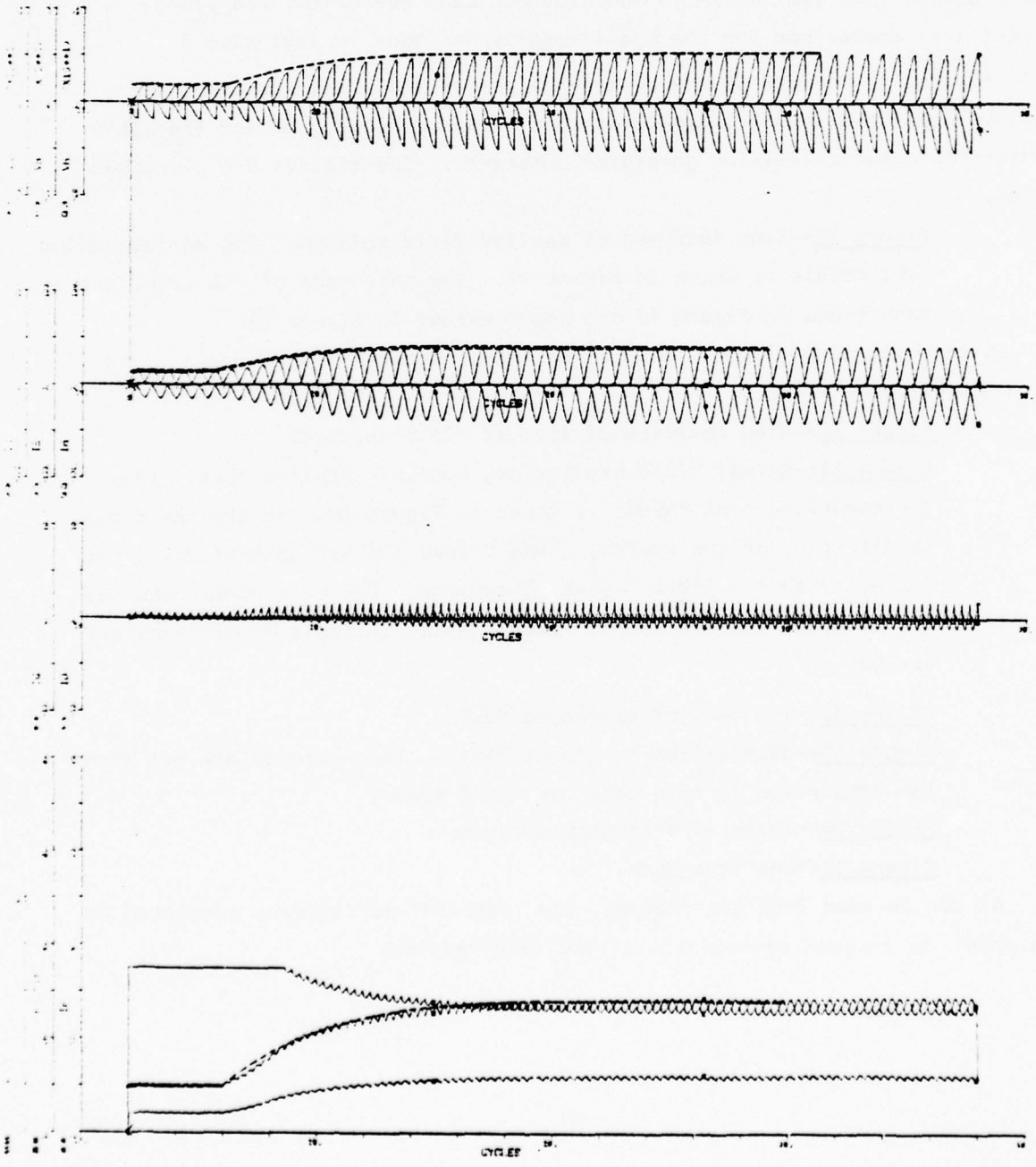

EXPERIMENTAL GENERATOR (COMPUTER CONSTANTS) --- LC 2

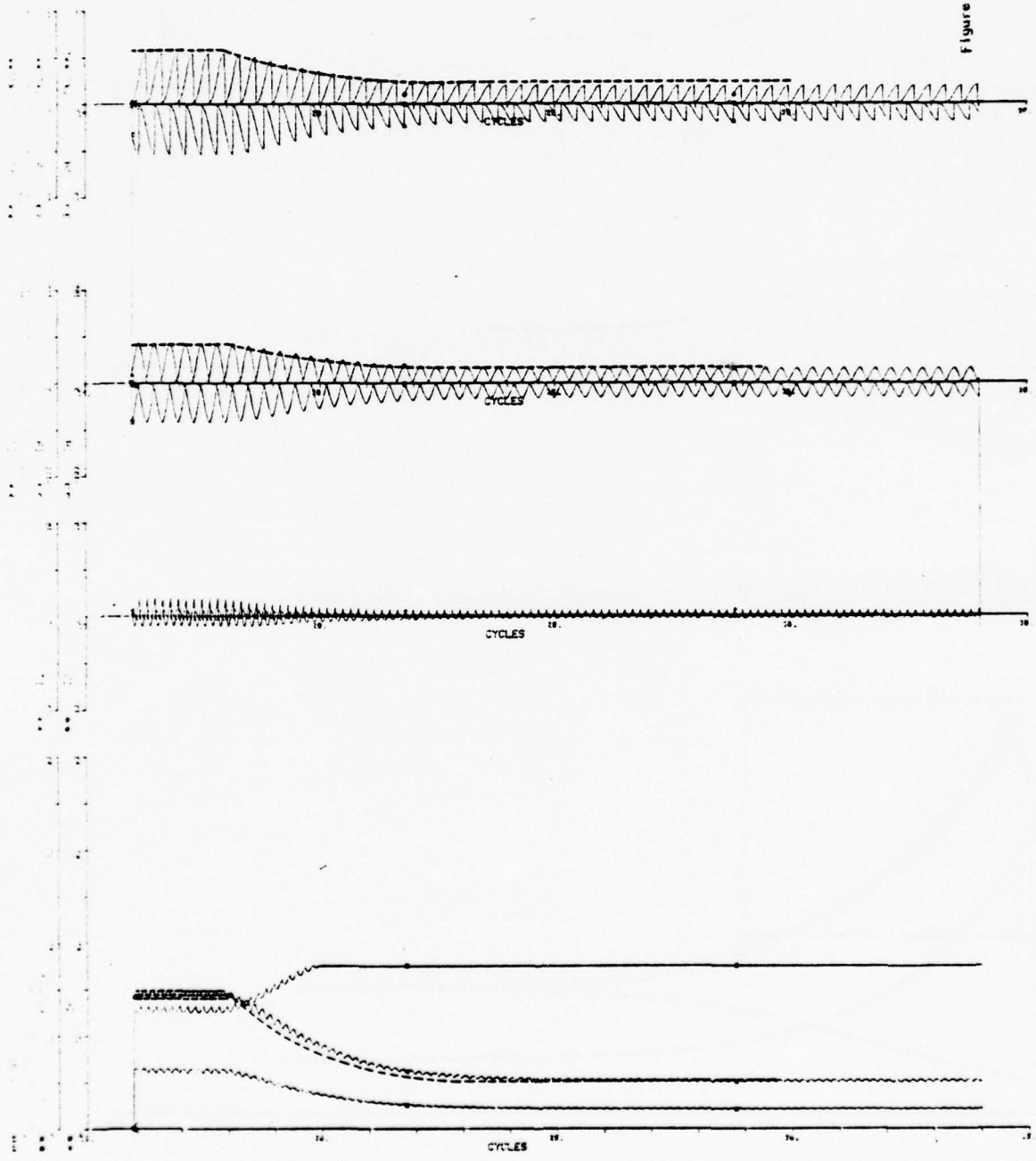

Figure 30. Load Case 2 Transient Response

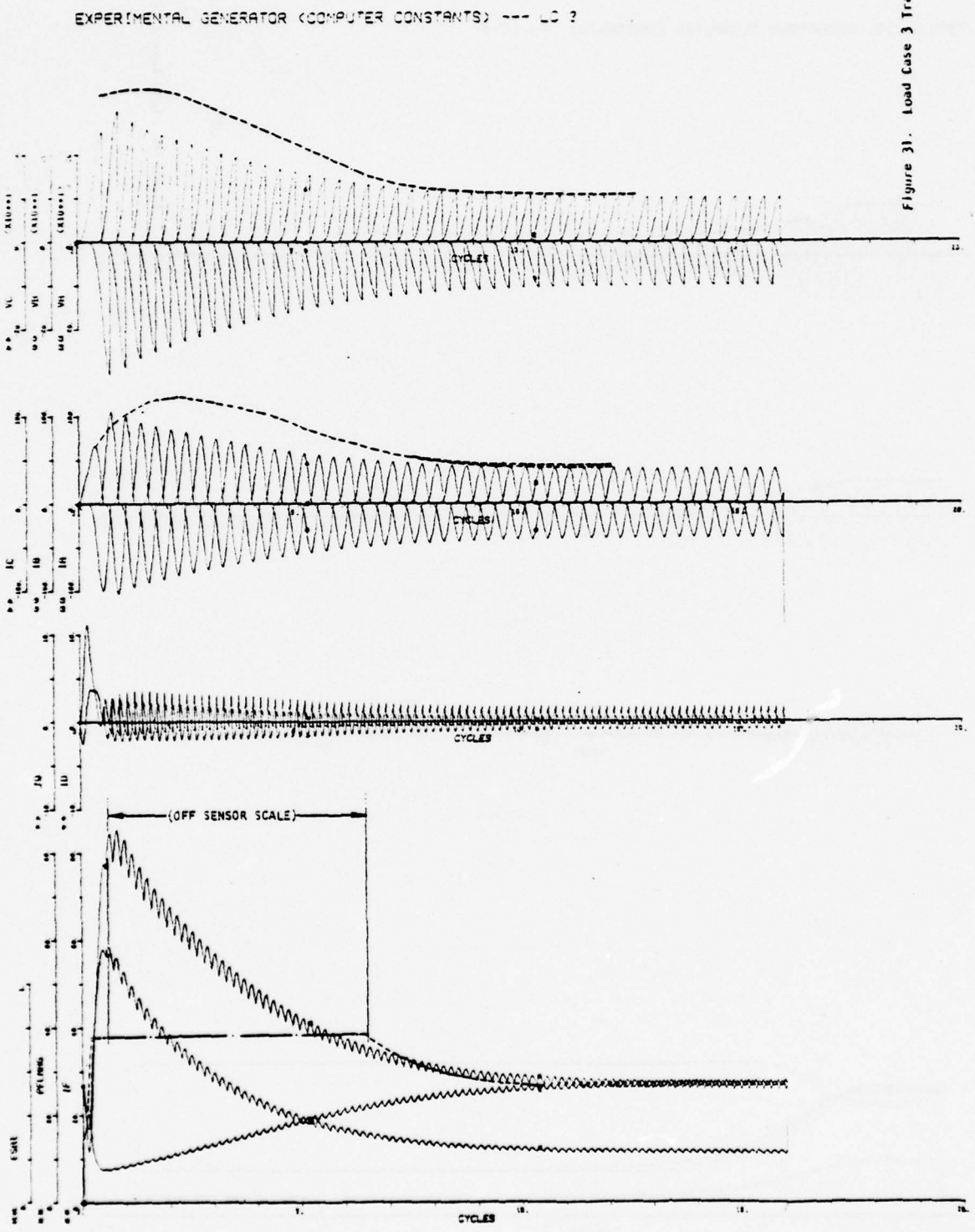

Figure 31. Load Case 3 Transient Response

EXPERIMENTAL GENERATOR (COMPUTER CONSTANTS) --- LC 4

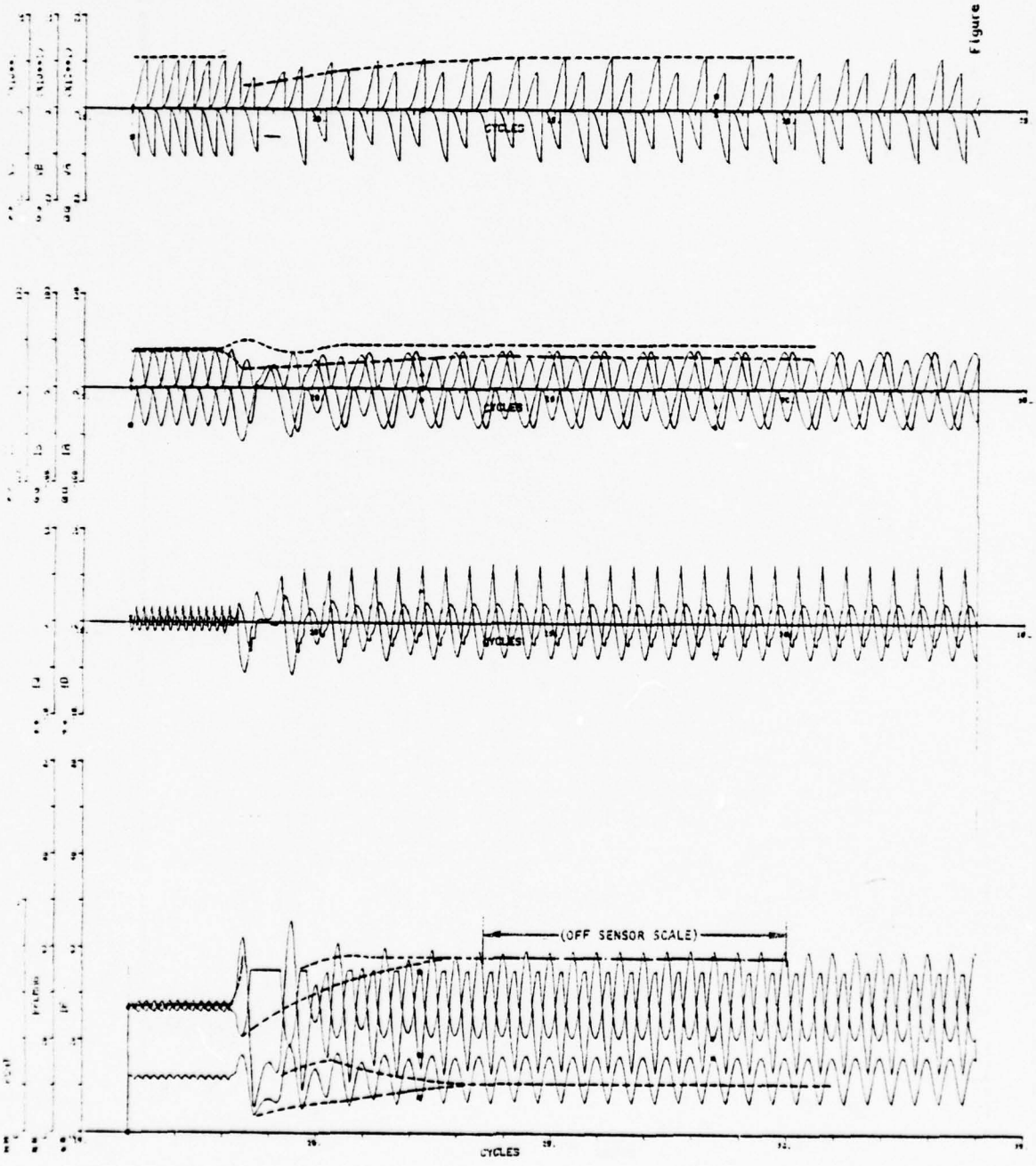

Figure 32. Load Case 4 Transient Response

EXPERIMENTAL GENERATOR (COMPUTER CONSTANTS) -- LOAD CASE DOUBLE LINE TO GROUND FAULT

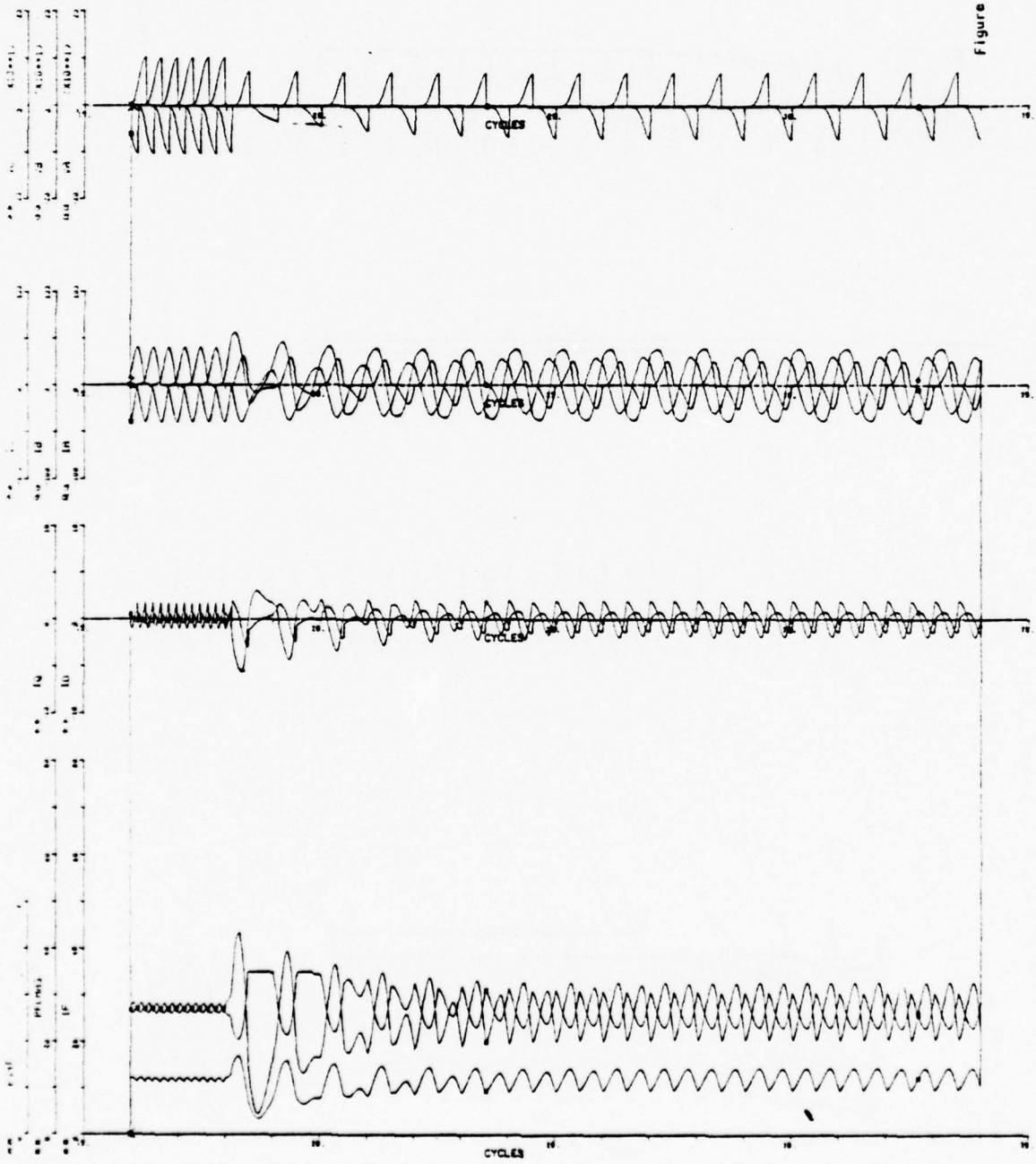

Figure 33. Load Case Double Line to Groun
Fault Transient Response

EXPERIMENTAL GENERATOR (COMPUTER CONSTANTS) --- LC 6

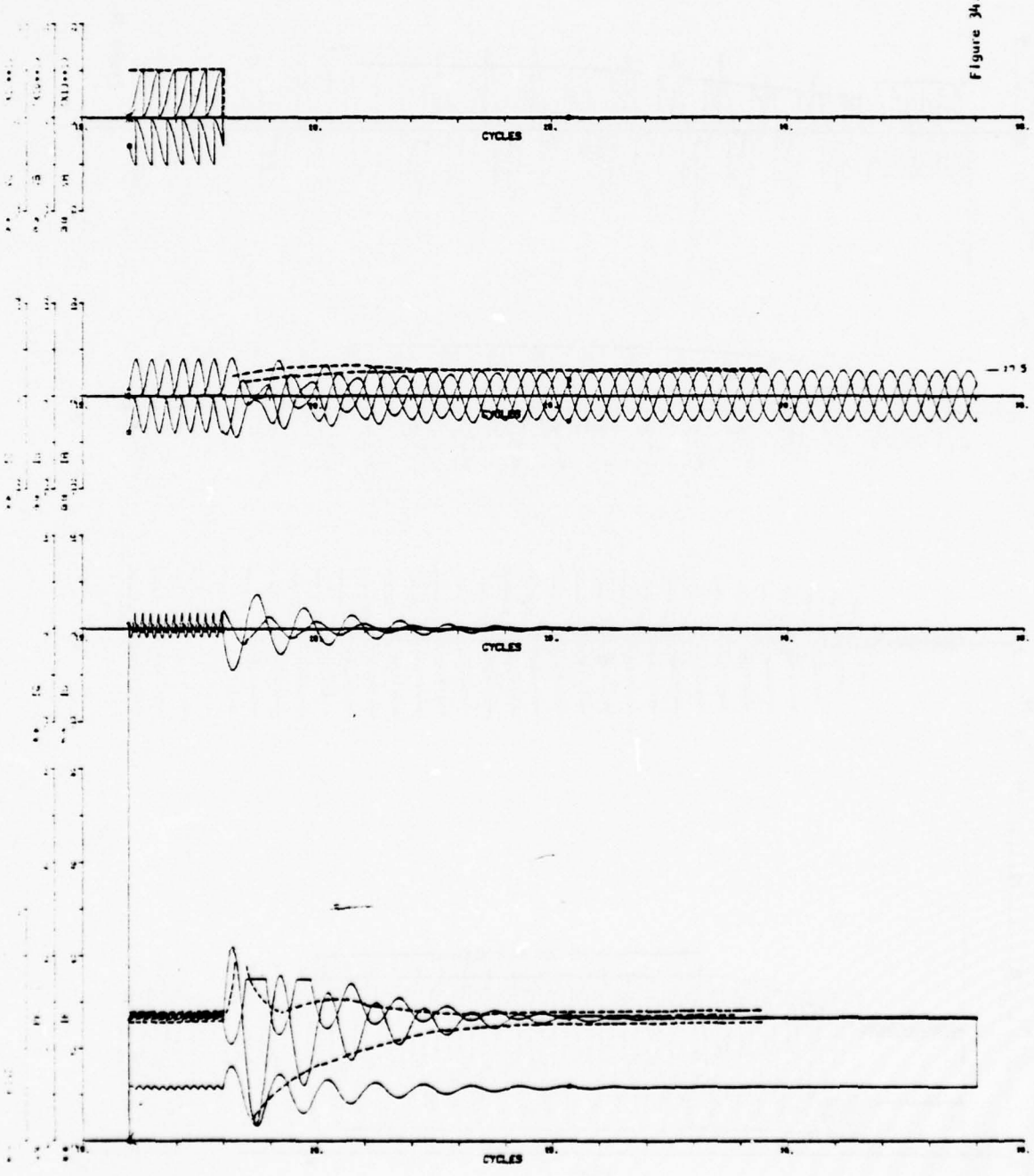

Figure 34. Load Case 6 Transient Response

EXPERIMENTAL GENERATOR (COMPUTER CONSTANTS) --- LC 7

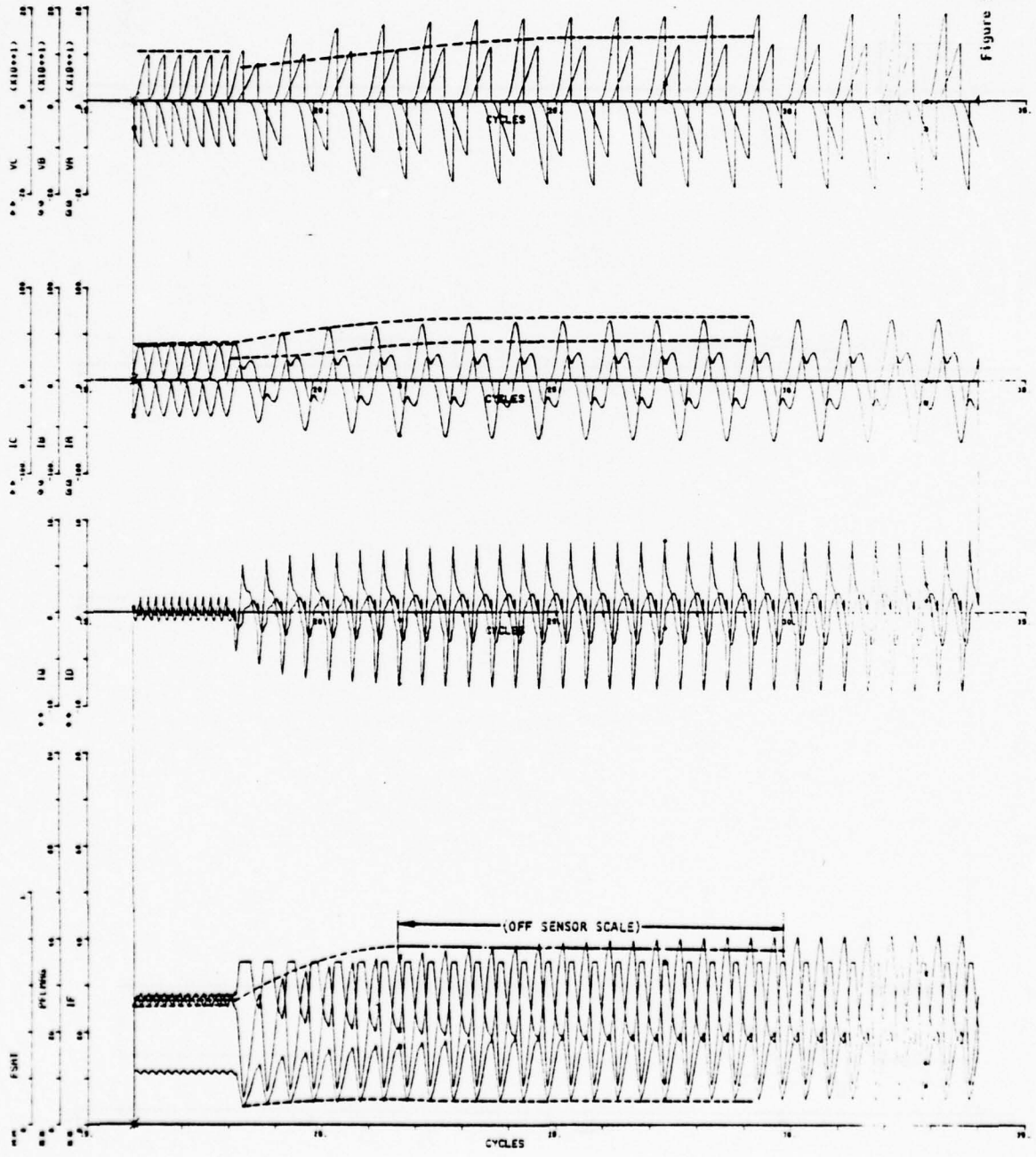

Figure 35. Load Case 7 Transient Response

Figure 36 shows single-line-to-ground fault case using the AiResearch model program and the combination test and manually computed alternator constants. As this comparison shows, these results are very close to those shown in Figure 32 (using the AiResearch model program and the AiResearch computer ROUND output constants).

The SCEPTRE program, although requiring more computer time, does yield the same output as that of the AiResearch model program. Figures 37 through 44 show the transient responses of i_f, MMF, i_a, i_c, V_{cal}, V_{cc1}, i_{Dd} and i_{Dq}, respectively, for a single-line-to-ground fault using the AiResearch computer ROUND output constants. These results also agree closely with those shown in Figure 32.

EXPERIMENTAL GENERATOR (APRIL 17 CONSTANTS) --- LC 4

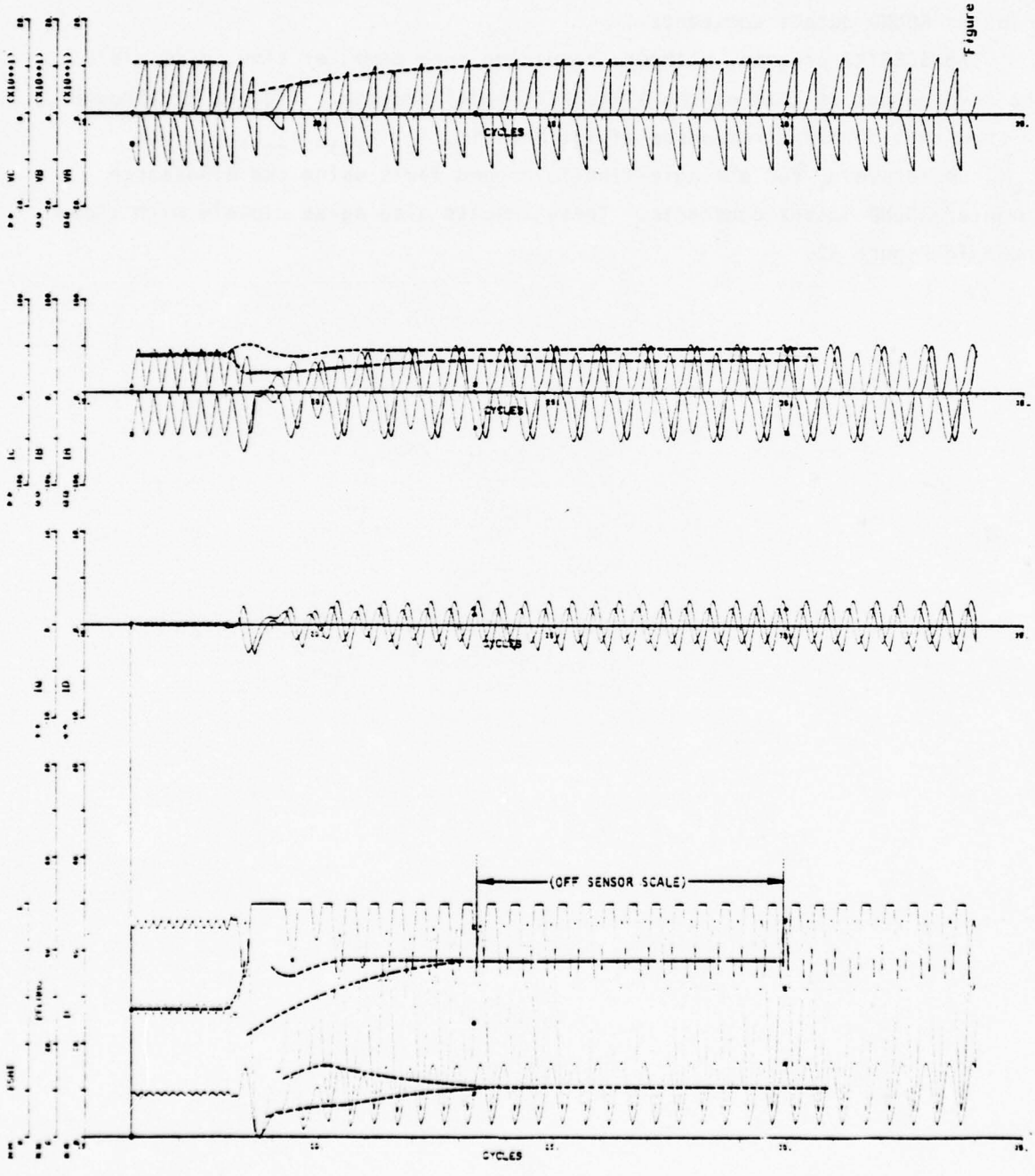

Figure 36. Load Case 4 Transient Response Using Combined Test and Calculated Data

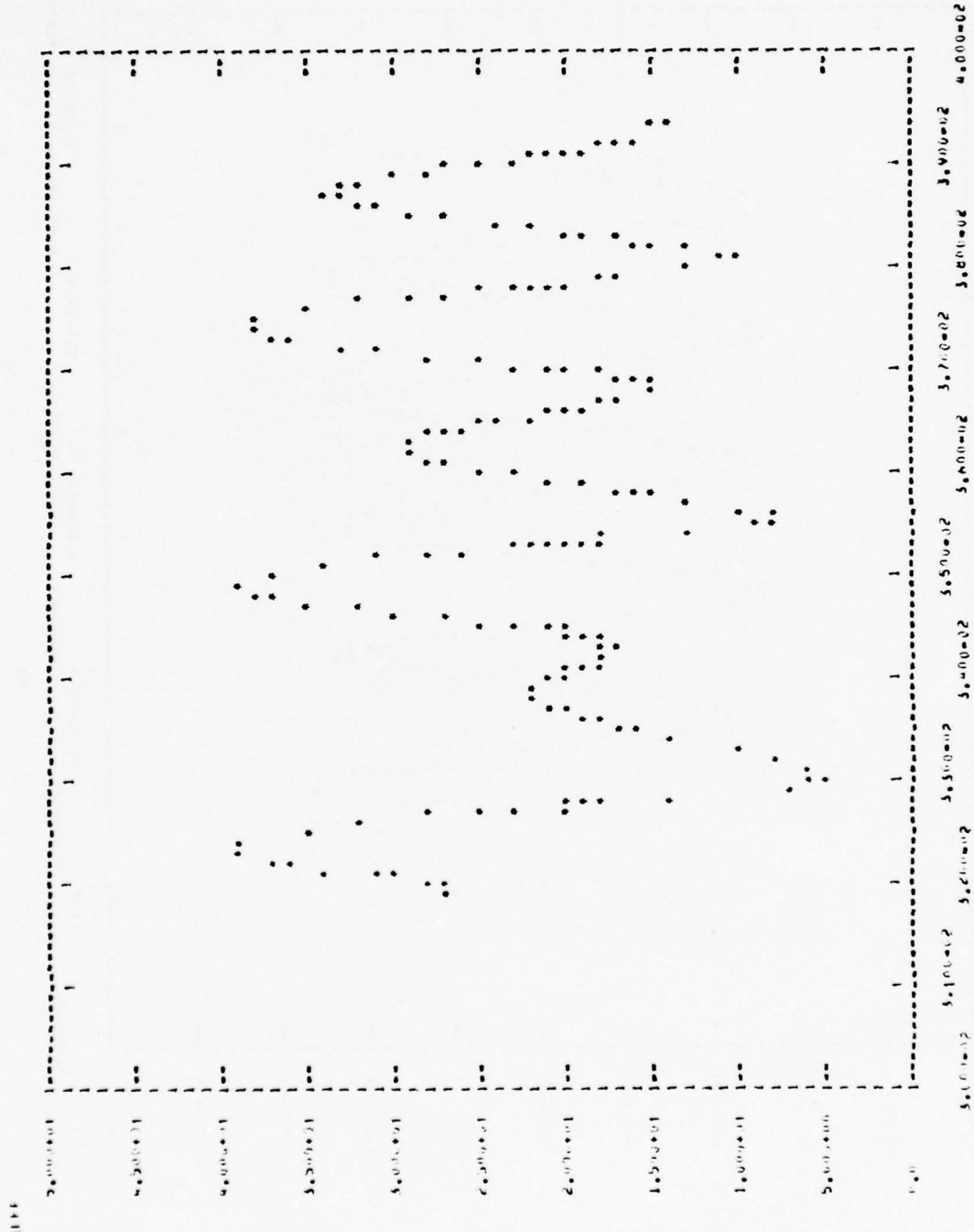

Figure 37a. Field Current, 0 to 3 Cycle Run

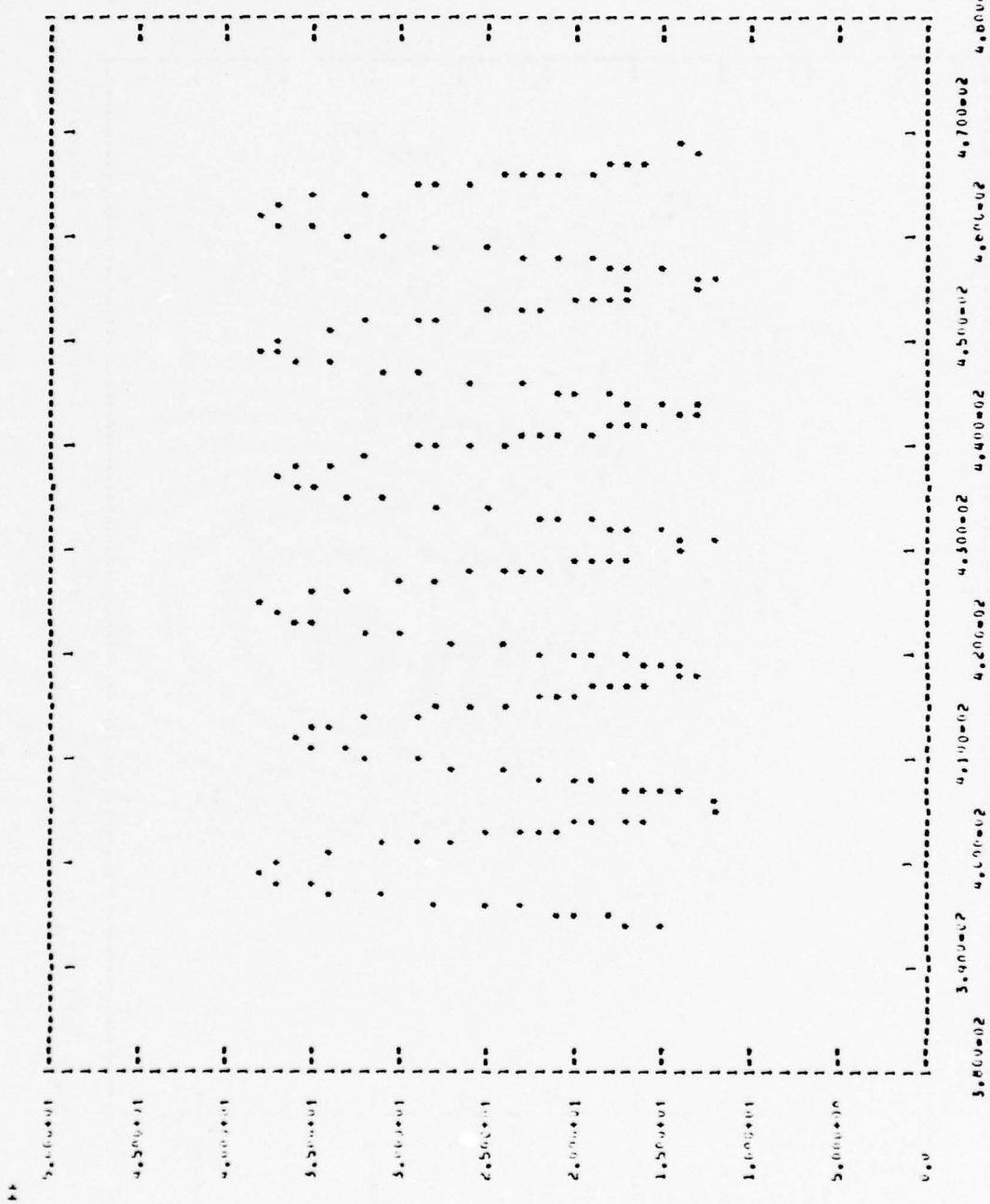

Figure 3/b. Field Current, 3 to 6 Cycle Run

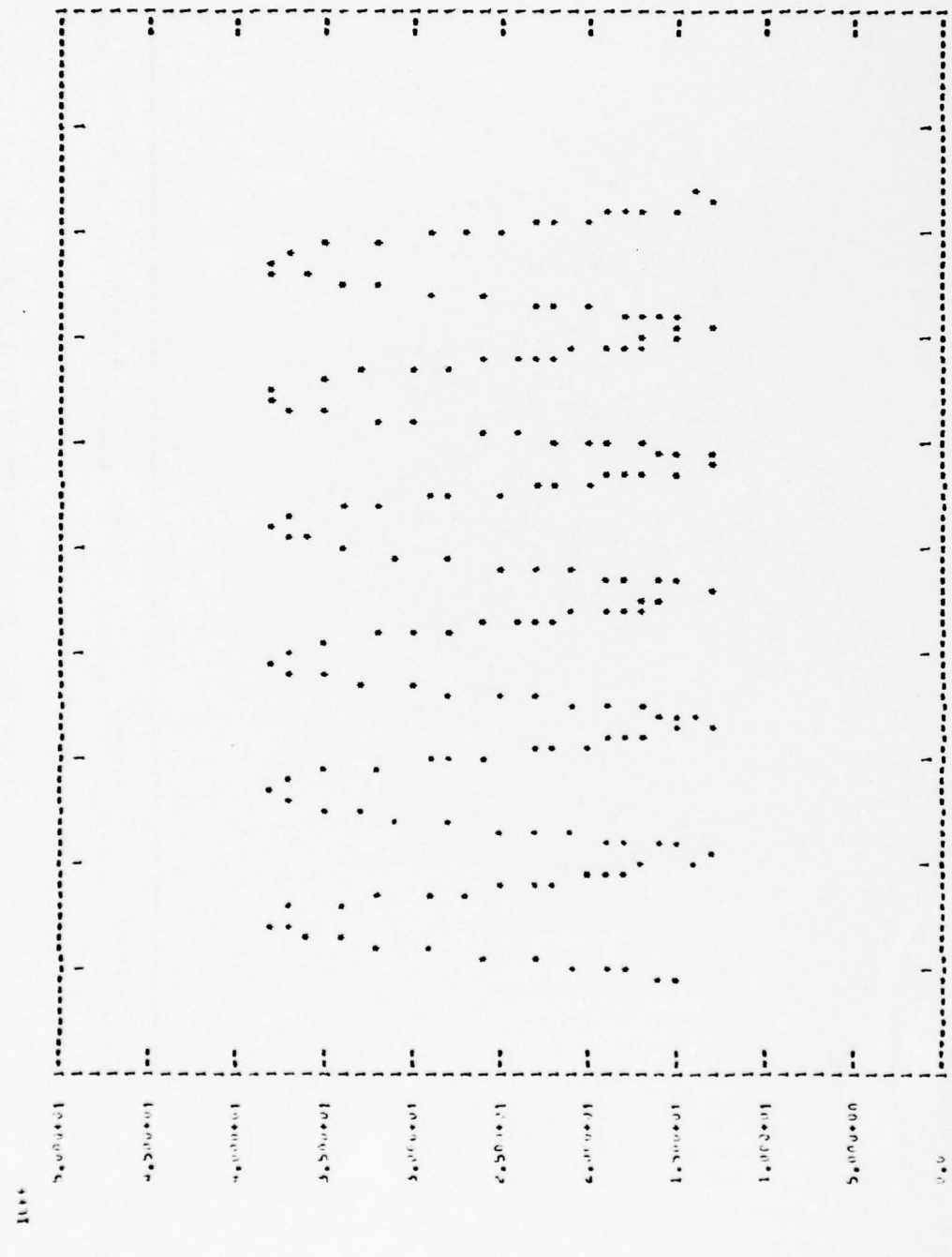

Figure 3/c. Field Current, 6 to 9 Cycle Run

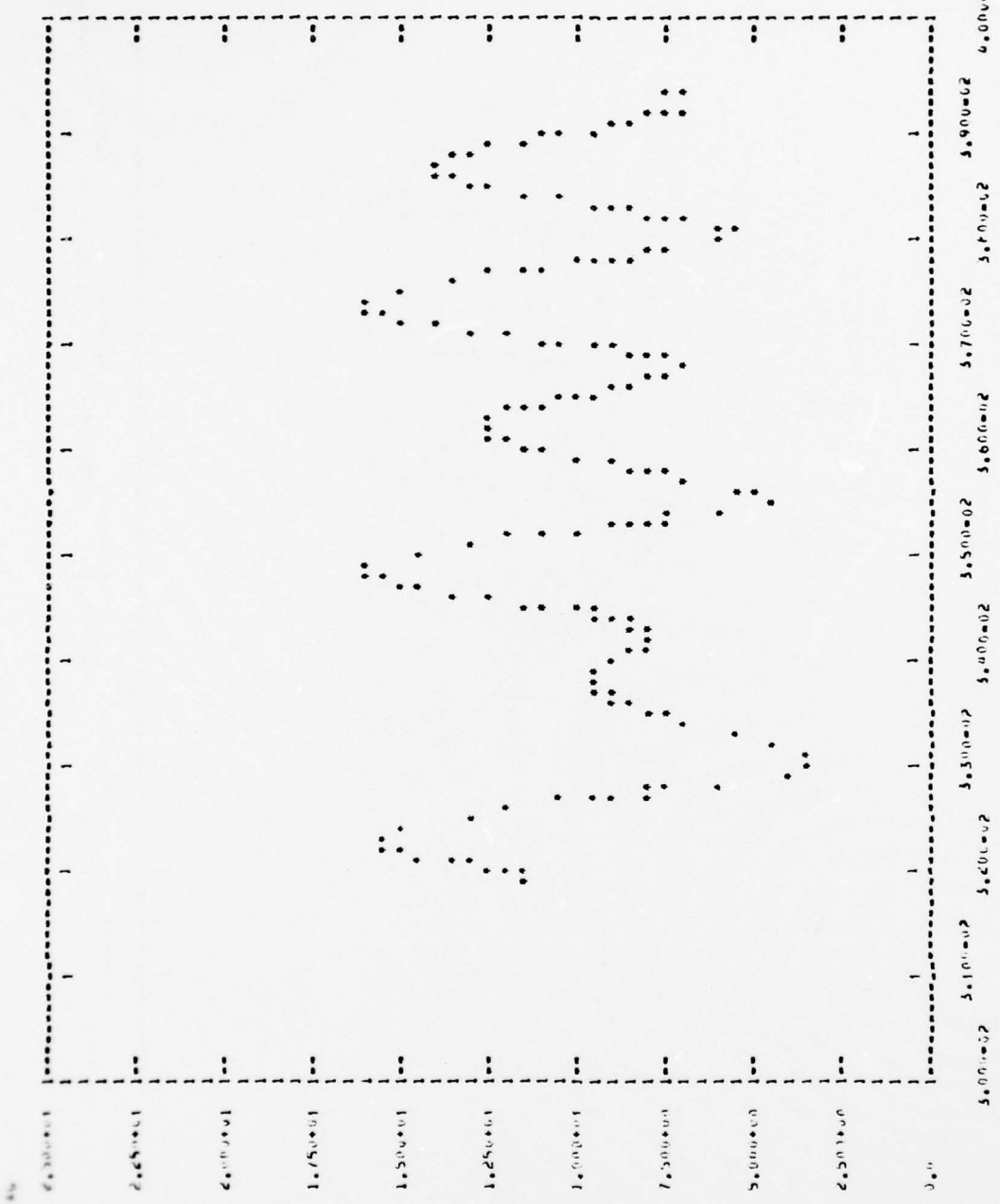

Figure 38a. Resultant MMF, 0 to 3 Cycle Run

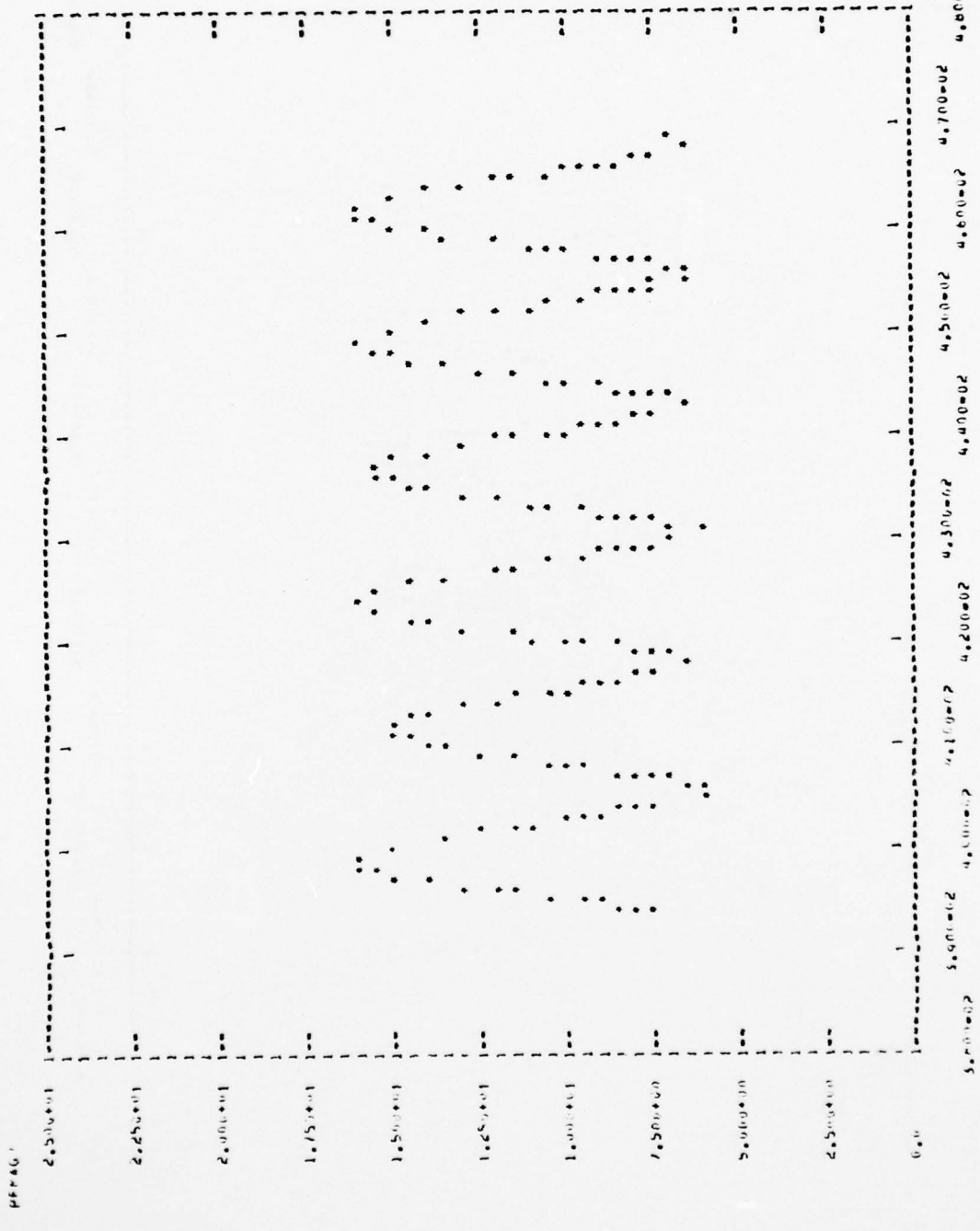

Figure 38b. Resultant MMF, 3 to 6 Cycle Run

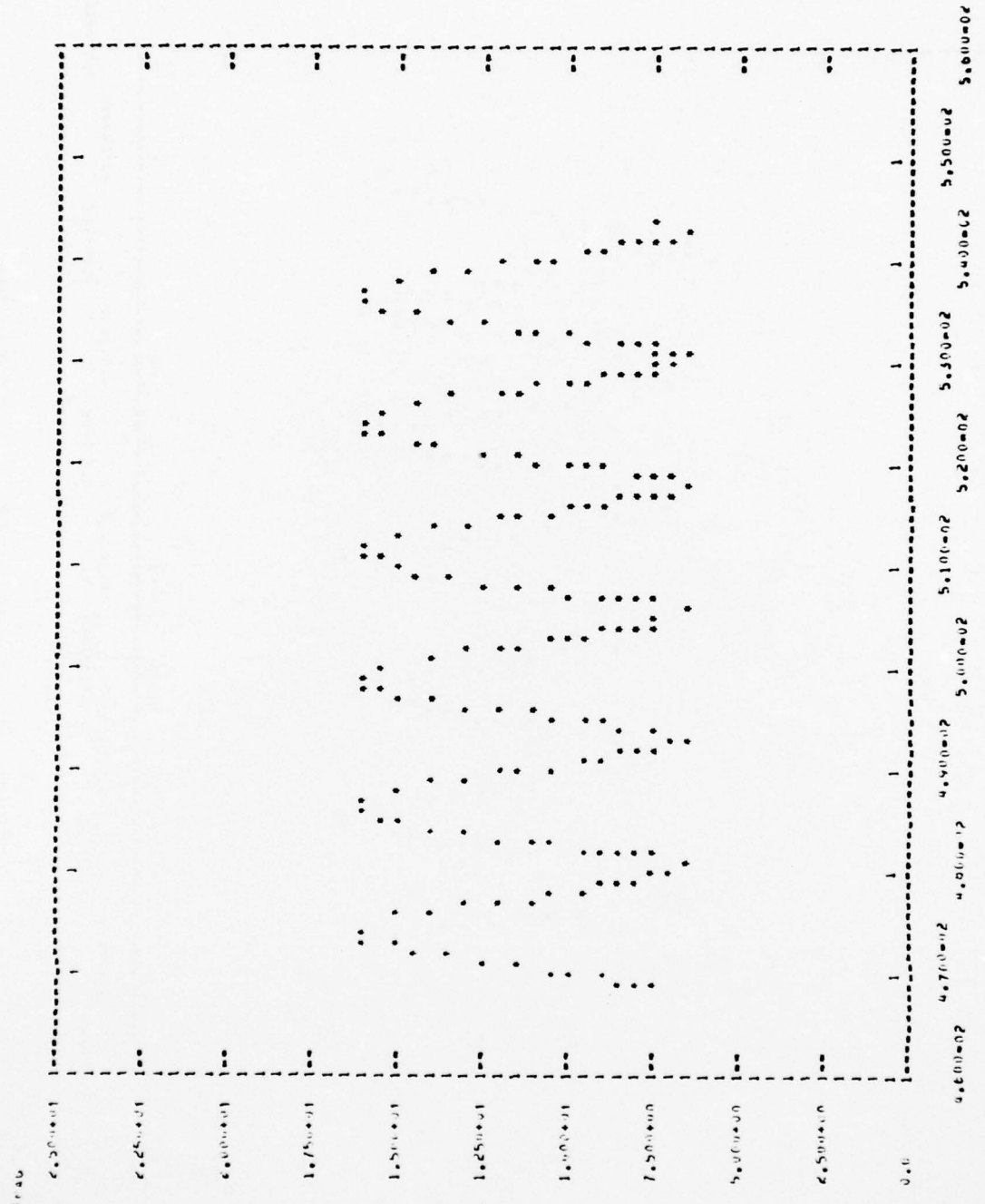

Figure 38c. Resultant MMF, 6 to 9 Cycle Run

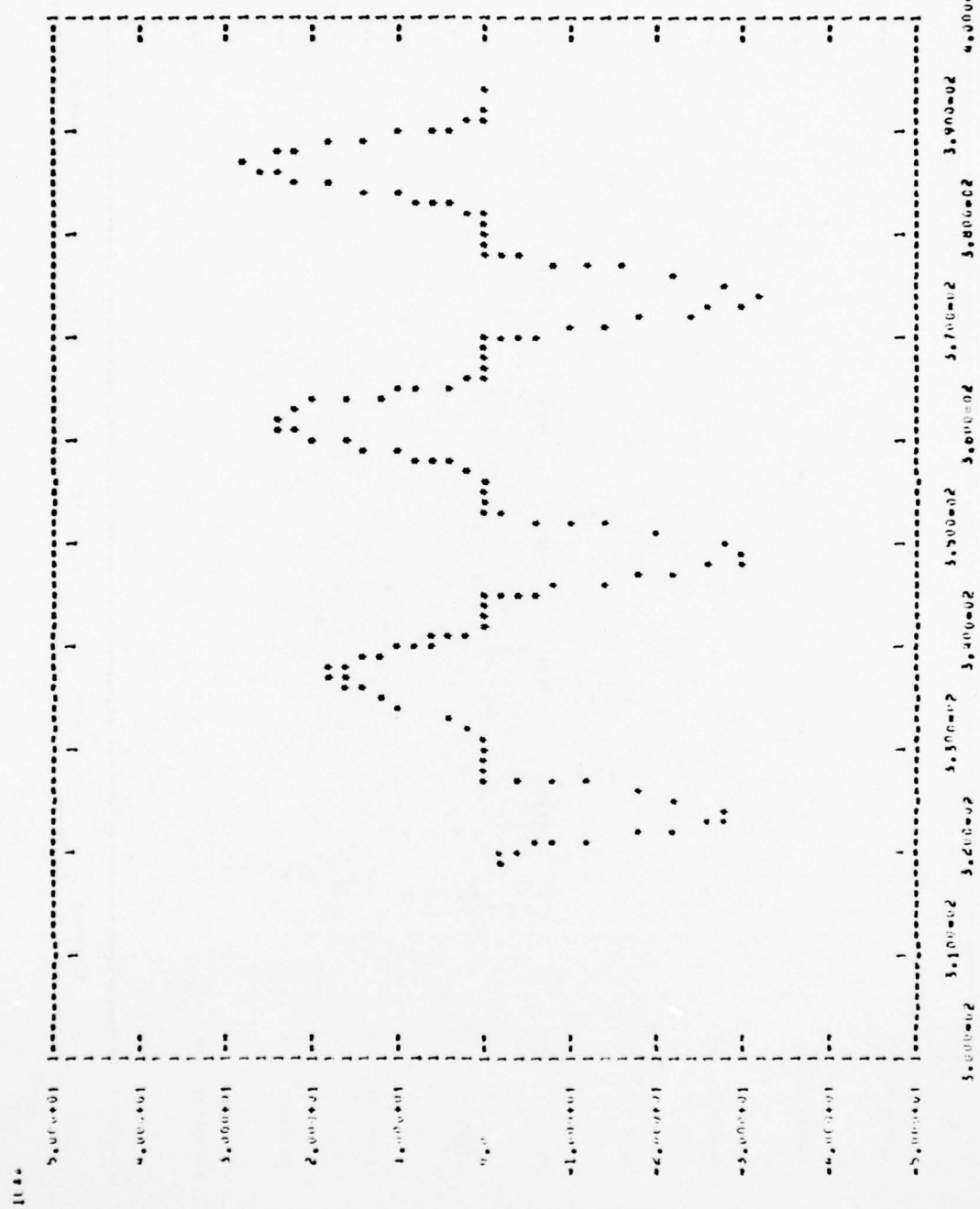

Figure 33a. Phase A Current, 0 to 3 Cycle Run

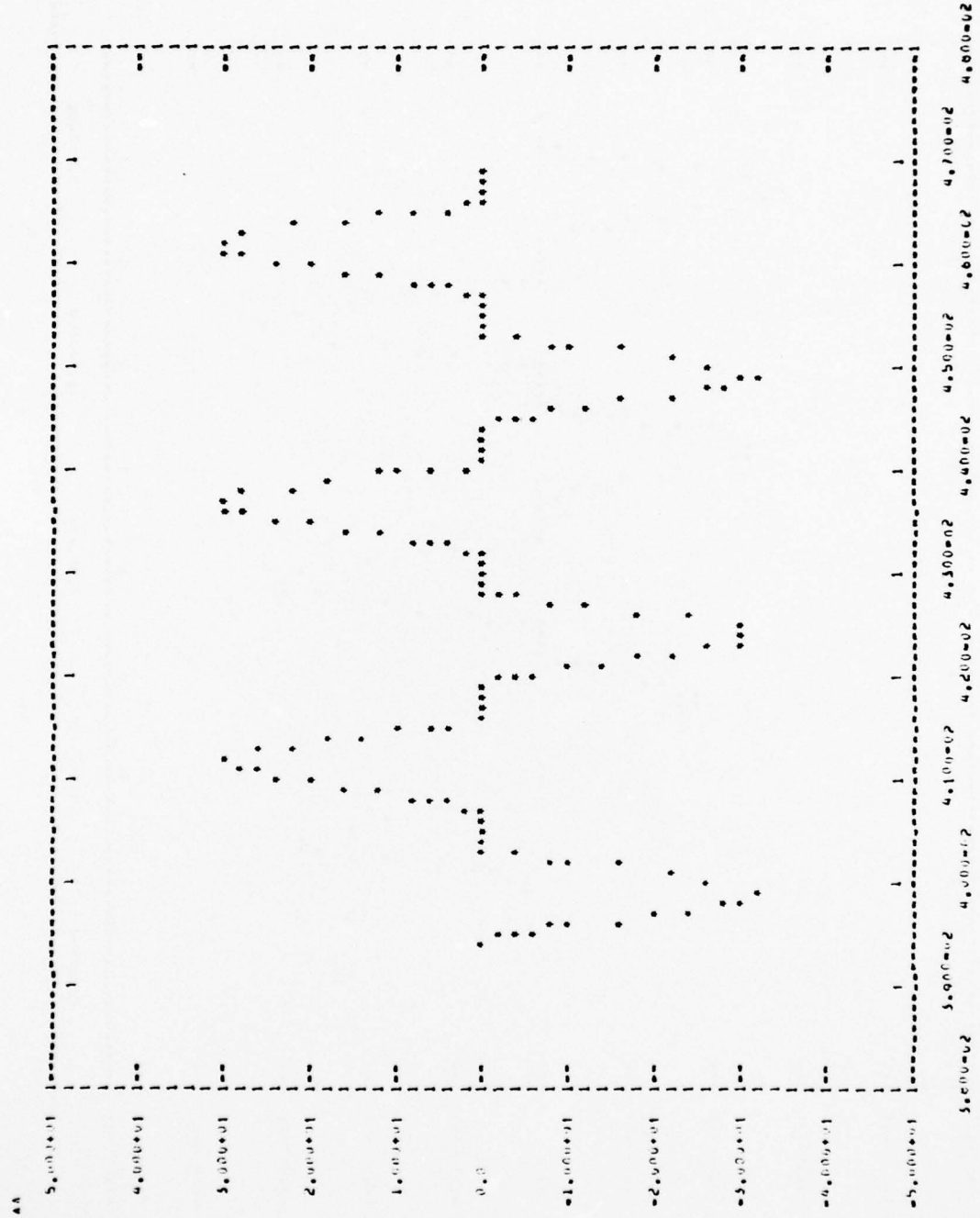

Figure 39b. Phase A Current, 3 to 6 Cycle Run

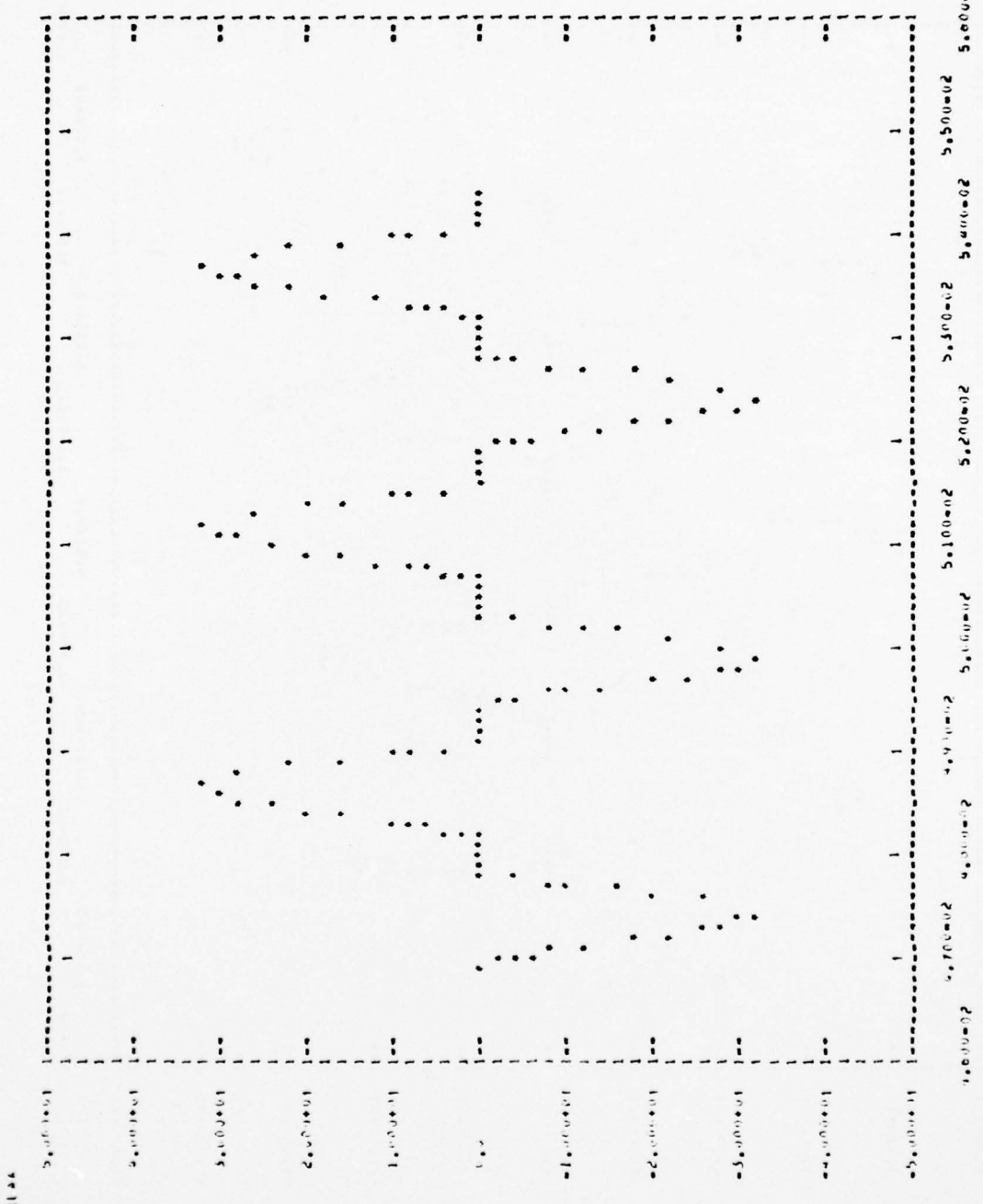

Figure 39c. Phase A Current, 6 to 9 Cycle Run

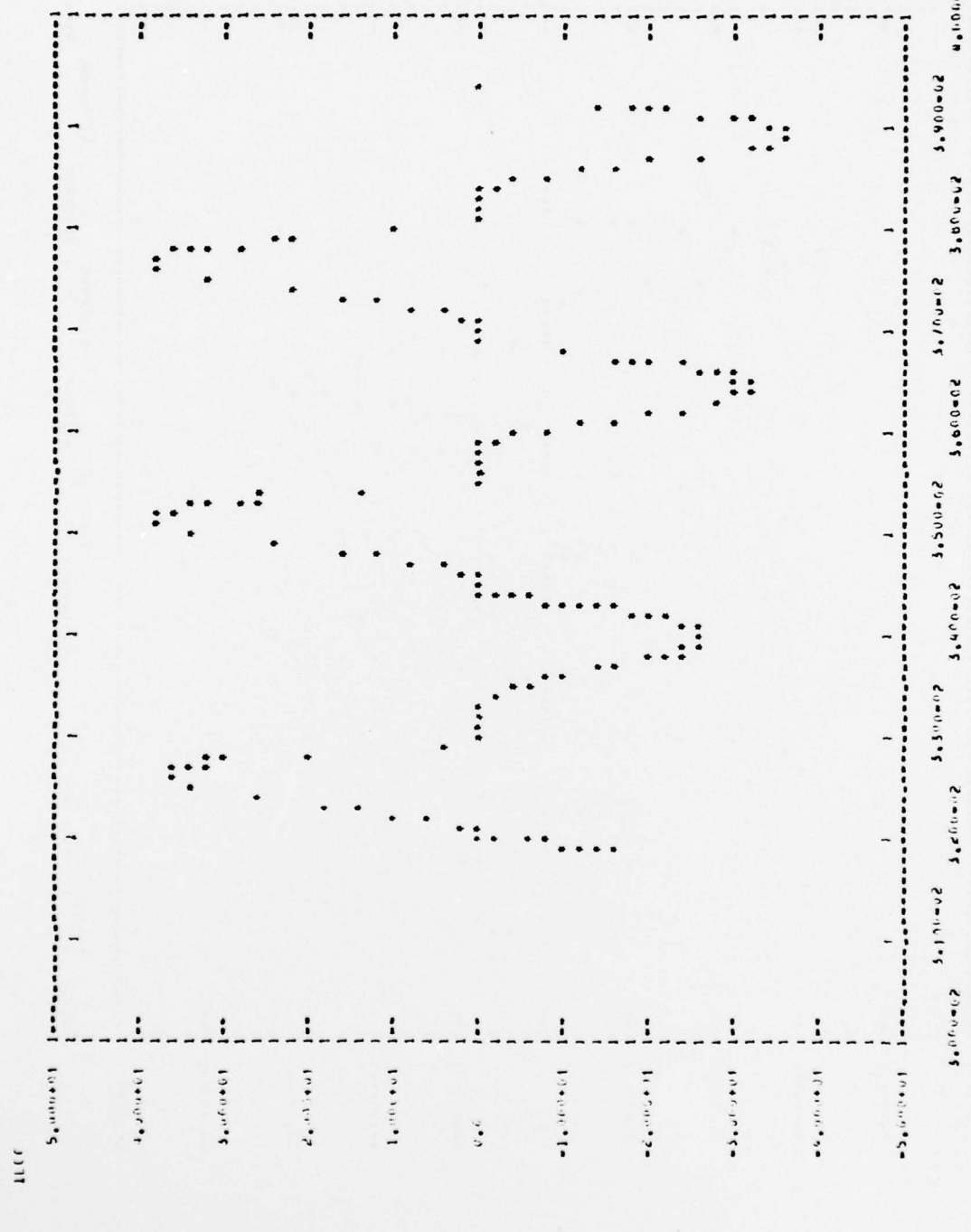

Figure 40a. Phase C Current, 0 to 3 Cycle Run

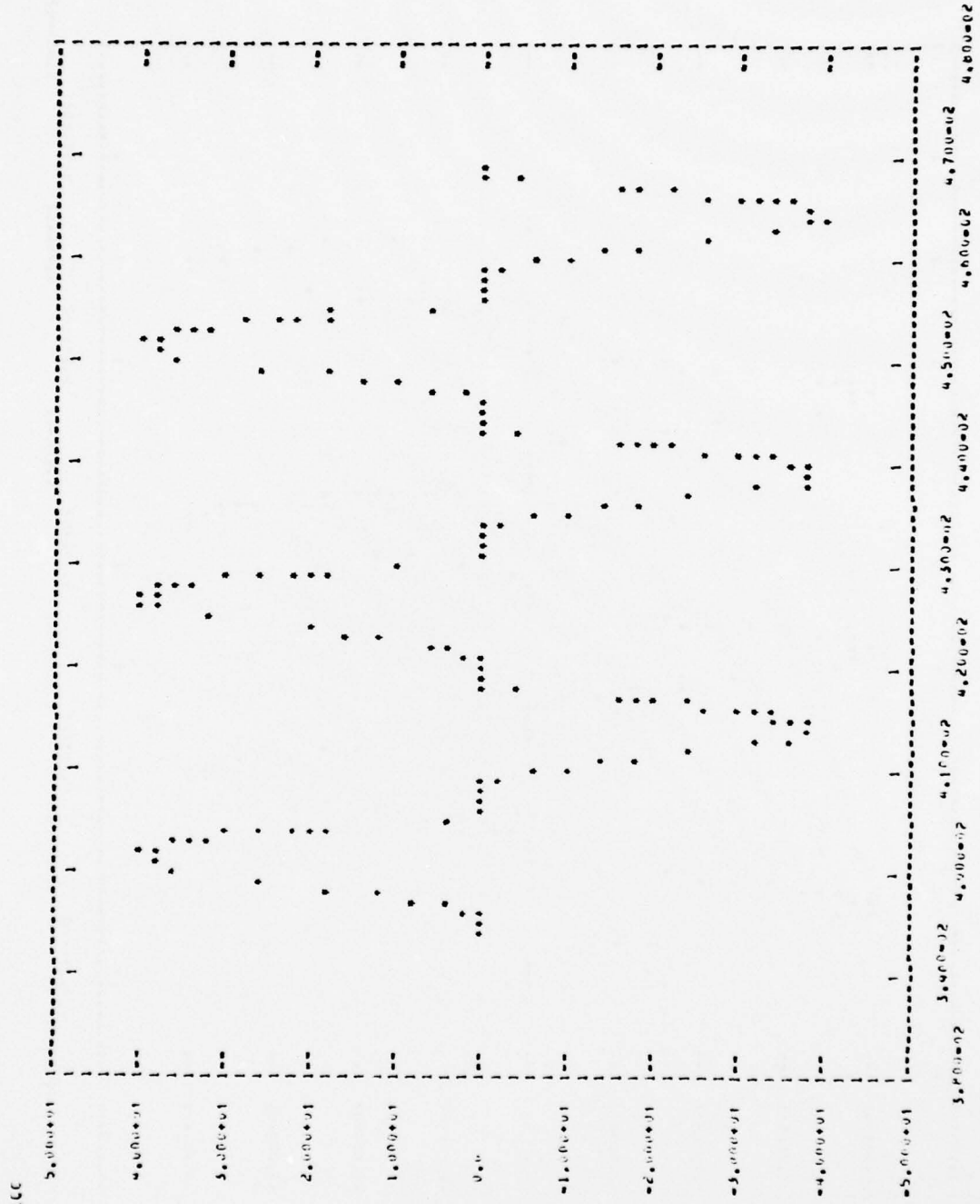

Figure 40b. Phase C Current, 3 to 6 Cycle Run

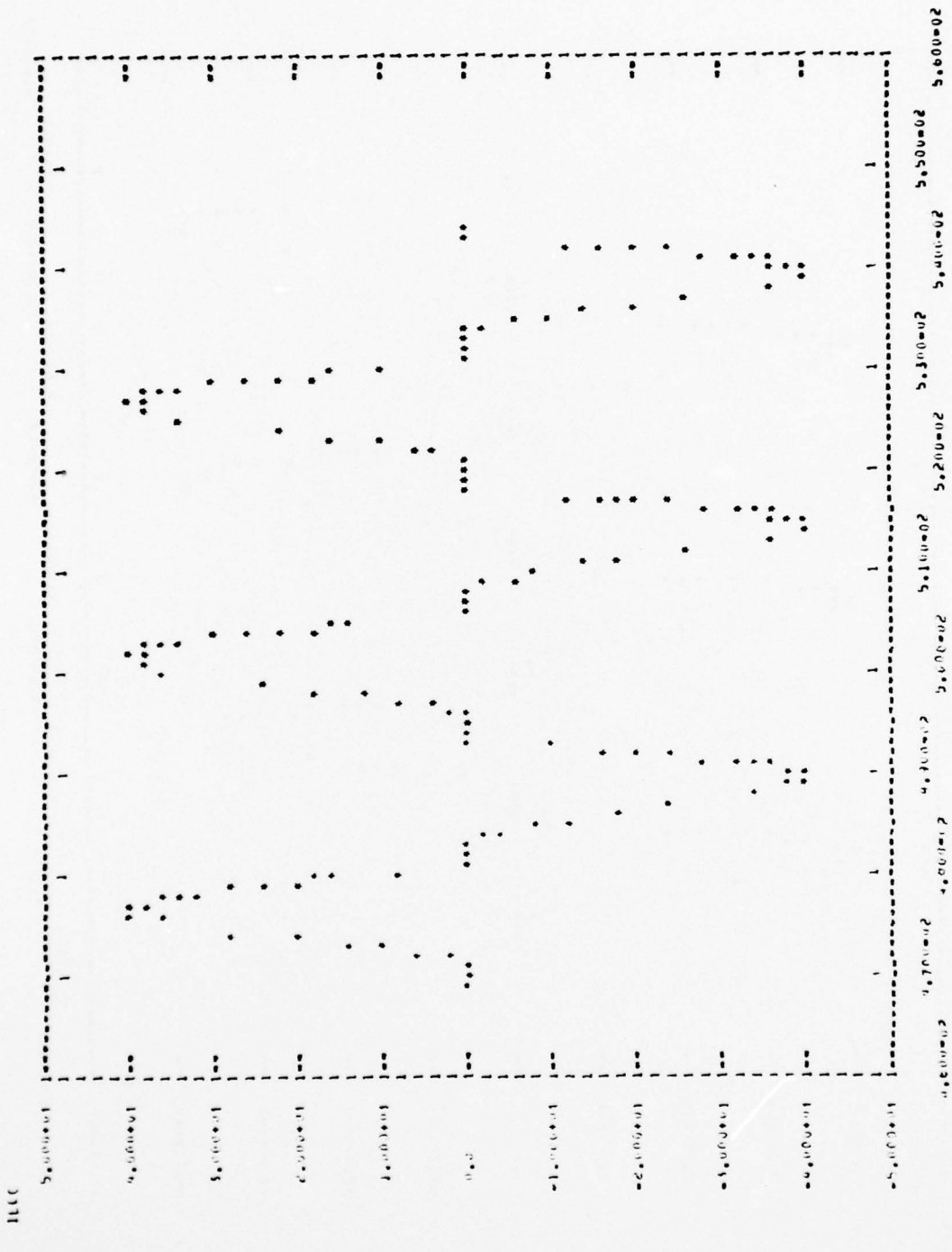

Figure 40c. Phase C Current, 6 to 9 Cycle Run

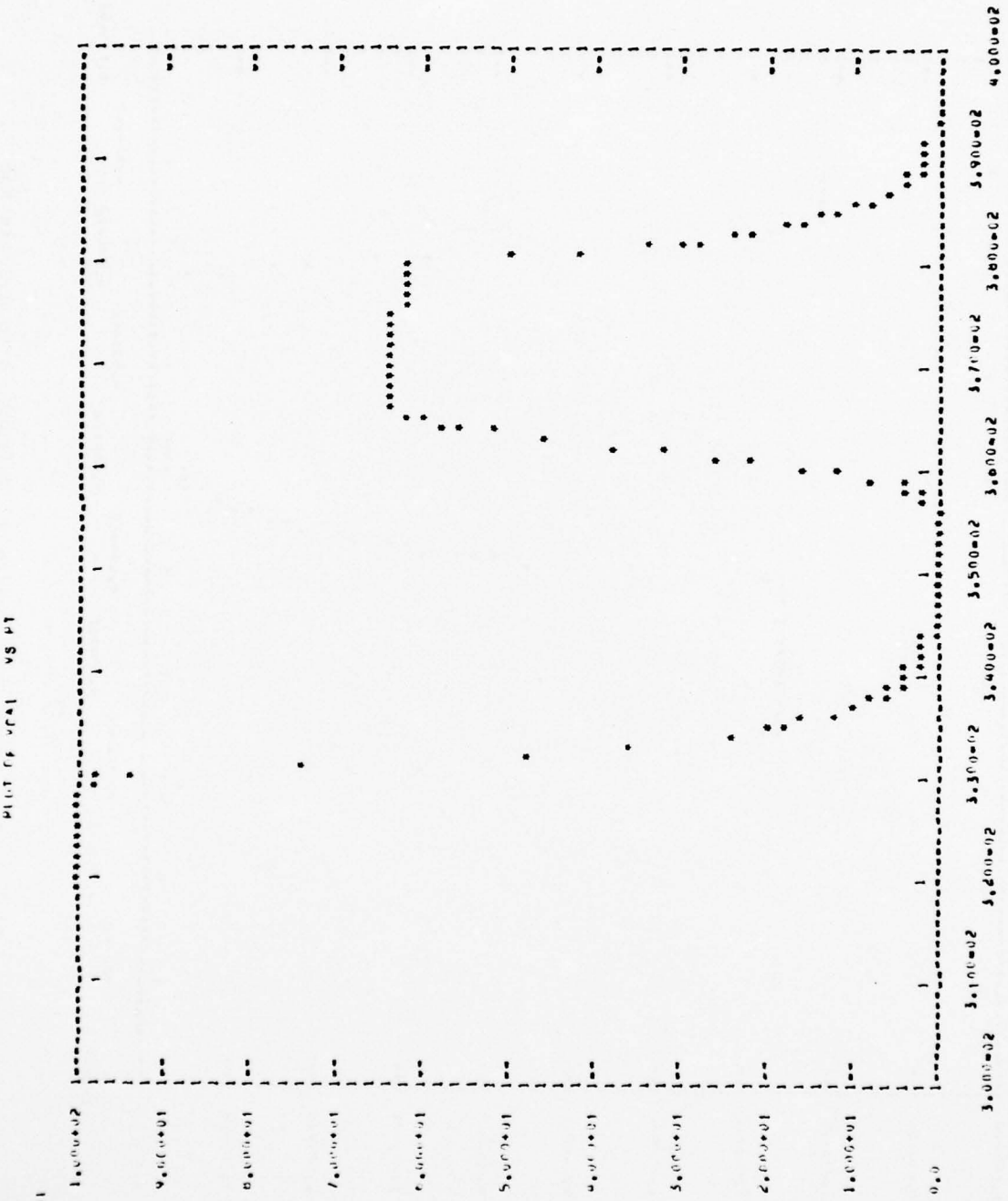

Figure 41a. Phase A Capacitor 1, Voltage, 0 to 3 Cycle Run

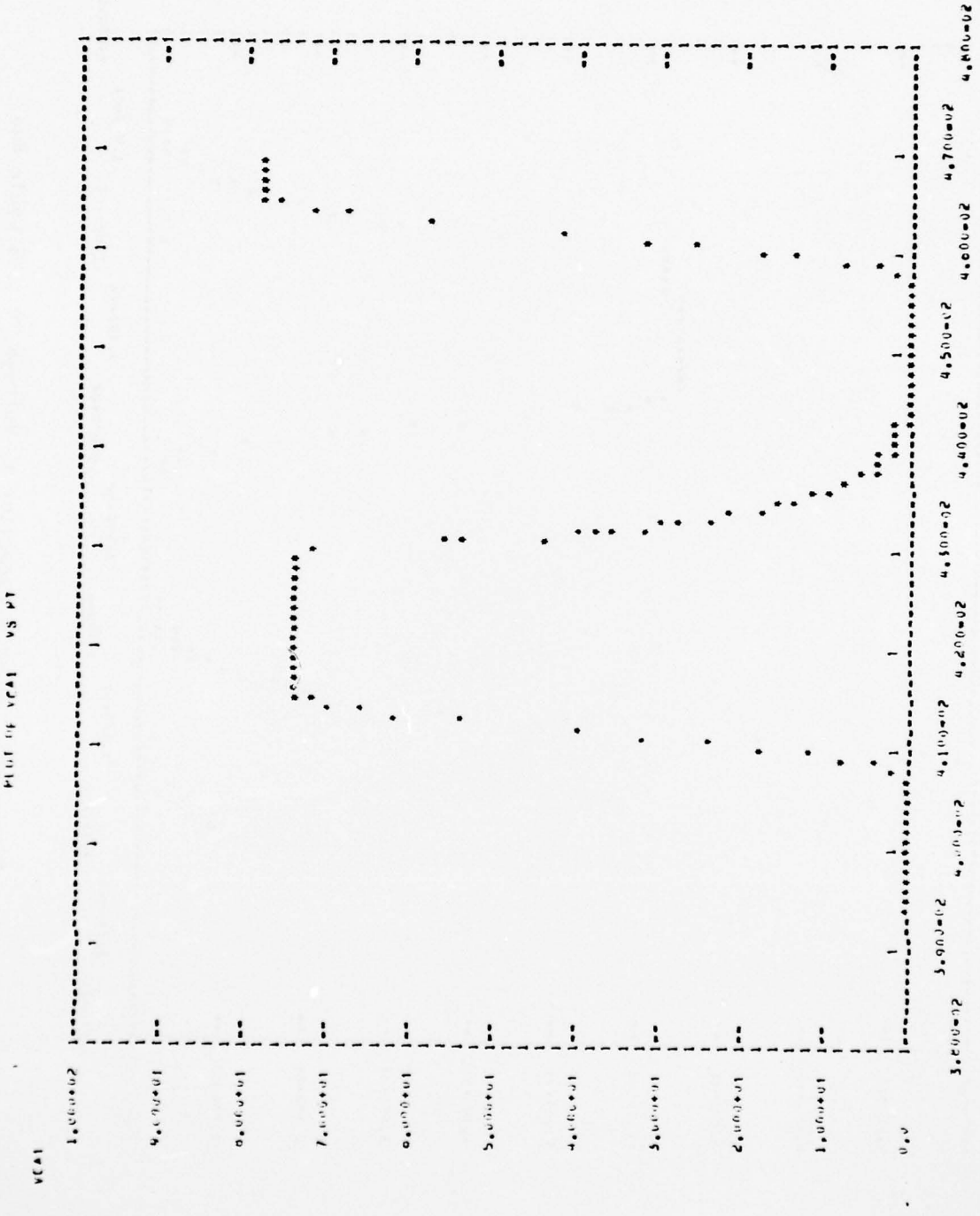

Figure 41b. Phase A Capacitor 1, Voltage, 3 to 6 Cycle Run

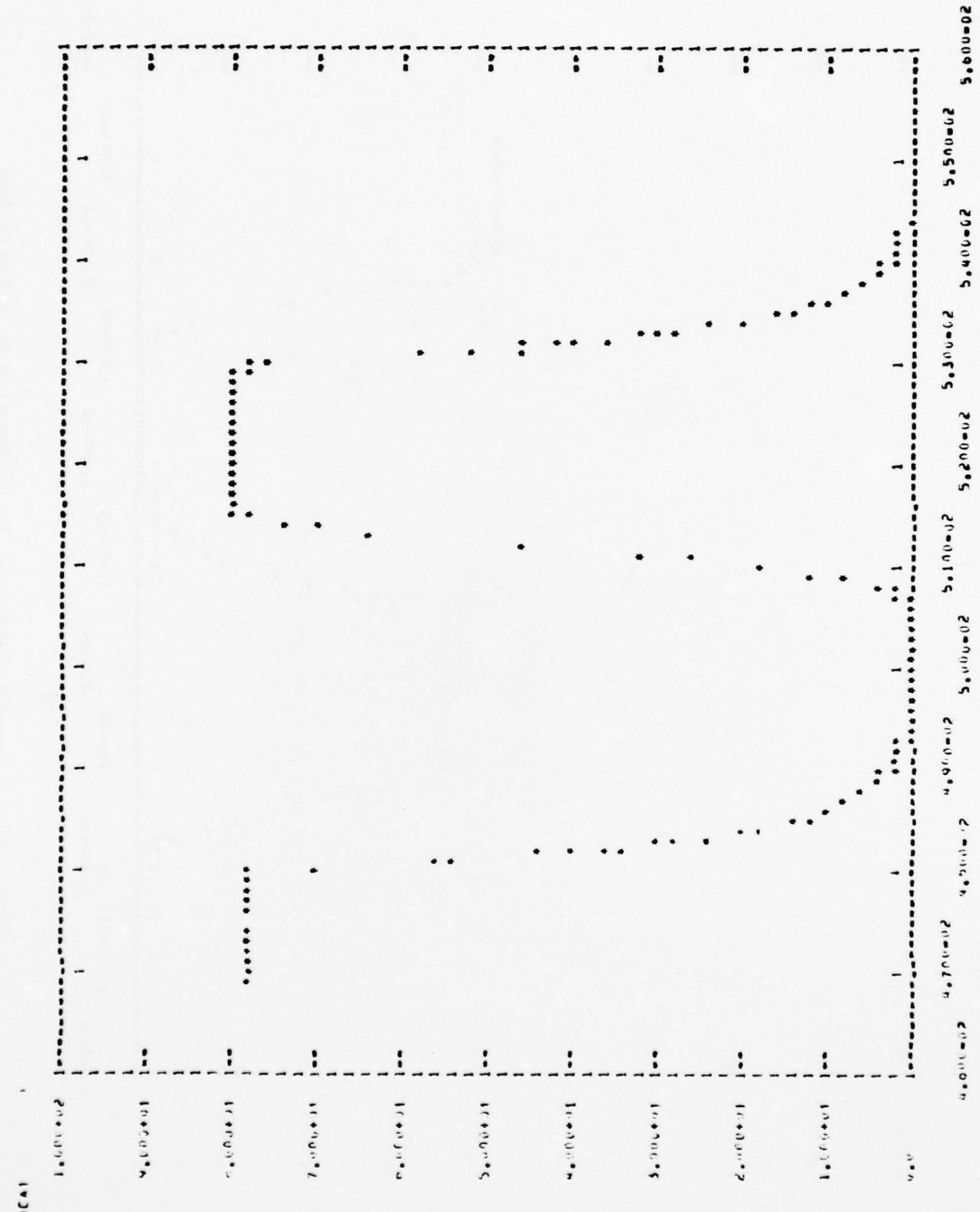

Figure 41c. Phase A Capacitor 1, Voltage, 6 to 9 Cycle Run

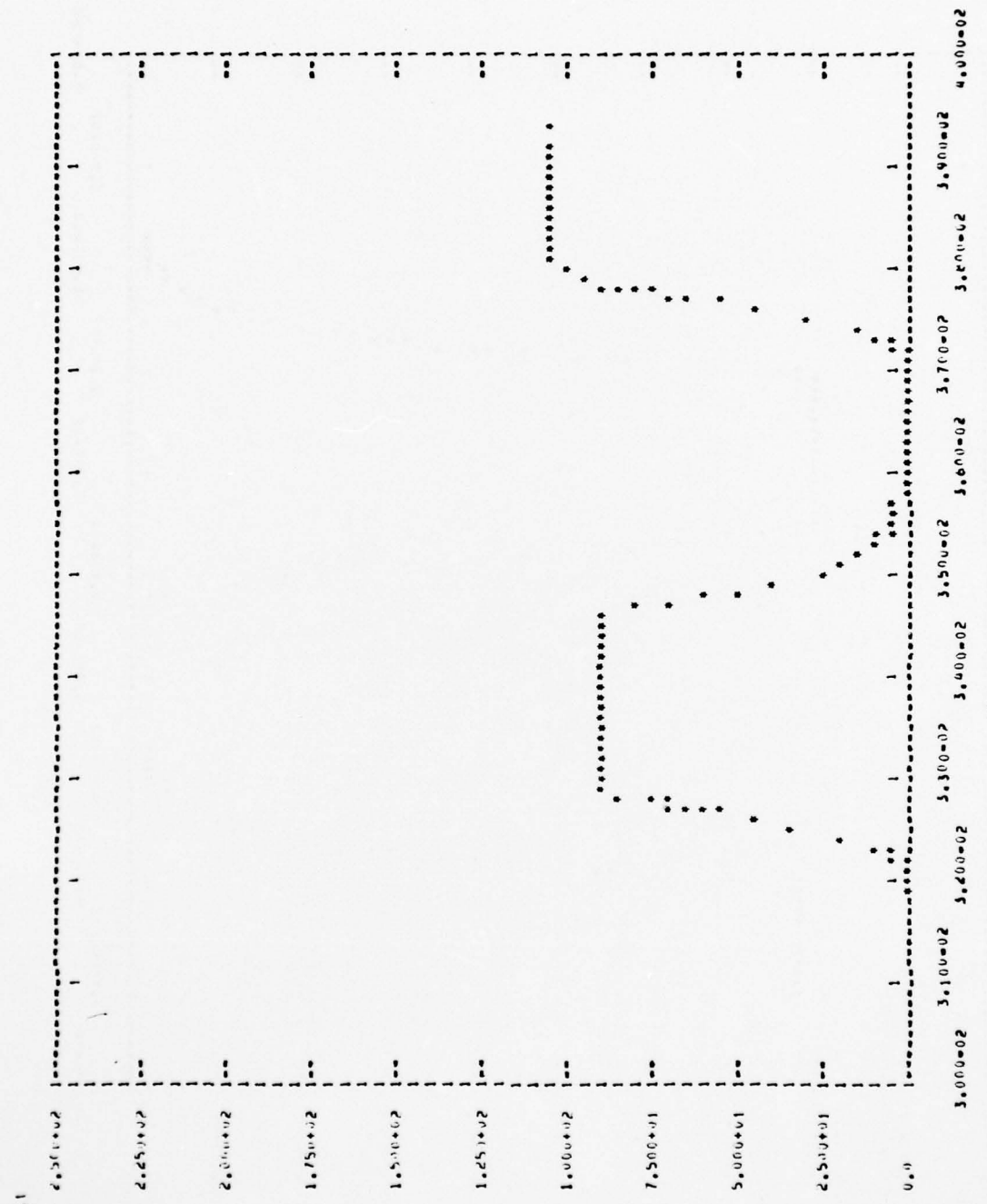

Figure 42a. Phase C Capacitor 1, Voltage, 0 to 3 Cycle Run

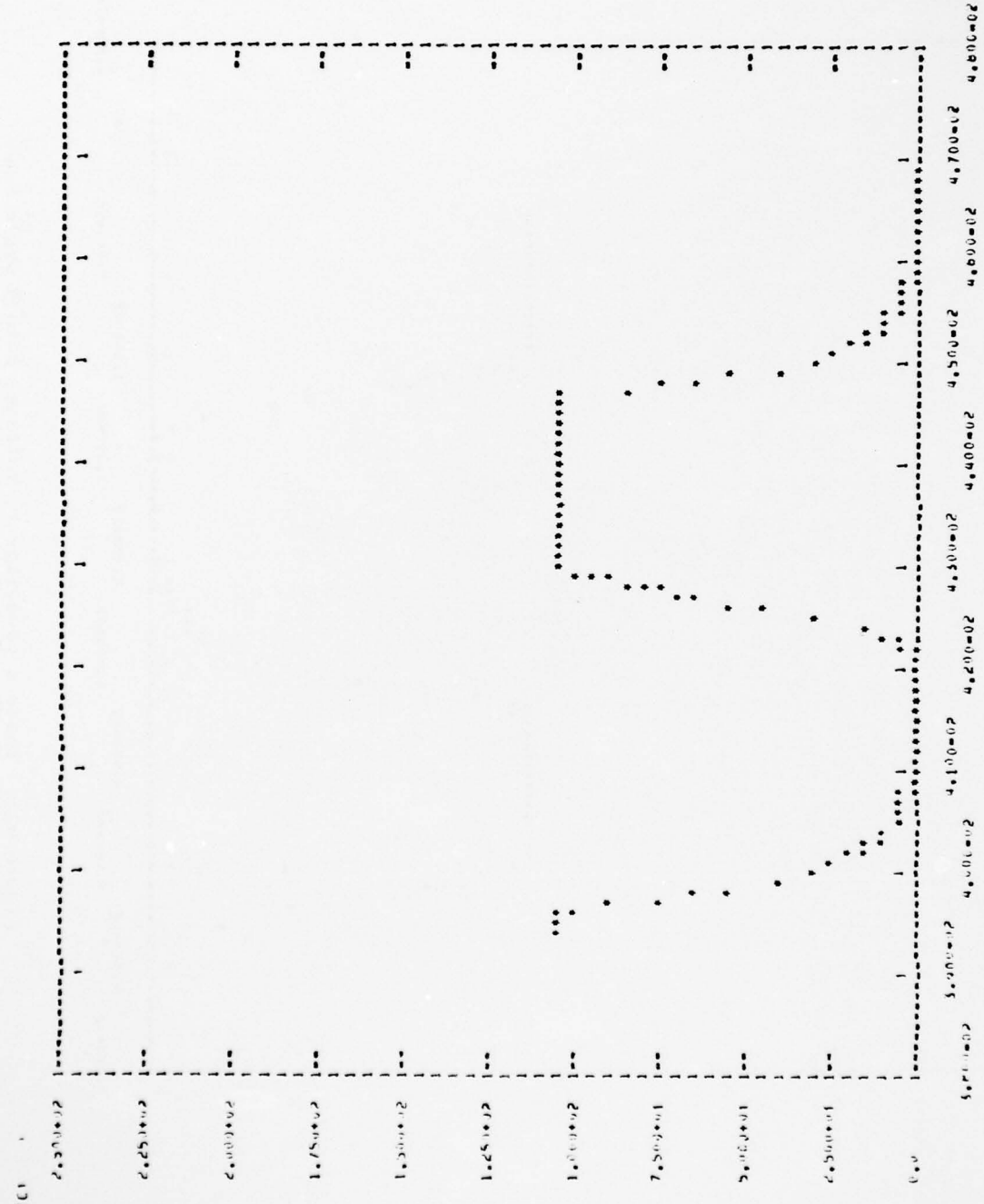

Figure 42b. Phase C Capacitor 1, Voltage, 3 to 6 Cycle Run

AD-A041 257 AIRESEARCH MFG CO OF CALIFORNIA TORRANCE F/G 10/2
SUBSYSTEM DESIGN ANALYSIS LIGHTWEIGHT ALTERNATOR (MODEL TEST PR--ETC(U)
MAR 77 C H LEE, D BERKER, G TATRO, P WALIA F29601-74-C-0055
UNCLASSIFIED AFWL-TR-75-66-ADD-2 NL

2 OF 2
AD A041257

END
DATE FILMED
7-77

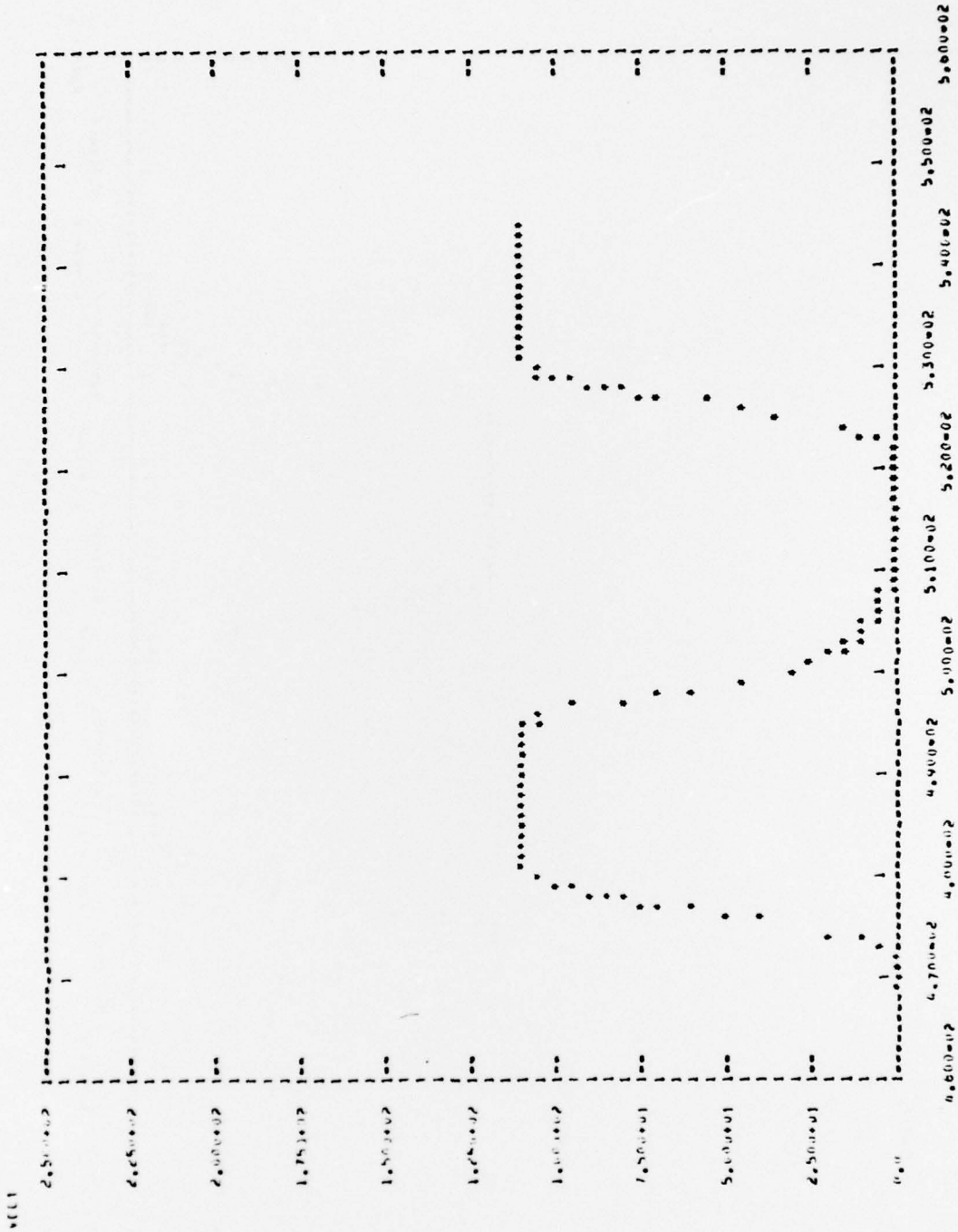

Figure 42c. Phase C Capacitor 1, Voltage, 6 to 9 Cycle Run

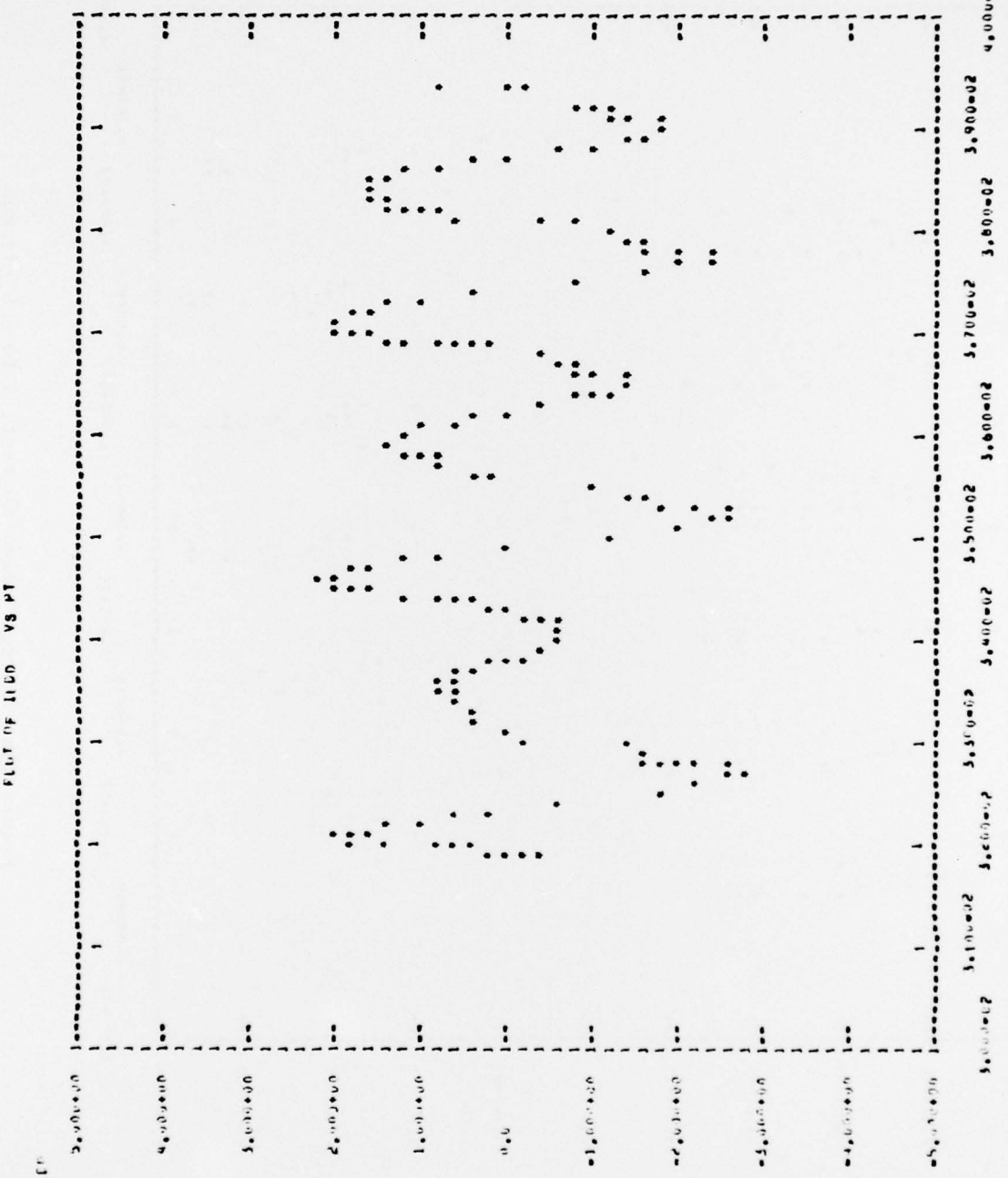

Figure 43d. Direct Damper Current, 0 to 3 Cycle Run

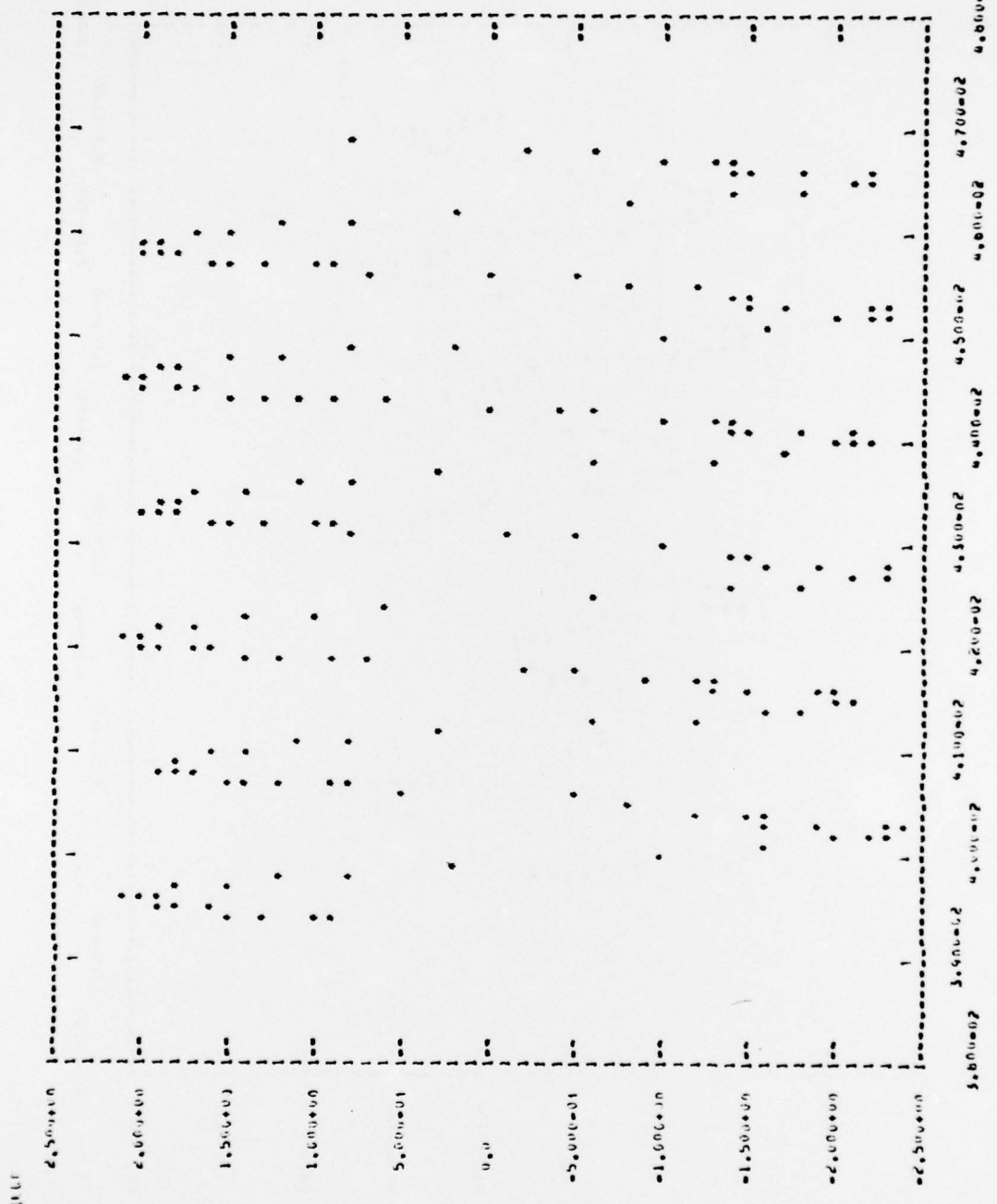

Figure 43b. Direct Damper Current, 3 to 6 Cycle Run

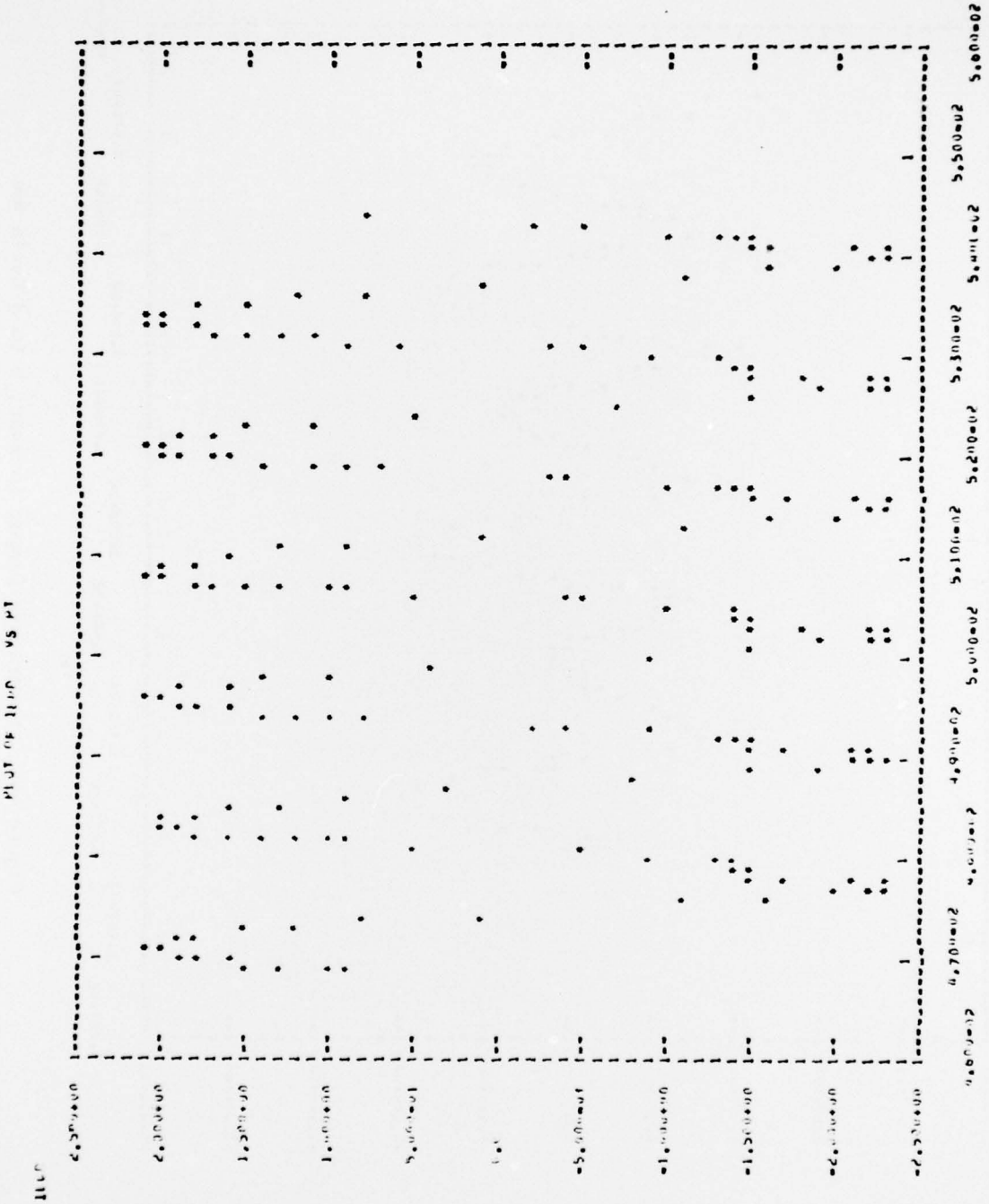

Figure 43c. Direct Damper Current, 6 to 9 Cycle Run

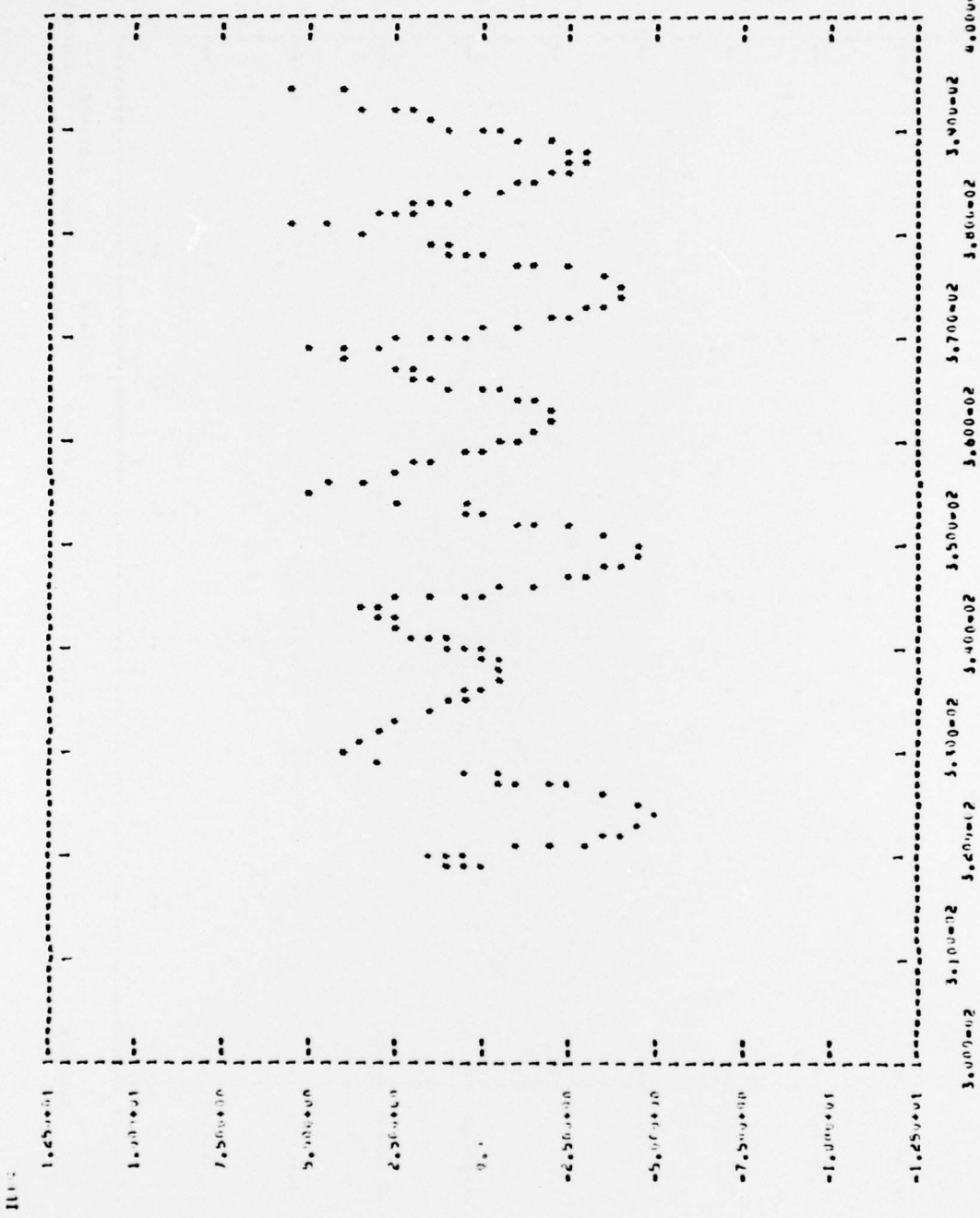

Figure 44a. Quadrature Damper Current, 0 to 3 Cycle Run

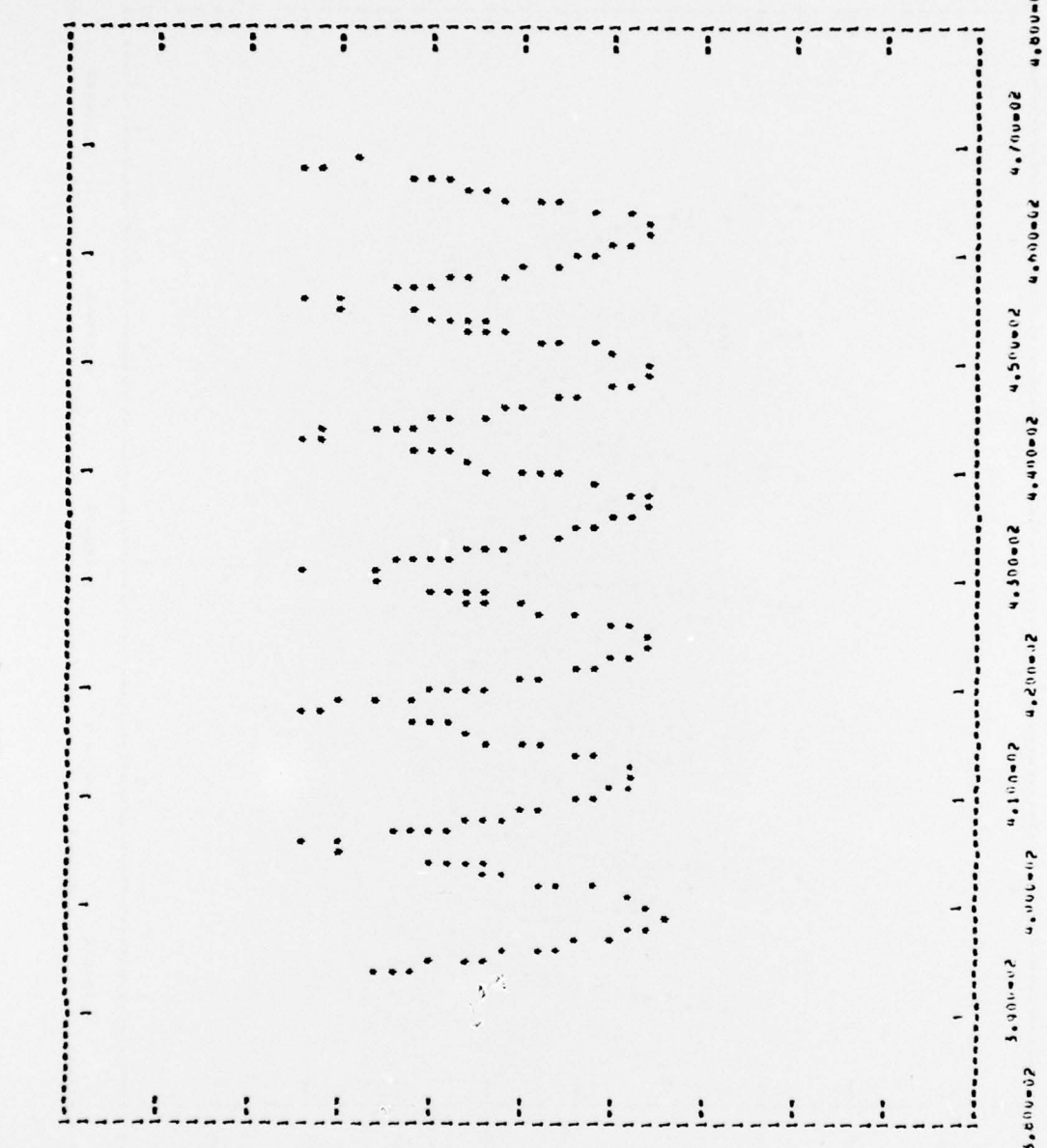

Figure 44b. Quadrature Damper Current, 3 to 6 Cycle Run

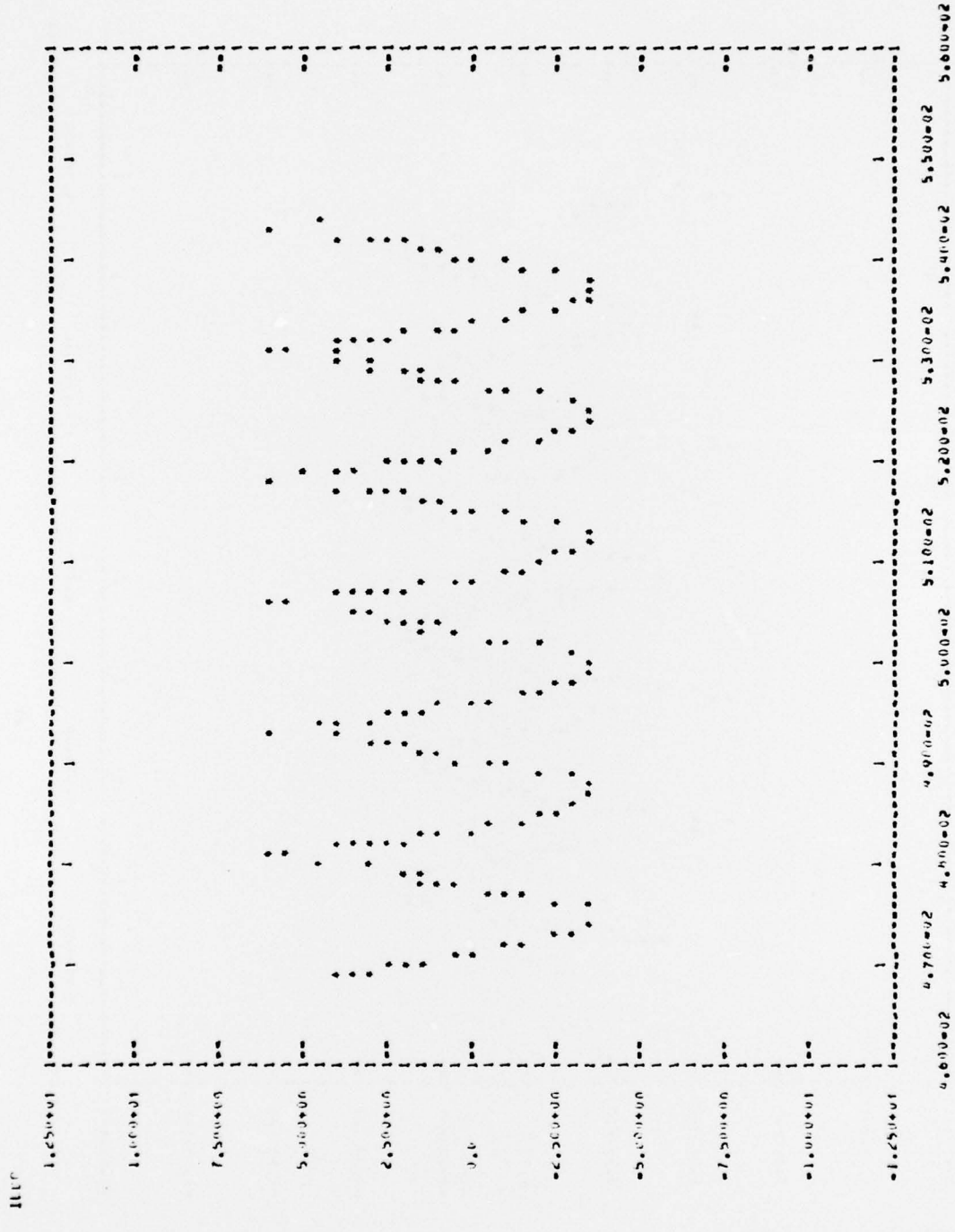

Figure 44c. Quadrature Damper Current, 6 to 9 Damper Run

SECTION X

CONCLUSIONS

Results of the alternator test and computer modeling work performed were positive. The following comments and conclusions are pertinent.

The test alternator and loading/control circuits performed as intended with no serious or unforeseen problems in construction or use. Although precise resonant operation was not realized, the alternator was operated at 400 Hz with two circuit resonant frequencies so that half-cycle current conduction angles of approximately 125 and 160 electrical degrees were achieved. (Note: emphasis in the program was on the test and modeling correlation activities in order to verify alternator design methods and approach. Achieving precise ac resonant operation was a secondary objective.)

Based on the test and modeling results, the AiResearch alternator design program ROUND does develop machine saturation data and constants that can be utilized to confidently predict alternator transient behavior.

Transient simulation results were checked using two sets of alternator saturation and reactance constant data: one directly taken from the AiResearch ROUND alternator design program, and one based on actual test of the alternator supported by manual calculation. These two input data sets generally were in close quantitative agreement and yielded similar results. It should nonetheless be noted that the accurate quantitative prediction or the determination by test of alternator damper circuit constants (particularly for nondiscrete elements like a solid rotor core) are presently dependent on largely empirical treatment. This is an area of possible interest for further analytical investigation.

The alternator/load model transient behavior cases were solved using two distinct mathematical/computer approaches: the SCEPTRE program and an AiResearch program. Results for a given input data set were in very close quantative agreement.

While SCEPTRE is capable of solving the alternator/load model cases and can do so with good accuracy, the computing time is still excessive. Accuracy of SCEPTRE results is essentially tied to the convergence and integration step size criteria selected. These, in turn, directly affect computer run

time and cost. Even when rather inexact solution is allowed, the SCEPTRE program requires long run time. Furthermore, the switching phenomena cannot be exactly treated. Finally, the output plot data, while it can be interpreted, is not conventiently graphic or complete. These are not serious defects, but should be noted.